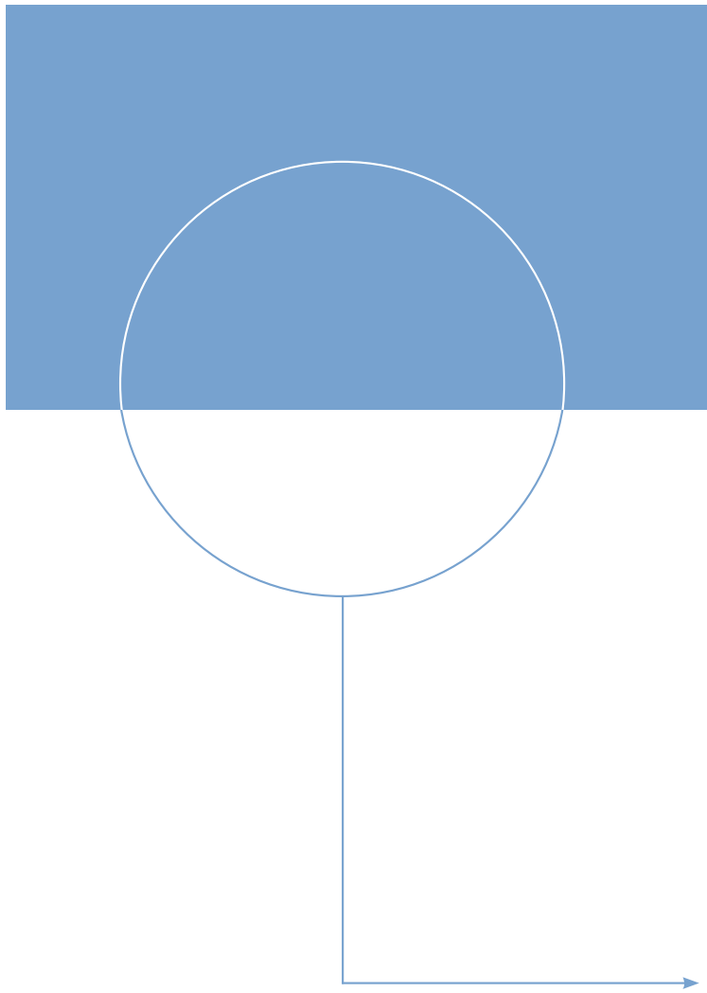

Master's thesis

2022

Erik Hjertnes Nygaard

NTNU
Norwegian University of
Science and Technology
Faculty of Engineering
Department of Civil and Environmental Engineering

Erik Hjertnes Nygaard

Experimental Investigation of an Inclined, Floating Breakwater with a Porous design and Bio-enhancing features

June 2022

NTNU
Department of Civil
and Environmental Engineering

UNIVERSITÉ CAEN NORMANDIE

ESITC CAEN
Ecole Supérieure d'Ingénieurs des Travaux de la Construction

NTNU
Norwegian University of
Science and Technology

NTNU
Norwegian University of
Science and Technology

NTNU

Norwegian University of
Science and Technology

Experimental Investigation of an Inclined, Floating Breakwater with a Porous design and Bio-enhancing features

Erik Hjertnes Nygaard

Civil and Environmental Engineering
Submission date: June 2022
Supervisor: Raed Lubbad (NTNU)
Co-supervisor: Dominique Mouazé (UniCaen)

Norwegian University of Science and Technology
Department of Civil and Environmental Engineering

Acknowledgements

This Thesis is concluding a Master's degree of Civil Engineering from the Norwegian University of Science and Technology (NTNU) in Trondheim. The practical work for the Thesis has been carried out on the Wave Flume Laboratory of ESITC in Caen, Normandie. I want to express my greatest gratitude to Raed Lubbad (NTNU) and Dominique Mouaze (UniCaen), my two supervisors, who have guided me through the work with valuable experience and important discussion. I want to thank Guillaume Carpentier who made it possible for me to conduct my experiments in the laboratory of ESITC, Iman Safari and Yoann Bonte who have helped me through the practical challenges I have met in the lab-work and all the wonderful people at ESITC and UniCaen who made my stay in France possible and into a great memory.

This degree would never have been possible without the company of my fellow students and student organizations in Trondheim, especially H.M. Aarhønen, Studentersamfundet and UKA, as they have been completing the student life in a way that makes the memories stay in my mind forever. I have a family who have been crucial supporters for me through my years of studies, and for that I am forever grateful.

NTNU

Trondheim, June 2022

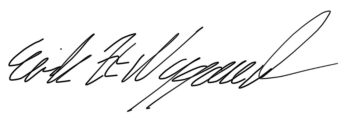

Erik Hjertnes Nygaard

Abstract

The world is facing bigger risks due to the climatic changes than previously described, including sea level rise and extreme weather conditions. The climatic changes have also caused substantial damages and increasingly irreversible losses in coastal and open marine ecosystem. Adaptions that decelerate the trend is a crucial remedy. Floating breakwaters are an established alternative to conventional rubble-mound breakwaters, where such a construction is unfavourable due to economical, environmental and practical constraints. The typical areas of use are those exposed to primarily wind waves as floating breakwaters do generally have a poor performance against long period swell waves.

This study presents a new design for a floating breakwater. The concept of the breakwater can be divided into a wave attenuating part and a biodiversity enhancing part, where the physical design play a role in both parts. The breakwater body will be inclined to the water surface in order to mimic a beach, with the purpose of making incoming waves shoal and break. The surface will be porous and partially permeable with the purpose of disturbing the flow over the volume as well as creating an aerated turbulence in, and around, the volume. The potential to implement bioenhancing features will be discussed and tested in order to investigate whether the breakwater can act as an artificial floating reef. Experimental studies are conducted on a physical model in a wave flume, where the main parameters of the tests will be surface porosity, inclination and fixations. Tests will be conducted using regular waves distributed over different frequencies and an irregular JONSWAP wave spectrum on a total of 8 porous configurations and one reference case. Wave transmission, wave reflection, body motion, mooring forces and hydraulic mechanisms are investigated. The results present a weak performance in terms of wave transmission for long waves, compared to other floating breakwaters. Body motions due to incident waves are the main limiting factor. Lower inclination leads to a decreased wave transmission due to increased wave breaking. Added porosity for fixations that allows movements, leads to no change in wave transmission, increased wave reflection, decreased mooring forces, decreased body motions, and enhanced aeration in and around the body. For rigid fixations, wave transmission and -reflection is reduced for porous configurations. Further investigations of the design are recommended, and several propositions for design changes and future testing are presented.

Keywords – wave flume, sloping, porous, floating breakwater, aquaculture, biodiversity

Contents

List of Figures

List of Tables

1 Introduction

The coastlines in the world are representing a considerable diversity, and the requirements to Coastal Engineering are highly influenced by this. The Norwegian coastline is mirroring this diversity, and its form, bathymetry, aquaculture and area of use will be parameters in this Master's Thesis. Climatic changes are no longer a projection for the future, but a reality we already experience which we must adjust to. Metrological conditions change and the marine life are facing big challenges, at the same time as industry must adjust to an increased demand of food. The thesis will investigate an alternative design to floating breakwater in sheltered fjords where certain conditions apply, and its design is proposed to enhance biodiversity and aquaculture while the ability to shore- and infrastructure protection is maintained.

1.1 Background

Floating Breakwaters are a type of breakwater which has been established as an alternative to the conventional solid breakwaters. Floating breakwaters are a floating construction fixed to the bottom by the use of poles, chains or other mooring systems. The typical area of use is in the proximity of marinas or marine industry, exposed to primarily wind waves (Jensen et al., 2018). Floating breakwaters are often considered as an alternative to conventional rubble mound breakwater, where such a construction is unfavourable due to i.e., construction cost in deep waters, foundation capability and circulation requirements (Oliver et al., 1994). Floating breakwaters have other advantages such as i.e., possibility for remote off-site construction, maintenance of natural sediment transportation and fish mitigation.

This type of breakwaters are often considered ineffective against long period swell waves, where waves exceeding 4-5 seconds period are usually given as an upper boundary (Oliver et al., 1994). Longer waves would require massive structures or a very innovative design. Incoming waves are in general partially reflected and partially transmitted under the floating breakwater. Some energy is initiating movement of the floating body. Wave dissipation is due to friction, damping, aeration and eddies generation. Floating breakwaters' efficiency is often characterized by the transmission coefficient, T_c, which is

the rate of the incident significant wave height to the transmitted wave height on the lee side of the breakwater. The transmission coefficient is generally dependent on the floating breakwaters' width, wave period and depth.

The world is facing bigger risks due to the climatic changes than previously described (IPCC, 2022). The recent published report is describing how sea level rise and extreme weather conditions will be making a significant increased impact on the world, especially in exposed and low altitude coastal areas. The climatic changes have also caused substantial damages and increasingly irreversible losses in coastal and open marine ecosystem, such as polewards shifting, increased and non-sustainable mortality and loss of kelp-forests. The report is also presenting the opportunity for future adaptions, such as developing ecosystem-based management in aquaculture, adapting human interference to natural processes in order to enhance biodiversity, sustainability and ecosystem services, as well as increase the size of natural areas for biological communities by restoration of degraded areas.

Coastal structures in general, including floating structures, with features that enhance biodiversity is a specific measure that can be categorized in the proposed adaptions from the IPCC report. However, such floating structures represent a challenge, as there are no natural, floating marine-ecological habitats in the ocean (Hadary et al., 2022). Absence of waterline varying tidal effects, shaded environments, overhangs and mooring systems are challenges linked to these such structures that should be discussed. The expression "ecological engineering" is introduced in literature and highlights three main categories of measures; material composition, texture and micro details, and Macro design (Firth et al., 2014).

1.2 Motivation

The evolution of the purpose for coastal development started with the humans building shelter and harbours in order to protect themselves from the nature and to access its resources in order to survive. Decades have passed, and the sheltered waters are reserved to industry and enormous cities. The ocean has changed position from an ally and supplier, to a bank of resources waiting to be exploited for economic profit. Despite its significant amount of fish, oil, waves, wind, etc., all resources are not without limits. As reports

are presented, consequences analysed and conclusion are confirmed again, the facts are unyielding. The next phase of the evolution is revealed; the humans are now the threat to the ocean.

The time to come will be crucial in order to develop solutions that compromise the needs for humans and the needs for the ocean. Every decision must be taken with the nature as a leading partner, and economic benefit must not be allowed to overrule the decisions enhancing sustainability. This thesis will explore a new concept that have a potential to do just that; enhance biodiversity in the marine ecosystem at the same time as it is providing protection to shore line and infrastructure exposed to rough marine conditions.

1.3 Problem Description

Climatic changes challenges humans to be creative in order to discover new technology where the biological and sustainable impact is a leading factor. Focusing on this impact is not equivalent to a weaker performance of the product. On the contrary, it might be an opportunity to let the interaction between human technology and nature improve the results.

Senior Researcher Dominique Mouaze at the Université de Caen (UniCaen), Normandie introduced his idea for a new breakwater during a meeting between the Norwegian University of Science and Technology (NTNU) and UniCaen. The motivation behind the idea was to investigate the potential for a new design of a floating breakwater that embraces the capacity to wave dissipation at the same time it is equipped with biodiversity enhancing features. This idea was the basis for the developed design concept investigated in this study.

The concept of the breakwater can be divided into a wave attenuating part and a biodiversity enhancing part, where the physical design play a role in both parts. The main idea of the design is taking advantage of an inclined beach in order to provoke wave breaking and energy dissipation, thus reducing the energy absorbed by the breakwater itself. By adding porous plates to the breakwater surface, it is intended to lead the water that is hitting the breakwater into the internal chambers. This process is believed to disturb the water flow by provoking more aeration, turbulence and friction forces, thus reducing the wave energy, and moreover the wave transmission. This process is

also believed to decrease the mooring- and anchoring forces, thus increasing the load on the system, which gives a positive engineering effect. The movement, current flow and aeration, in and around the breakwater body, is intended to be optimized for marine growth for different species. The design is also developed to be protecting itself, and its ecosystem, by letting waves break over the structure and force a submersion of the structure in extreme weather conditions. This is due to the two main objectives of the breakwater, which is enhancing marine biodiversity and to improve the working service conditions for the infrastructure it will protect. Intended area of use are in connection to fish farms and near-shore infrastructure, where the industry could be decreasing the living conditions for marine ecological diversity.

The performance will be evaluated based on physical parameters, counting wave response, free body movements and flow mechanisms inside and around the model. The biological performance will be discussed based on these observations.

1.4 Research Objectives and Questions

The aim of this study is to develop a new design of a floating breakwater, while enhancing biodiversity and aquaculture. There will be conducted a literature review in order to explore existing solutions that are similar or relevant to use in the design. The literature review will also have the purpose of exploring solutions within aquaculture and biodiversity for floating marine structures. Experimental studies will be conducted to assess the performance of the presented breakwater design. Through the discussions, performance will be evaluated and this will make the foundation for recommendations for future use and development of the proposed breakwater design.

The thesis will aim to make a solid foundation for answers to the following research questions:

- How will the proposed design, and its different configurations and inclinations, affect the main parameters of the study; wave transmission, -reflection and -breaking?
- What effect will different configurations and inclinations for the design have in terms of body motions and mooring forces.
- How will different configurations, inclination and design alterations affect the

hydraulic mechanisms, and can these mechanisms have a bioenhancing effect?

1.5 Research Methodology

The Research Methodology for this Thesis is consisting of four parts, as illustrated in Figure 1.1. As the concept described in this study is different from previous studies, it is expected that evaluations will be exhibited at each step. These evaluations might reveal the need of alterations in the previous steps. Hence, moving to a previous step might be necessary to reevaluate and alter design and methods.

The first part is a presentation of existing studies relevant to the problem. The literature study is executed with the intention to form a theoretical basis for the following:

1. Comprehensive background knowledge for the reader to get acquainted to State-Of-The-Art.
2. Obtain the methodical and theoretical basis for the physical model testing.

The second part is the process of developing and constructing a physical model for the experiments. Different designs are discussed and evaluated, and the final result is used in the next phases.

The third part is the execution of physical testing and data acquisition. Evaluation of the methods from step one and the model from step two will be important in this part, and changes are expected.

The fourth part will consist of analysing and interpretation of the data obtained from the physical tests, in order to get the answers of the research questions.

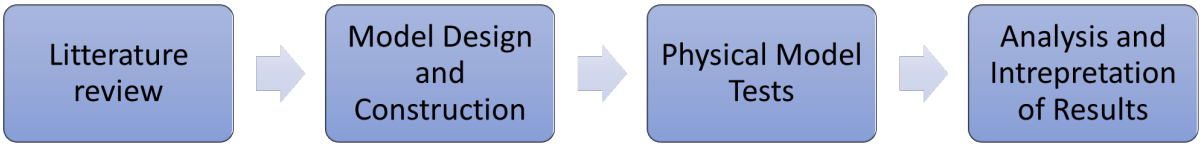

Figure 1.1: Flowchart of Research Approach.

1.6 Structure of the Report

Chapter 1: Introduction, scope of the thesis and overview.

Chapter 2: Presentation of state-of-the-art and background for floating breakwater, floating marine structures, aquaculture and Norwegian conditions.

Chapter 3: Introduction to parameters for physical modelling.

Chapter 4: Description of the experiments and the experimental set-up.

Chapter 5: Presentation of results and discussions regarding the performance and potential for the breakwater design.

Chapter 6: Conclusions and recommendations for future work.

1.7 Readership

This thesis is a Master Thesis within coastal engineering and physical modelling, concluding a five-year university education in Civil Engineering with marine construction and constructional analysis as specialization. The thesis is recommended for readers with a university-level knowledge about floating coastal structures, ocean wave theory and physical laboratory work. Practical understanding of concrete structures and basic marine ecological knowledge are recommended. Usage of this thesis is recommended for further research within the topic.

2 State-of-the-art

2.1 Floating Breakwaters

Breakwaters are a very common coastal engineering structure, with the main purpose of protecting coastal infrastructure, ships and coastlines against incoming waves. Growing activity within offshore and maritime industry have led to the growing need for larger ports with deeper fairway depth. Conventional bottom-founded breakwaters are the traditional way to construct breakwaters. However, they represent a major cost as the material demand increases with increasing depth. Consequently, floating breakwaters have been an appealing alternative. The concept has been subjected to a significant increase of interest through the last decades, illustrated in published papers about the subject, see Figure 2.1. Positive properties in terms of construction and characteristics are often given to the low effect on seabed conditions and water depth, a low profile which is minimizing the visual impact and adaptation for natural water circulation underneath the construction (Oliver et al., 1994). However, they are often criticized for their low effect against long waves and a mooring system that are prone to damage during severe environmental conditions.

This section will review existing floating breakwater solution that exploit porosity, inclinations, plate design and other relevant designs for the model of interest in this thesis.

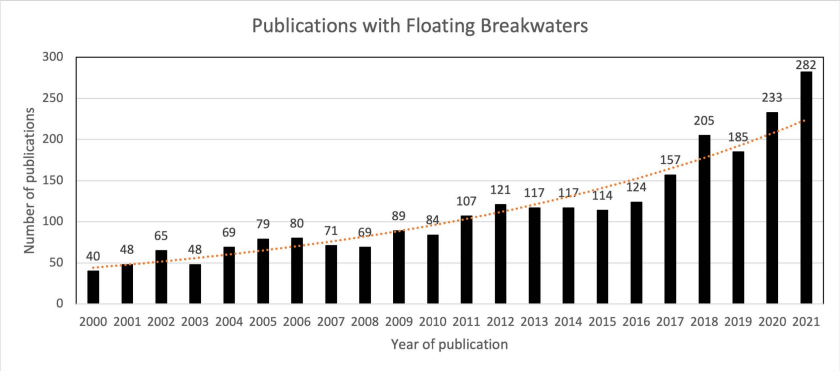

Figure 2.1: Trend in number of publications containing the keyword "floating breakwater" on Google Scholar (Google, 2021).

Studies of porous, or perforated, breakwaters, both fixed and floating, have been conducted since the 1960s. Consistent results from representative studies show some trends.

Jarlan (1961) was one of the first to discuss a caisson breakwater with perforated wall, a design that today bears his name. The basis design of a Jarlan-type breakwater consists of a perforated front wall and a vertical impermeable back-wall. Advantages of the slotted/perforated coastal structures are the saving in construction cost in relatively deep water and less disturbance to coastal water environments. While numerous designs of the design exists today, certain general characteristics apply. Huang et al. (2011) gives an extensive review of the transmission- and reflection coefficient for the design, describing how the relations between wavelength, geometrical factors controlling porosity and width of the wave chamber between the two walls are the most important contribution to the wave reflection. Depending on the specific design, different reflection trends can be observed, where the similarities are big variations of the reflected wave. Variations of the reflection coefficient for a fully perforated Jarlan-type structure plotted according to B/L, the width of the wave chamber and wavelength, is shown in Figure 2.2, showing one of the reflection trends presented in the review article.

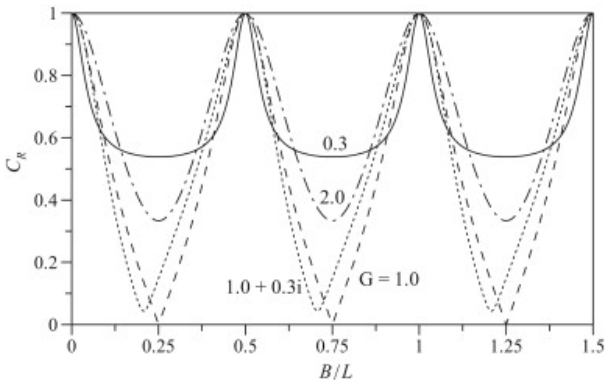

Figure 2.2: Variations of the reflection coefficient for a fully perforated Jarlan-type structure versus B/L (Huang et al., 2011).

Design and performance of floating breakwaters are dependent on different factors, where a selection of studies are investigating the effect of porous solutions. Wang and Sun (2010) designed a porous floating breakwater with a large number of diamond-shaped blocks (see Figure 2.3a) to reduce transmitted wave height and the mooring force. The experimental study revealed favourable performance, presenting results of its capacity to reduce incident wave height and decrease mooring forces by dissipating more energy than reflecting it. Another design of a porous floating breakwater, studied by Shih (2012), presented a porous perpendicular pipe breakwater (see Figure 2.3b) where the performance were found to be

highly influenced by the wave height for short incident waves, and that larger pipe length effectively reduced the reflection coefficient. Ji et al. (2019) presented results from an experimental study of a single-row and double-row rectangular floating breakwater with porous plates (see Figure 2.3c) where the design effectively attenuated incident waves with slight motion responses and small mooring forces. Christensen et al. (2018) analysed three basic cross-sections of floating breakwaters in an experimental and numeric study: a regular pontoon, a regular pontoon with wing plates attached, and a regular pontoon with wing plates and porous media attached to the sides. The study showed results that the cross-sections with wing plates and porous media attached to the sides reduced the reflection and the transmission most effectively.

(a) Model from an experimental study of a porous floating breakwater (Wang and Sun, 2010).

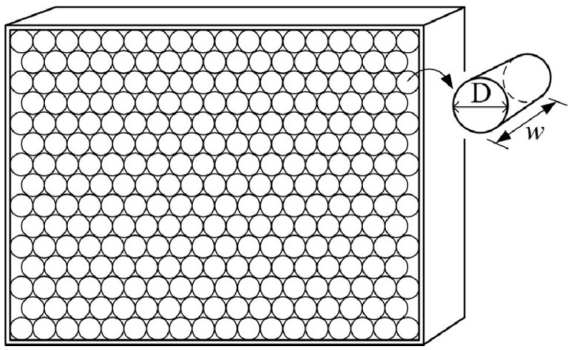

(b) Illustration of porous box element with perpendicular pipes, from an experimental breakwater study(Shih, 2012).

(c) Rectangular floating breakwaters with porous plates (Ji et al., 2019).

Figure 2.3: Examples of porous floating breakwaters found in literature.

Sloping floating breakwaters is a less studied subject, and few relevant studies are found matching the search criteria. One experimental study is investigating the effect of an

inclined breakwater sloping *against* the wave direction, with the purpose of using the angled mass to dissipate the wave force (Bayram, 2000). It was reported that the inclination of the float is a crucial factor controlling the transmission coefficient, which was found to decrease with the increase in wave period and mooring length, where a bottom-fixed installation performed more poor than one with a bottom clearance. A joint numerical and physical study investigated a sloping, floating breakwater that had a gap between two floaters (Sohrabi et al., 2021), see Figure 2.4. The study compares the results to a conventional vertical faced breakwater. The design is proposed in order to minimize the effect of overtopping due to the sloping face of the construction. The design is shown in Figure 2.4. Two anchoring systems were tested, a one-degree of freedom pole system and a 3-degree of freedom mooring line system. The system was also tested with a chain net added to the model to test the effect on transmission coefficient. The results of the experiments show a sloping floating breakwater that has a 15% better performance than a rectangular bow type in terms of a decreased transmission coefficient. Pole-fixed is the best anchoring system and the model with a chain net exhibits a better performance compared to the model without it, both in terms of decreased transmission coefficient and increased dissipation coefficient. The study does not comment the difference in the reflection coefficient from a sloping and a vertical breakwater face. Experimental studies of stepped-slope floating breakwaters have showed that wave attenuating can have up to 80% efficiency for the model under shallow water conditions while having an effective reflection structure (Teh and Ismail, 2013). Koftis and Prinos (2005) compared a trapezoidal design with a box-type barrier, showing that the trapezoidal structure triggered more complex wave-structure hydrodynamics, including vorticity development at the edges of the structure, with the associated turbulence, wave run-up and run-down on the sloping face of the structure.

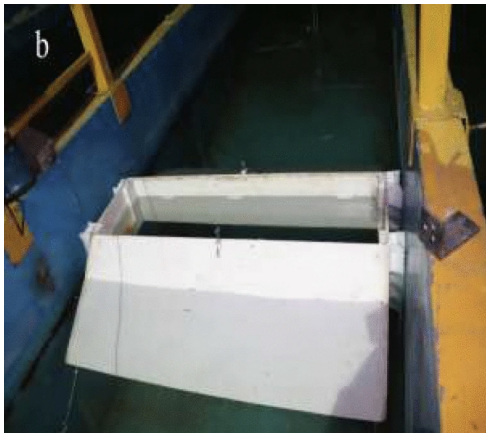

Figure 2.4: Sloping breakwater with centred gap to attenuate forces due to overtopping (Sohrabi et al., 2021).

Elastic and porous plate breakwaters has been subject to studies. An analytic model for oblique wave scattering on floating and submerged porous elastic plates of different structural parameters produced observations of a significant amount of dissipated wave energy due to the presence of the plates, thus resulting in less wave reflection and transmission (Behera and Ng, 2017). Illustrated in Figure 2.5a. Correlating results are presented in the analytic testing of a porous circular plate where results showed that wave-energy dissipation due to porosity initially increases as the plate becomes more porous, but reaches a maximum and then slowly decreases as the porosity increases further (Meylan et al., 2017). Testing of fixed plates are conducted with both horizontal and inclined configurations. Testing of a fixed horizontal porous plate, with both analytical and physical experiments, indicated an ideal porosity at 10% after testing with different wave conditions (Cho and Kim, 2013). Results from analytical testing of an inclined submerged plate fixed on top and moored at bottom showed results indicating that as the plate moves from vertical to horizontal position, reflection coefficient decreases, transmission coefficient increases and hydrodynamic forces decrease (Kundu et al., 2018). Physical tests on a rigid fixed plate with inclination from 0 to 180 degrees, see Figure 2.5b displayed results that the inclination of 60 degrees was found to be most efficient for the whole range of the wave parameters considered (Rao et al., 2009).

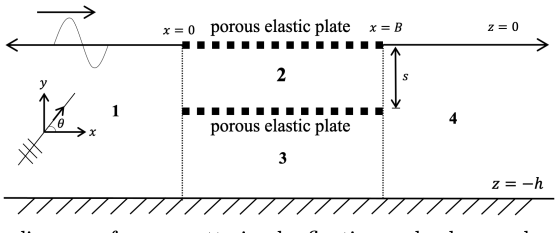

(a) System of floating and submerged porous elastic plates (Behera and Ng, 2017).

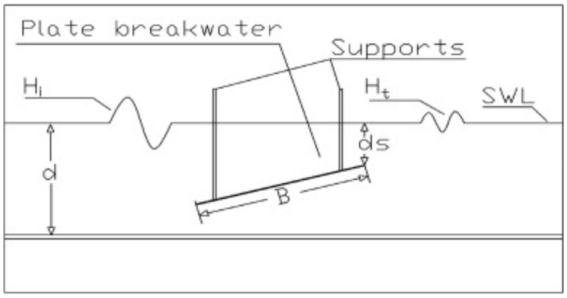

(b) Physical studies conducted on a submerged inclined plate breakwater (Rao et al., 2009).

Figure 2.5: Examples of plate breakwaters found in litterature.

2.2 Aquaculture and Biodiversity for Floating Structures

2.2.1 Floating structures and artificial habitats

The construction of floating infrastructure leads to a colonization of marine life in an ecosystem that has no real comparison in the natural world, and there is a constant increase of floating structures throughout the coastlines of the world (Hadary et al., 2022). Floating structures can be defined by everything from buoys to floating cities prospected for the future. In Norway, nearshore floating structures are often floating marinas, while offshore structures are represented by mainly oil rigs on the Norwegian shelf and fish farms in protected waters inside the fjords. Floating structures are prone to considerations that must be taken on a different basis than conventional non-floating structures. A recent study has presented challenges and design factors that influence the colonization by marine life on floating structures. The study enlightens the necessity for bridging knowledge and technology gaps, most of them related to the ability to develop robust structures in rough marine environments. The following challenges and proposals for solutions are presented:

- **Structural Performance and Longevity:** Most floating structures are made of steel and/or concrete. Structural considerations must de done to assure a good performance and a long lifespan. However, both steel and concrete have known disadvantages in marine environments. The growth of marine organisms that produce Calcium Chloride can create a biofilm on the surface that reduce the

Chloride penetration and abrasion on concrete. Presence of molluscs on the steel surface can inhibit corrosion, and biofouling can in some cases be more protective than anticorrosive paint.

- **Dynamic movement:** Wind, waves and currents should be carefully studied in the design phase as they will affect the movements of the construction. The mooring system must keep the structure in place, but must allow displacements in order to allow dampening effect and minimize peak loads on the system. Fatigue analysis must be conducted on the whole system. Furthermore, mooring lines are recommended to avoid contact to the seabed in order to minimize ecological impact.
- **Drag and load:** The addition of marine growth to the structure implies the gain of extra weight and can increase the drag forces around the structure. However, some marine growth might reduce the drag forces. Studies of flow around piles indicated that growth of oysters will disrupt the viscous flow of currents, and instead produce turbulent eddies.
- **Maintenance:** Bioprotection of the structure can reduce the maintenance cost thanks to increased lifespan. However, intense growth might disrupt visual surveys of the infrastructures' state. Inspection can in such cases be conducted by scraping off sections of the growth from the surface, within certain limits such that reproduction of growth is still possible.

Hadary et al. (2022) do also elaborate how nature inclusive designs are an important part of eco-engineering. Three pillars are presented that influence the marine life that will adhere to the structure, and subsequently, influence the local biodiversity and productivity.

- **Material composition:** Portland cement-based concrete is a widely used material for marine constructions. This is known as a poor substrate in terms of biological requirement, due to high surface alkalinity and leaching of compounds that are toxic to marine life. Thus, the ability for concrete based floating structures to provide ecosystem services similar to those offered by natural habitats is severely compromised. There has been developed an environmental sensitive alternative, a Bio-enhancing concrete admixtures tailored to double biodiversity and species richness compared to standard Portland cement based concrete elements.

- **Texture:** The traditional smooth surface of concrete constructions does not provide suitable conditions for the development of diverse biological assemblages. As a result, these are often dominated by nuisance and invasive species, and do not function as surrogates to natural reef environments. Eco engineered surfaces that have high surface rugosity, helps marine larvae adhere and attach to the concrete surface, by creating micro turbulence, thus breaking the laminar flow across the element and facilitating settlement processes.

- **Macro-Design:** Non-enhanced marine constructions are highly homogenous and offer limited shelter, leading to low diversity assemblages. Examples of eco-engineering can include different designed habitats, and shelter, that can be tailored to specific species. Biological environments related to marine constructions are often subjected to unnatural overhangs and shaded habitats. These conditions are often dominated by invasive species that typically thrive in such conditions. Adding elements like moon pools, 3D complexity and light penetrating features can diminish the shading effect and improve habitat conditions. The mooring system can also be adjusted to more eco-friendly designs by implementing growth enhancing materials to the mooring line for surface growth and design anchors with habitats and shelters for species living on the sea bed.

A comparative study of the difference between submerged artificial habitats on given depths revealed differences between pole fixed and free floating configurations in reefal conditions in the Red Sea (Perkol-Finkel et al., 2006). Such habitats, when able to move, offer unique environmental conditions, mainly in terms of hydrodynamic aspects. The study tested whether floating habitats would develop unique communities compared to the identical fixed ones, due to different flow regime. Significant differences in hydrodynamic features were found, where floating installations had greater flow velocities and shear stress on their surfaces compared to fixed ones, encouraging massive settlement of benthic macroinvertebrates while fixed habitats had less biomass and more coral settlements, especially close to the seabed.

Artificial reefs have some appearances along the Norwegian coast, but most of them are in deep waters, incomparable to the floating design. However, there is an area of relevance. Tjuvholmen is an area in Oslo, located in Bjørvika, in the inner Oslofjord, subjected to a

comprehensive recent urban renewal. The Oslofjord in general, and Bjørvika specially, has experienced a critical decline in biodiversity and marine fauna due to years of ship industry, urban emission and traffic in the area (Rinde et al., 2019). In an attempt to remedy, 100 artificial reefs were deployed at the sea bottom as well as 1000 mussel ropes under the pier. Mussel ropes, also called *fuzzy ropes*, have proven to be a success, as they have a significant amount of growth. Mussels are considered a *"super-filter"*, which means it can filter polluted water. Scientists from the Norwegian Institute for Water Research (NIVA) estimate the mussels in Bjørvika to cleanse up to $6000m^3$ water per hour. Colonies of oysters have also been facilitated in parts of the Oslofjord, using oyster cages.

2.2.2 Aquaculture in Norway

The industry of aquaculture in Norway is primarily production of salmon, and other fish species used to support the industry, in fish farms (Misund, 2021). The traditional, and most applied, technology for fish farm are open cages located in sheltered or exposed water. In open cages, fish are separated from the free water using nets. The facilities are exposed to natural currents and waves, which results in a life close to the nature for the fish, but also exposes the nature to nutrition waste, bacteria and salmon louse, and the facilities to occasional rough environmental conditions where human operations are exposed to risks.

The Norwegian salmon industry is in a great scale using lumpsuckers as a remedy against salmon louse (Stranden, 2021). The cleaning fish is eating salmon louse as a "snack", and is therefore contributing to prevent massive blooms of the parasite. This has contributed to an increase in the amount of lumpsuckers being farmed or caught in their natural habitats along the shore, whereafter they are put into farms. These fishes are primarily juvenile, and they do not have their natural habitat in deep sea where they do not have access to low depth kelp, low current conditions and hiding spots. This is an important condition for the species that are using a big amount of energy while swimming in free water. It is estimated that 40% of the lumpsuckers die after being deployed in fish farms, while unknown amounts disappear without a clear reason.

The industry of offshore floating aquaculture is projected to several challenges. Dissolved oxygen in culture water is considered one of the dominating limiting factors in aquaculture

(Grundvig et al. (2014). The oxygen demand in aquaculture systems increases with rising temperatures, caused by two well known factors. The solubility of dissolved oxygen is reduced with increasing temperatures, making less oxygen available for fish, shrimps etc. In addition, the oxygen consumption rate of different stock increase concurrently with the temperature. As a consequence, rising temperatures are a limiting factor in the productivity of both aquaculture farms and natural marine ecosystems. Two remedies for low values are available. Injection of pure oxygen, oxygenation, is a high cost and energy demanding solution. Aeration is the other alternative, which is forcing air into the water using i.e. electrical powered pressured air tubes or mechanical paddle wheels.

2.3 Norwegian conditons

2.3.1 Climate and climatic changes

Norway is characterized with large climatic variations. The mainland has a mild climate in the lowland, while Arctic climate is found in the mountains, along the coast of the county Finmark and on the island Svalbard. A mild and humid climate describes the rest of the coast, where also the winters are mild. The climate in Norway, and at the coast specifically, is milder than comparable areas in the same latitude due to the heat transfer from warmer climates, orchestrated by the Gulf Stream and global wind systems.

As the world is facing climatic changes, Norway is no exception. The Norwegian coastal zone climate has experienced, and will experience changes due to the global climatic trends (Hanssen-Bauer et al., 2015). Registrations with available instrumental tools throughout the past decades describe the trends to

- changes in temperature, currents and salinity in the North-, Norwegian-, North-Atlantic and Barents Sea,
- decreasing thickness and withdrawing edge of the Arctic sea ice,
- increased intensity and level of precipitation,
- and local increasing sea level.

The future changes in the coastal climate correlate with observations from the past, but are projected to increase more rapid. The expected changes are based on the climatic

situation the world is experiencing today, with a continuation of emissions of greenhouse gasses. The climatic changes expected in Norway in 2100 are presented below, where relevant points are highlighted.

- **an average national temperature rise of 4.5°C,**
- 18% increase in annual precipitation,
- more frequent torrential rainfall,
- rain floods will be bigger, with higher frequency,
- snow melting floods will be smaller, with lower frequency,
- snow will be absent in the lowlands for several years and the highlands will experience higher snow levels,
- fewer and smaller glaciers,
- **stronger and more often storms,**
- **and sea level will increase between 15 and 55 cm.**

2.3.2 Bathymetry, coastal zones and effect on wave conditions

The Norwegian coastline is among the longest in the world. The diversity of bathymetry, wave conditions and climate require a divided description of different characteristics.

The Norwegian continental shelf is a plateau located in the eastern part of the Norwegian Sea, with the southern part in the North Sea and the northern part in the Barents Sea. The shelf is of a varying shape with numerous trenches and irregular peaks, making the depth vary between 200 and 500 meters along the 40-200 kilometres wide area. The Norwegian Sea is experiencing the most extreme wave conditions in Norwegian waters, and hence the outermost western coast of Norway is exposed to strong deep water swell, some of them propagated from the North Atlantic Ocean. Wave conditions are described with a significant maximum wave height of $H_s < 12m$, maximum wave height, $H_{max} < 16m$ with a duration up to 3h (Christakos et al., 2020). Long term wave statistics are of good value for the area, and accuracy of wave models have shown good quality.

The description of the Norwegian coast gets more complex inside the outermost parts of

the coast and inside the fjords. The behaviour of waves, winds and currents are influenced by islands, shallow water, tides, tidal currents and complex orography and bathymetry (Christakos et al., 2021). These areas are generally exposed to wind waves with lower significant wave height and shorter periods. Wave statistics, simulations and studies must be done individually to retrieve specific data for sites in interest. Fetch length, width of the fjord and natural sheltering are important factors. The fjords have characteristics in the bathymetry and topography that are different from most coastlines in the world, with a deep and narrow body of water. Fjords can be a couple of hundred meters wide, and a thousand meters deep. The bathymetry makes traditional computational wave modelling challenging, as most programmes are made for a more uniform bottom topography with monotone changes. The Norwegian coastline is as a result subject to many studies regarding numerical wave modelling, but field measurements are still very important to identify the local conditions.

3 Aspects of Physical Modelling

3.1 Wave characteristics

The physical testing will be subject to varying wave conditions. The sea state that is the basis for the laboratory tests is wind waves. Characteristics of wind waves are typically steep waves with short wave period. Wave conditions are described principally by (CIRIA/CUR/CETMEF, 2007):

- the incident wave height, H_i(m), usually given as the significant wave height, H_s(m)
- the wave period given as either the mean period, T_m(s), the mean energy period, $T_{m-1,0}$ (s), or the peak period, T_p(s)
- the angle of wave attack, β (°)
- the local water depth, h (m)
- the wave length L (m)

The relation between wavelength, L, wave period, T, and water depth, h, is called the dispersion relation, and is described by

$$L = \frac{g}{2\pi} T^2 \tanh\left(2\pi \frac{h}{L}\right) \tag{3.1}$$

where g is the acceleration of gravity.

The influence of the wave period is often described using the fictitious wave steepness, s_0,

$$s_0 = H/L_0 = \frac{2\pi}{g} \frac{H}{T^2} \tag{3.2}$$

which is based on the local wave height, H, and the theoretical deep-water wavelength, L_0, or wave period, T.

An important parameter for describing wave action on a slope is the surf similarity or breaker parameter, ξ, also known as the Irribarren number. The Irribarren number is

described by

$$\xi = \tan\alpha / \sqrt{s_o}, \tag{3.3}$$

where α is the angle of the structure slope facing the waves. The Irribarren number has often been used as a device to describe the form of breaking waves on a beach or towards a structure. Different breaker types as a function of the Irribarren number are displayed in Figure 3.1.

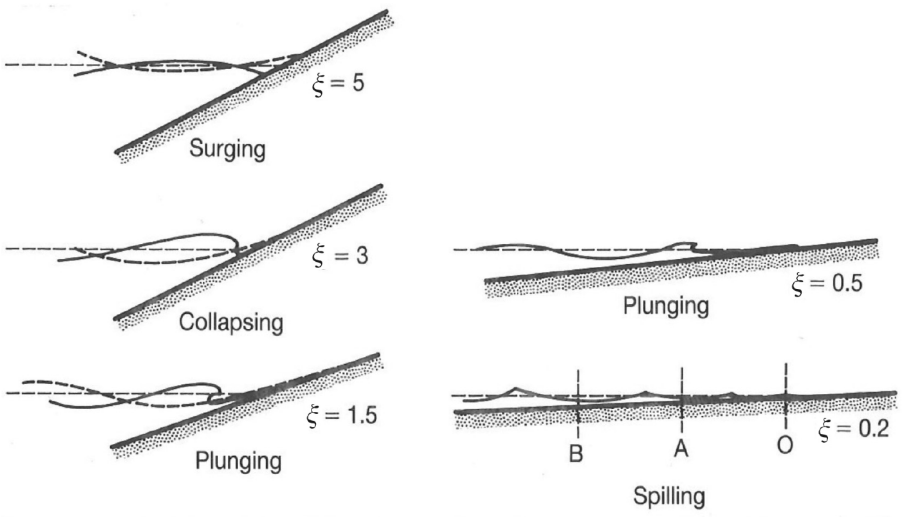

Figure 3.1: Breaker types as a function of the surf similarity parameter or Irribarren number, ξ (Battjes, 1974).

Mean wave energy density can be described based on linear wave theory, and consists of two contribution (CIRIA/CUR/CETMEF, 2007). The mean potential energy density of surface gravity waves can be described by

$$\begin{aligned} E_{\text{pot}} &= \overline{\int_{-h}^{\eta} \rho g z \, \mathrm{d}z} - \int_{-h}^{0} \rho g z \, \mathrm{d}z \\ &= \overline{\frac{1}{2}\rho g \eta^2} = \frac{1}{4}\rho g a^2 \end{aligned}$$

where ρ is the water density, g is the gravitational acceleration, η the free surface elevation, h the mean water depth and a the wave amplitude. The overbar denotes the mean value, taken as a time- or space average.

The mean kinetic energy over the wave motion is found to be

$$E_{\text{kin}} = \frac{1}{4}\rho \frac{\sigma^2}{k \tanh kh} a^2$$

which, by using the dispersion relation, results in

$E_{\text{kin}} = \frac{1}{4}\rho g a^2$

where σ is intrinsic frequency and k the angular wave number.

Hence, the mean energy density is dependent on the wave amplitude and can be described by

$E = E_{\text{pot}} + E_{\text{kin}} = \frac{1}{2}\rho g a^2.$

Breaking characteristics are an important reference when describing the wave energy dissipation. The main contribution to wave dissipation, where magnitude is dependent on breaker types, can be distinguished into the energy content in surrounding air, surface tension effects, viscous dissipation in water and the friction work done against the propagation of the pressure field (Iafrati, 2011). It is shown that the rate of dissipation for surging waves are lower, hence the relative time of the breaking process will be longer and the pressure field that occurs under the wave will be distributed along a bigger part of the beach. Breaking waves will have a relative quicker dissipation from the moment the breaking is initialized. The pressure to the bottom will be significantly higher, but distributed over a shorter time and smaller area. Breaking wave mechanisms have a higher transfer of energy to surrounding air and viscous effects, thus the total ground pressure will be lower than for surging waves.

3.2 Hydraulic Performance

Ocean waves can be described by linear wave theory.

The performance of the breakwater will be depending on the hydraulic interactions related to the incoming waves and governing parameters. Descriptions are obtained from the Rockmanual (2007).

- **Wave run-up / run-down:** Wave action on the slope of the breakwater will cause the water surface to oscillate over a vertical range that is generally greater than the incident wave height. The extreme levels reached for each wave is known as run-up, R_u, and run-down, R_d. These are defined vertically relative to the still water level and expressed in meters, m. The run-up level shall be used in the design of the breakwater to determine the height and slope angle. In the case of a run-up higher than the height of the breakwater, overtopping will occur as described below. Wave

run-down will be used to decide the depth of the breakwater. If the run-down is not low enough, waves will go underneath the breakwater and lifting- and/or slamming forces will occur. Run-up and run-down can be measured in the lab by using video analysis, measuring the wet area on the surface of the slope after testing (only applicable for run-up), or visual observation if accurate quantification is unnecessary. Wave run-up/run-down is affected by rugosity, described by the following equation (CIRIA/CUR/CETMEF, 2007),

$$R_{u2\%}/H_{m0} = A\gamma_b\gamma_f\gamma_\beta\xi_{m-1,0}$$

where $R_{u2\%}$ is the 2 per-cent run up level, H_{m0} is the spectral significant wave height (H_s can be used for regular wave conditions), A is a fitting coefficient, γ is correction factors where γ_f is a friction coefficient ($0 \leq \gamma_f \leq 1$) varying for rugosity, and $\xi_{m-1,0}$ is a wave breaking parameter.

- **Wave overtopping:** If the wave run-up is higher than the breakwater, wave overtopping will occur. This may occur for a few or for several waves. The magnitude of overtopping can be quantified in experiments, but can also just be visually considered and registered in test logs in order to detect rough correlation between different test results.

- **Wave Transmission:** The wave transmission is a measure of how much of the wave energy that is transmitted through the breakwater. Wave transmission through the breakwater may happen due to wave overtopping, energy transmission below the breakwater, water flow through the breakwater and heave, roll and sway movements by the breakwater. The transmission performance is described by the coefficient of transmission, C_t, defined as the ratio of the transmitted to incident wave heights H_t and H_i respectively, given by the equation

$$C_t = H_t/H_i, \tag{3.4}$$

where H_t and H_i is measured according to methods described in Chapter 4.1.1.1.

- **Wave Reflection:** Wave reflections are of importance on the open coast, at harbour entrances and inside harbours. The interaction of incident and reflected waves often leads to a confused sea state in front of the breakwater, with occasional steep

and unstable waves. This can complicate ship manoeuvring, cause unintentional ship movements inside harbours and may affect previously sheltered areas. Wave reflection is described by a reflection coefficient, C_r, defined in terms of the ratio of the reflected to incident wave heights, H_i and H_r, respectively, and are defined by the equation

$$C_r = H_r/H_i. \tag{3.5}$$

3.3 Model scaling

In an ideal situation, transformation from a full scale-model to a scaled model applicable for lab testing will make a system that act in full similarity. Similarity will generally include the similitude in acceleration, velocity, mass transport and fluid forces, and the state of similitude is achieved when all the major factors related to fluid action are in proportion between the model and the prototype (Hughes, 1993). The definition of scales is defined as the proportions of measurable characteristics between model and prototype, whereas the scale ratio is given by the prototype value and the model value of a given parameter. The scaling is determined by the Scaling Criteria, or the Criteria of similitude. These criteria must meet mathematical conditions which represent physical properties. Similitude criteria can be divided into three categories:

- **Geometric similitude:** Similitude is dependent only of the linear geometrical relationship between the prototype and the model, with conserved angles. If the criteria is met, by having the same geometric scale in both horizontal and vertical direction, the model is *undistorted*. If the criteria is not met, then the model is *distorted*. The following equation represents the similarity in length,

$$L_r = \frac{L_m}{L_p}, \tag{3.6}$$

  where L_r represents length scale factor, L_m the model dimension and L_p the prototype dimension.

- **Kinematic similitude:** A similitude that require the ratio of the velocities and accelerations must be kept constant. The ratio can be defined by

$$U_r = \frac{u_m}{u_p} = \frac{v_m}{v_p} = \frac{w_m}{w_p} \tag{3.7}$$

and

$$\dot{U}_r = \frac{\dot{u}_m}{\dot{u}_p} = \frac{\dot{v}_m}{\dot{v}_p} = \frac{\dot{w}_m}{\dot{w}_p} \tag{3.8}$$

for velocity and acceleration, where u, v and w are the velocities in x,y and z directions respectively.

- **Dynamic similitude:** The criterion requires that all types of forces are scaled by the same ratio. Newton's second law of motion is the basis for the derivation of the scaling criterion. It is important that both magnitude and direction of forces are represented correctly in model and prototype. The dynamic similitude criterion is fulfilled by distinguishing the dominating forces.

In order to satisfy the criteria for dynamic similitude, theories for the different incident forces must be satisfied. The relevant forces for wave models include gravity, inertia, friction and surface tension, hence to have dynamic similarity, Froude number (F_r), Reynolds number (R_e) and Weber number (W_e) must be similar for model and prototype. These numbers are defined by

$$F_r = \sqrt{\frac{\text{InertialForce}}{\text{GravitationalForce}}} = \sqrt{\frac{\rho L^2 V^2}{\rho L^3 g}} = \frac{V}{\sqrt{gL}}, \tag{3.9}$$

$$R_e = \frac{\text{InertialForce}}{Viscous\ \text{Force}} = \frac{\rho L^2 V^2}{\mu V L} = \frac{\rho L V}{\mu} \tag{3.10}$$

and

$$W_e = \frac{\text{InertialForce}}{\text{SurfaceTensionForce}} = \frac{\rho L^2 V^2}{\sigma L} = \frac{\rho V^2 L}{\sigma} \tag{3.11}$$

where

$V =$ Velocity of flow

$L =$ Length

$g =$ Gravitational Acceleration

$\rho =$ Fluid Density

$\mu =$ Kinematic Viscosity of Fluid

$\sigma =$ Surface Tension

Satisfying similarity for all parameters is not possible when testing is conducted on a prototype and a scaled model, due to limitations of changing the fluid in a way that is proportional to the scaled values. As gravity and inertia are dominant parameters in a wave field model, Froude modelling is generally applied. The Reynolds number is important when viscous forces dominate, such as laminar boundary layer problems in open-channels of free-surface flows. Surface tension is not dominant in wave action, therefore Weber number can be neglected as testing is not conducted in very small scales. Model testing in this thesis will be based on Froude scaling. Flow conditions must be observed and kept in a non-laminar state to keep viscosity negligible, with a Reynolds number above 10^4.

The Froude number, F_r, should be the same in both model and prototype to satisfy Froude scaling, thus the condition is given by

$$\left(\frac{V}{\sqrt{gL}}\right)_p = \left(\frac{V}{\sqrt{gL}}\right)_m$$

This results in:

$$\frac{V_p}{V_m} = \sqrt{\left(\frac{g_p}{g_m}\right)\left(\frac{L_p}{L_m}\right)}$$

which can be rearranged in terms of scale ratios (L) as;

$$\frac{U_v}{\sqrt{N_g L_r}} = 1 \quad \text{or} \quad N_{Fr} = 1$$

Relations for scaling based on Froude law can be expressed in terms of length scale factor

L_r. Table 3.1 show similitude ratios for Froude scaling in terms of L_r.

Table 3.1: Scaling factor based on the Froude criterion.

Froude Scaling factors		
Parameter	**Dimension**	**Scaling factor**
Length	L	L_r
Area	L^2	L_r^2
Volume	HL^3	L_r^3
Time	T	$L_r^{1/2}$
Speed	LT^{-1}	$L_r^{1/2}$
Acceleration	CLT^{-2}	1
Mass	M	L_r^3
Force	MLT^{-2}	L_r^3
Pressure	$ML^{-1}T^{-2}$	L_r
Energy/work	ML^2T^{-2}	WL_r^4
Power	ML^2T^{-3}	$L_r^{7/2}$

3.4 Hydraulic conditions

3.4.1 Reference location

A report from a consulting firm in Norway is the basis for the wave conditions that will be tested in this study (Norconsult, 2017). The report was an order from an undisclosed developer of floating breakwaters in Norway, and it studied the efficiency of an existing floating breakwater protecting a marina in Midtfjorden, Norway. The floating breakwater is a 5-meter wide and 3.5-meter high concrete structure with hollow core. The location is exposed to conditions typical for closed fjords, where the waves are highly dependent on the wind conditions in the area, as indicated in Figure 3.2. The position of the existing floating breakwater and the dominant fetch- and wave direction are shown in Figure 3.3a. Wave data were retrieved using two wave gauges located on the outside, and inside, of the floating breakwater, as shown in Figure 3.3b. The collected data consists of statistical wave parameters considering wave height, wave period and wave direction. Wind data is retrieved from 10 meter altitude on the nearby airport. Position of airport and reference location is shown in Figure 3.2. The report is only presenting measured data, not statistical return period for the area.

As illustrated in Figure 3.2, multiple peaks are recorded in the time domain of the tests,

with one specified peak which will be used as a reference for this current study. Retrieved wave conditions for the selected peak are displayed in Table 3.2. Based on the recordings, an estimate for the breakwater efficiency can be given by the transmission coefficient. Consequently, the transmission coefficient for significant wave height, H_s, and maximum wave height, H_{max}, are given by

$$C_{r,H_s} = \frac{H_{s,inner}}{H_{s,outer}} = 0.17 \tag{3.12}$$

and

$$C_{r,H_{max}} = \frac{H_{max,inner}}{H_{max,outer}} = 0.16. \tag{3.13}$$

Table 3.2: Wave conditions recorded by inner and outer wave gauge at reference location

	Outer gauge	Inner gauge
H_s	1.5 m	0.25 m
H_{max}	2.5 m	0.4 m
T_p	5.0 s	5.0 s
T_m	3.8 s	2.9 s
s_{0,H_s}	0.038	0.006
$s_{0,H_{max}}$	0.064	0.010

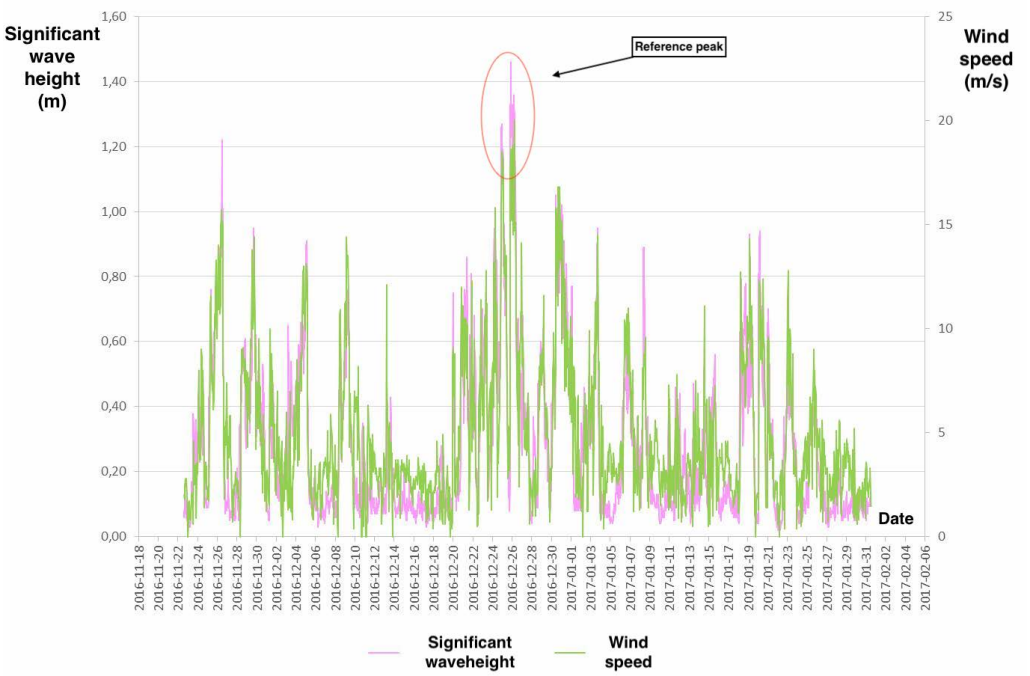

Figure 3.2: Significant wave height outside floating breakwater, and wind speed from nearby airport, Midtfjorden, Norway.

(a) Reference location, nearby airport and dominant fetch- and wind direction, Midtfjorden, Norway (Google Maps, 2022).

(b) Position of wave gauges on reference location.

Figure 3.3: Reference location (Norconsult, 2017).

4 Description of the Experiments

4.1 Wave Flume

The experiments are conducted in a two-dimensional wave flume located at the ESITC (École Supérieure d'Ingénieurs des Travaux de la Construction de Caen) in Caen, Normandie, France. The flume has a total length of 8.2 meters and internal width of 350 mm. Water depth is 0.5 meter. The total length is including the regions of the pistol wave paddle and the absorption zone. The absorption zone is a 2-meter-long, triangular shaped foam beach. See Appendix A1 for drawings of the flume. Figure 4.1 shows a representative sketch of the experimental set-up.

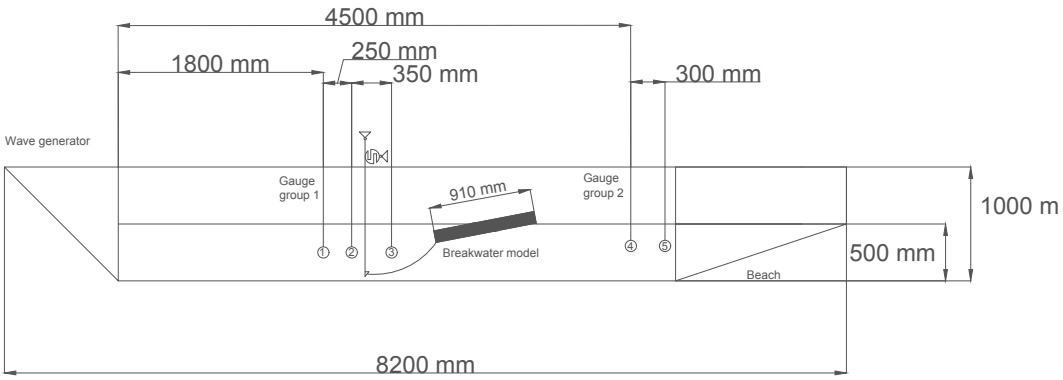

Figure 4.1: Test set-up in Laboratory.

4.1.1 Flume instrumentations

Wave conditions in the flume are measured using wave gauges. Such measurements are important in order to describe the hydraulic performance, explained in Section 3.2.

4.1.1.1 Surface elevation

Surface elevations are measured in order to retrieve data for wave propagation on specific places in the wave flume. Resistive wave gauges are used for the purpose. Resistive gauges consist of two parallel steel rods fixed with a set distance apart, and these are mounted perpendicular to the flow direction (HydraWiki, 2019). The rods are subjected to a high frequency alternating voltage, and the conductance between the rods are recorded. The

conductance will be dependent on the rod submergence, hence the measured conductance can be converted into surface elevation. This requires a calibration procedure, where records of the instrument output voltage linked to different measured submersion are linearly correlated.

Wave gauges used for this report are from Edinburgh design and are sampling with a frequency of 128 Hz (EdinburghDesigns, 2016). Njordr Wave Synthesizer and Njordr Controller are used for calibration and data collection, both developed by Edinburgh Design.

In order to measure data of necessary quality while taking into account spatial limitations in the wave flume and availability concerning a consistent wave gauge system, five wave gauges were used during the testing in groups of three and two, see Figure 4.1. The group of three were placed in front of the floating body in order to measure incident and reflected waves. The group of two gauges were placed behind the floating body to measure transmitted waves.

4.1.1.2 Wave height and reflection analysis

Sampled data are throughout the testing treated in three different programs.

- **Matlab:** Regular waves were analysed using the zero up-crossing method, where wave height and wave period were retrieved from the individual wave gauges and averaged for each gauge group. The method has weaknesses in terms of distinguishing incident and reflected waves, even though averaging using several wave gauges will reduce some error. Error is caused by harmony between incident and reflected waves. In the case of perfect harmony, there will be no variations in the recording of a super positioned wave measured by one gauge, making the deviance uniform for the test run. For non-harmonic waves, the deviance problem will be averaged away for each individual wave gauge. The WaFo toolbox is used in order to produce wave- and force spectrum during the testing of irregular sea states (WaFo, 2017).
- **Wavelab:** Wavelab is a software package for data acquisition and data analysis specifically designed for wave laboratories, developed by Aalborg University, Denmark (Wavelab, 2019). The program is used for regular and irregular time series-, spectrum- and reflection analysis. The case of regular waves separation is done using the

nonlinear Andersen et al. (2017) method, and for linear waves using the Lin and Huang (2004) method. Irregular waves are analysed by the Zelt and Skjelbreia (1993) method for linear waves and by Røge Eldrup and Lykke Andersen (2019) for nonlinear waves.

- **Njordr Wave Synthesizer:** Edinburgh Designs has developed a suite of software tools specifically for running experiments in a wave flume. Njordr Wave Synthesizer outputs files to the paddle controller for the wave flume, based on user inputs. The program can also be used as a data acquitting tool for the wave gauges where the data is analysed, and if necessary, used to correct for flume effects in the generated wave. The program is used for time series- and reflection analyses of regular and irregular waves using three and four gauges, by the method of Mansard and Funke (1980).

4.2 Breakwater model

As presented in the literature review regarding existing studies and literature in Chapter 2.1, there are not discovered any breakwater with high resemblance to the characteristics for the model proposed for this thesis. However, there are different studies and concepts with resemblance to individual parts of the proposed model. Results and designs from these studies will be attempted implemented and compared to this study.

4.2.1 Material

The material used for the model is plates made by KÖMATEX® PVC white 662. The general properties of the material are listed in table 4.1. The choice of material is due to the versatile use and simplicity in terms of assembly. The material is giving a base for further implementation of components, meaning that the buoyancy can be adjusted by added weight and roughness adjusted by adding 3d-texture to the surface. The simple basis for the material makes it easier to interpret results when manipulating the input parameters. During assembling of the parts, glue was used to stick the pieces together.

Table 4.1: Material properties for PVC plates used for the model.

KÖMATEX® PVC white 662	
Thickness	10 mm
Density	0.60 g/cm^3
Flexural strength	$>$ 25 MPa
Roughness	$<$4 μm

A full size prototype is likely to be consisting of reinforced concrete or a PVC-composite, depending on factors such as size, weight, economy, influence from external forces and bio enhancing effects. Both materials are possible to manipulate towards similar properties as the PVC used in the model presented in this thesis.

4.2.2 Model design

4.2.2.1 Frame

The PVC plates used have a small thickness and intermediate flexural strength, thereby the frame were constructed with double side walls, end walls and two transverse walls to assure a rigid base for additional components. The frame were also equipped with ballast chambers which assured that ballast could be evenly distributed along the width of the model. The main contribution to the inclination of the model was the ballast, but the model did also have a moveable steel bar that could be slid along the length of the model in order to do fine adjustments to the inclination angle. The inner side wall were extended and equipped with drilled holes which function were to make fixation points for the model tests. Aluminium strips with rotational freedom were used to hold the surface plates in its place. The basis drawing for the frame is presented in Figure 4.2 and measurements are presented in Table 4.2

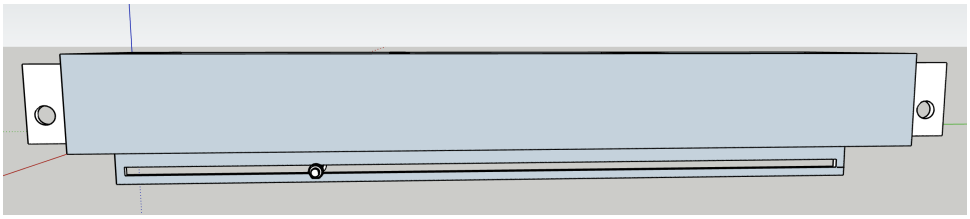

(a) Side view.

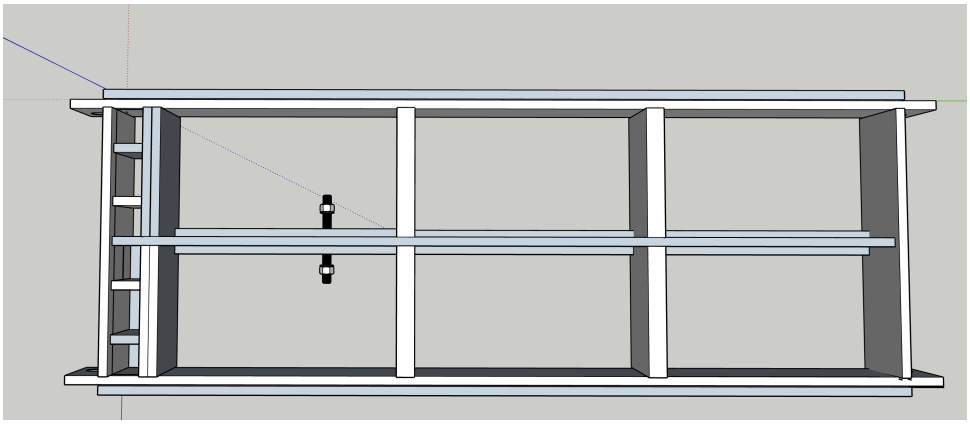

(b) top view.

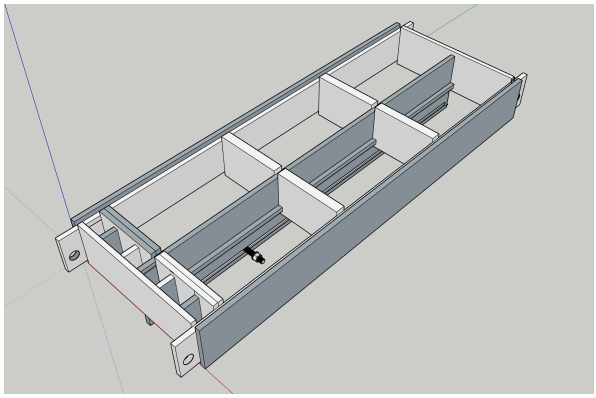

(c) 3D view.

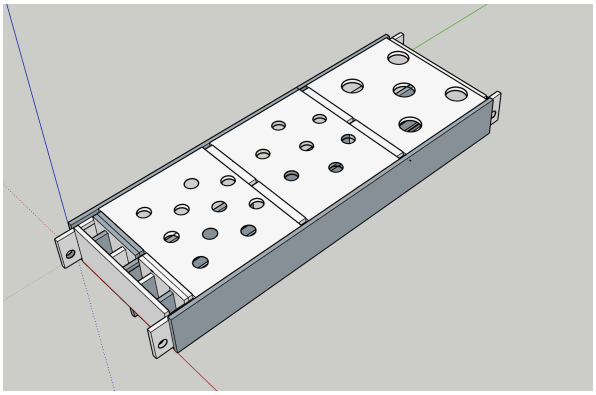

(d) 3D view with porosity plates.

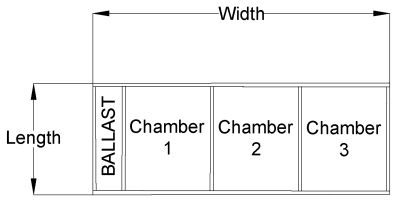

(e) Dimension direction and chamber positions.

Figure 4.2: Model drawings describing frame, porosity and dimension directions.

4.2.2.2 Porosity plates

Top plates cover the whole inner width of the breakwater, while the bottom plates are divided by the extended longitudinal middle wall. Plates are perforated with patterns with circular holes to make porosity. Porosity-holes are made in two different sizes; ø

55 mm and ø 30 mm, pattern illustrated in Figure 4.3. In addition to porous plates, configurations with rock filled chambers and beaching foam were included in the tests.

Table 4.2: Model dimensions for floating breakwater body.

Model dimensions	
Width $[W]$	910 mm
Length $[L_m]$	340 mm
Height $[H_m]$	100 mm
Top plates - width/length	320/260 mm
Bottom plates - width/length	155/260 mm

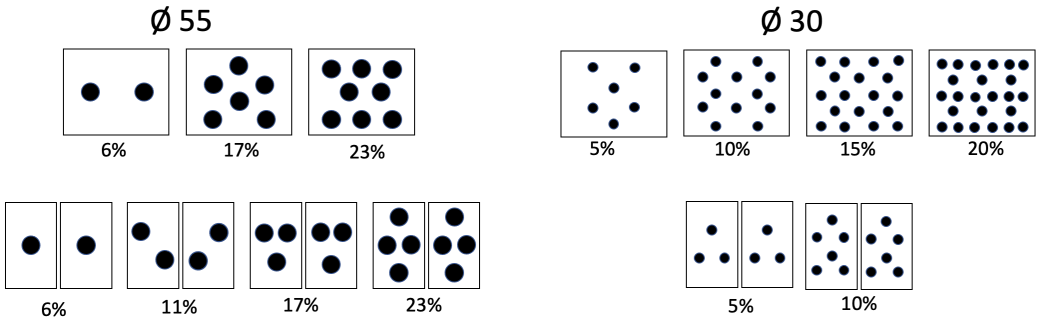

Figure 4.3: Porosity plates.

4.2.2.3 Model configurations

One of the purposes with the testing is to see what effect different porosities have on the performance. In Table 4.3, different configurations are described. Porosities are listed in the order of the chambers described in Figure 4.2e.

Table 4.3: Porosity plate-configurations for the floating breakwater body.

Model configurations

Configuration		Chamber 1	Chamber 2	Chamber 3
Reference case	Top plate	No porosity		
	Bottom plate	No porosity		
Configuration 1	Top plate	10% (ø30)	15% (ø30)	20% (ø30)
	Bottom plate	No porosity	5% (ø30)	10% (ø30)
Configuration 2	Top plate	10% (ø30)	20% (ø30)	5% (ø30)
	Bottom plate	No porosity	5% (ø30)	10% (ø30)
Configuration 3	Top plate	10% (ø30)	6% (ø55)	5% (ø30)
	Bottom plate	10% (ø30)	17% (ø55)	23% (ø55)
Configuration 4	Top plate	5% (ø55)	17% (ø55)	23% (ø55)
	Bottom plate	10%(ø30)	17% (ø55)	23% (ø55)
Configuration 5	Top plate	5% (ø55)	17% (ø55)	23% (ø55)
	Bottom plate	5% (ø30)	10% (ø30)	6% (ø55)
Configuration 6	Top plate	23% (ø55)	Open chamber	17% (ø55)
	Bottom plate	5% (ø30)	No porosity	6% (ø55)
Configuration 7	Top plate	Rocks	23% (ø55)	17% (ø55)
	Bottom plate	5% (ø35)	No porosity	5% (ø55)
Configuration 8	Top plate	5% (ø55)	Foam	14% (ø30)
	Bottom plate	6% (ø55)	Foam	10% (ø30)

4.2.2.4 Model fixation

Four different fixations are being used in the testing, with the purpose of isolating the effect of varying parameters. Different fixations are shown in Figure 4.4, while placement in the wave flume is illustrated in Figure 4.1.

- **Semi-rigid:** The model is fixed with semi-flexible poles in the submerged end. This allows moderate horizontal-, and full rotational movement in the fixation point, and free movement at the free end.
- **Rigid:** Fully rigid fixation of the model, allowing no movement in neither ends.
- **Long mooring:** Moored to anchor with 1,46 m chain, connected to the model with 0,35 m rope, allowing all movements.
- **Short mooring:** Moored to load cell with short mooring line. Mooring length is limiting movements, as the load cell pole is subjected to absorb as much of the force as possible.

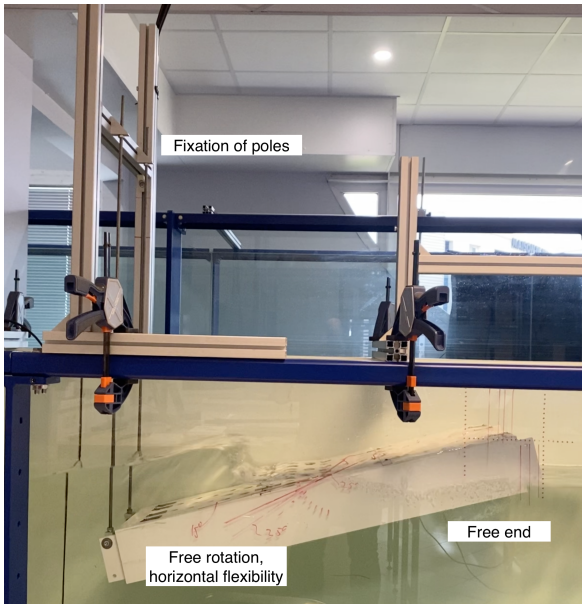

(a) Semi-rigid fixation.

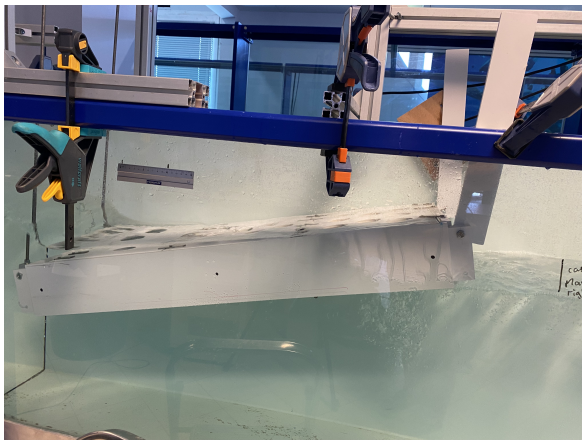

(b) Rigid fixation.

(c) Long-moored fixation.

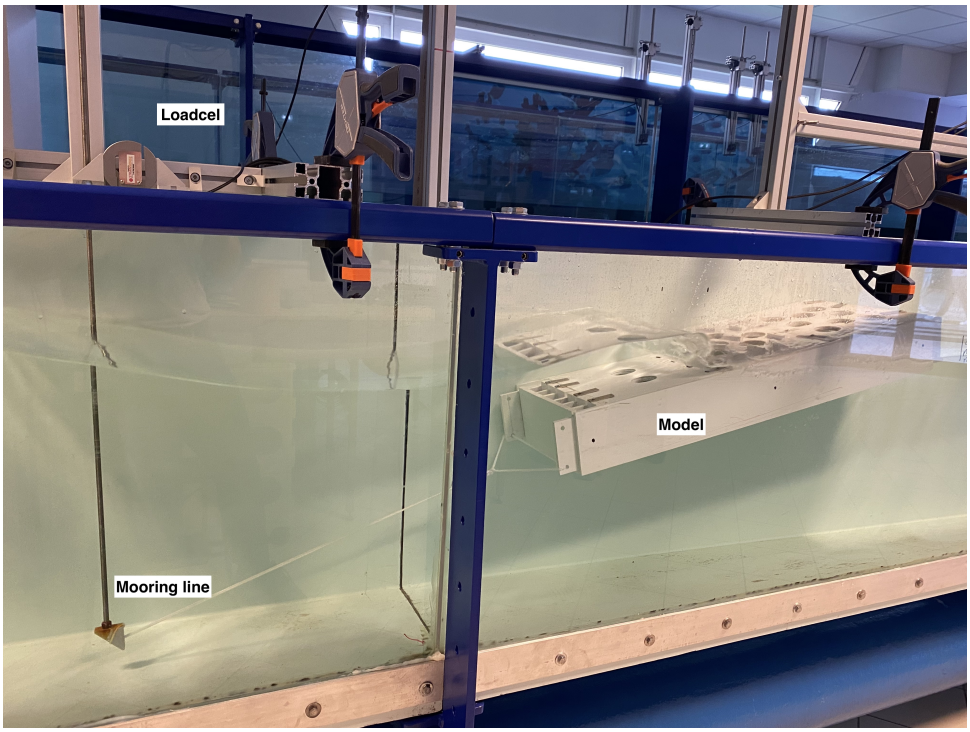

(d) Short-moored fixation with loadcell.

Figure 4.4: Model fixations.

4.2.3 Model instrumentations

4.2.3.1 Mooring forces

Mooring forces are measured using a load cell from National Instruments, which measures tension and compression. The load cell is mounted inside a cantilever system to prevent the cell to be submerged into the water. This is due to the water resistance of the load cell which is limited to one hour, hence more considerations would have been required in the execution of the experiments.

The set-up is presented in Figure 4.5, and placement in the wave flume is illustrated in Figure 4.1. The system is calibrated by exposing it to a known load case while logging the output signal. This method will give a linear connection between force and output. The set-up will give the magnitude of the mooring force, but not the direction. Wavelab is used for data acquisition and Matlab for analysis. The force signal were analysed using an established average up-crossing analysis.

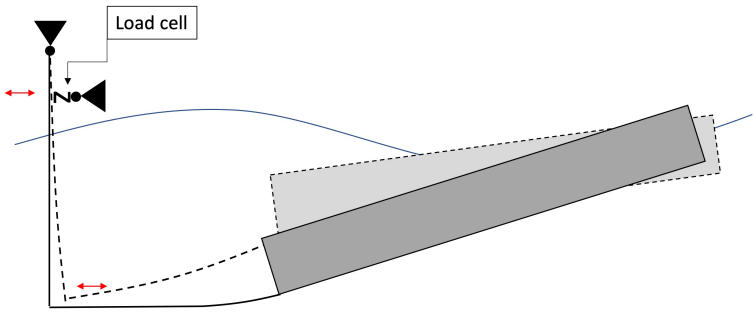

Figure 4.5: Illustration of load cell set-up.

4.2.3.2 Free Body Movements

Roll, heave and sway movements are recorded using a mounted video camera. The free body is equipped with three tracing points. By doing this, tracking programs can easily track the movements frame-by-frame by pixel-recognition. The open-source program

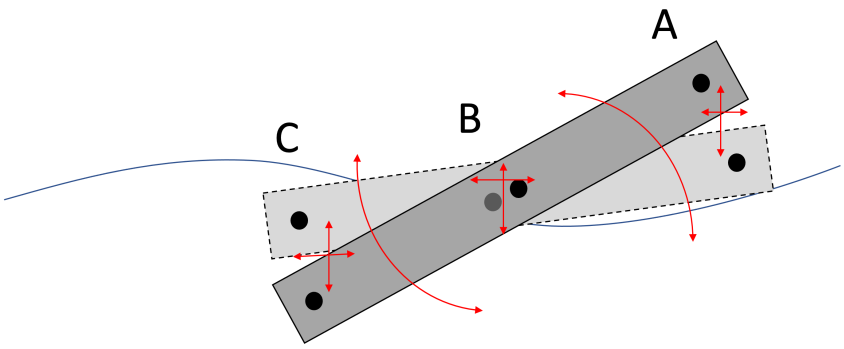

Figure 4.6: Illustration of body movements, with labels for tracking point A-C.

Tracker (Brown et al., 2022) is used to track the movements and produce the output data. The analysis of movement were very capacity demanding, resulting in a limited amount of tests being analysed.

Figure 4.6 illustrates the position of the tracing points and which movements they are expected to produce.

4.3 Test Methodology

Testing were divided into four different fixation configuration, as described in Section 4.2.2.4. Test methodology is given below, with details specific for the different tests schemes.

1. Wave flume is filled with water to reach 0.5 m depth.
2. Wave paddle is powered and prepared with corrected input data from Njordr synthesizer.
3. Wave gauges are calibrated as described in 4.1.1.1 and the data acquisition is armed ready for testing.
4. The breakwater model is placed in the wave flume with the fixation set for the round of testing. Adjustments of inclination and porosity are done according to the configuration of interest.
5. Activation of measuring devises, in the cases where these are used:
    - Load cell device is connected to the computer and data acquisition is armed.

- The camera for motion tracking is placed in correct position and armed.

6. Wave paddle is activated, together with measuring advices. Paddle and data acquisition is running for the set time for the selected wave run. Observation are written down into test log.
7. In the case of several consecutive tests, activity 4-6 is repeated.
8. Collected data is organized together with observations, readied for analysis. The model is taken out of the water, and measuring tools and paddle are disconnected.
9. Wave flume is emptied.

   In order to reduce the water consumption and reduce changes in the water qualities, activity 1 and 9 are only executed before the very first test and before/after periods of high inactivity.

4.3.1 Test matrix

A significant amount of tests is conducted for different model fixations, porosity configurations and wave conditions. The results are categorized based on fixation, in the order the tests were conducted. Table 4.4 shows the tests conducted.

Table 4.4: Test matrix for laboratory testing.

Fixation	**Configuration**	**Number of tests**	**Model inclination(s)***	**Wave conditions (Different runs)**	**Test main focus**
Without breakwater model	*Without breakwater model*	N/A	N/A	Regular(r) Irregular(i)	Synchronizing wave paddle and wave conditions input. Reflection of flume beach.
Semi-rigid	Ref. case Conf. 1 Conf. 2	3x14r 2x14r 2x14r	15 / 25 / 35 15 / 25 15 / 25.	Regular(r) (14)	Effect of inclination. Wave transmission. Effect of porosity.
Long mooring	Ref. case Conf. 1 Conf. 2 Conf. 3 Conf. 4 Conf. 5	14r+1i 14r+1i 14r+1i 14r+1i 14r+2i 14r+1i	23 29 / 19 31 / 19 20 21 / 20 21	Regular(r) (14) Irregular(i) (1)	Effect of porosities. Wave transmission. Wave reflection.
	Conf. 6 Conf. 7 Conf. 8	1i 1i 1i	22 13 / 19 16	Irregular(i) (1)	Effect of porosity /rocks/foam. Wave transmission. Wave reflection.
Short mooring	Ref. case Conf. 4 Conf. 5 Conf. 5 (3d)** Conf. 8	10r+1i 1i 10r+1i 10r+1i 1i	23 20 21 21 16	Regular(r) (10) Irregular(i) (1)	Porosity effect on forces. Wave reflection. Free-body movements. Mooring load
Rigid	Ref. case Conf. 5	14r+1i 14r+1i	15 15	Regular(r) (14) Irregular(i) (1)	Wave reflection Wave Transmission
	Total	257			

* Inclination is the inclination of the model in still water without any movements.
** 3D-pattern illustrated in Figure A3.1 in Appendix.

4.3.2 Wave conditions and test runs

Wave conditions from the reference location are scaled according to a scaling factor of $L_r = 1/25$. Leading parameters for wave conditions are displayed in Table 4.5, where scaling is done according to Table 3.1

Table 4.5: Wave parameters for reference case and model test.

Parameter	Reference case	Scaled values
H_s	1.5 m	0.06 m
H_{max}	2.5 m	0.10 m
T_p	5.0 s	1.0 s
T_m	3.8 s	0.76 s

The test scheme is prepared with the purpose of retrieving results that are comparable to

different runs, as well as other studies. Two test schemes are used in the model tests, one consisting of regular waves and one consisting of a JONSWAP spectrum. In the regular wave scheme, wave height is fixed while the period is varying. The parameters for the JONSWAP spectrum are presented in Table 4.7.

The wave runs, both regular and irregular, are tested through calibration runs without the breakwater model in the wave flume prior to the experiments in order to assure correct wave production from the wave paddle. Deviances from input parameters and measured waves were found, and the input values were gained using built-in functions in Njordr Wave Synthesizer.

Table 4.6: Regular wave runs for experimental testing.

Regular wave runs					
Run number	Frequency	Period	Wave height	Wavelength	Duration
1	0.60 /s	1.667 s	0.10 m	3.245 m	5 min
2	0.70 /s	1.429 s		2.645 m	
3	0.80 /s	1.250 s		2.182 m	
4	0.85 /s	1.176 s		1.985 m	
5	0.90 /s	1.111 s		1.811 m	
6	0.95 /s	1.053 s		1.651 m	
7	1.00 /s	1.000 s		1.519 m	
8	1.05 /s	0.952 s		1.387 m	
9	1.10 /s	0.909 s		1.276 m	
10	1.15 /s	0.869 s		1.172 m	
11	1.20 /s	0.833 s		1.079 m	
12	1.25 /s	0.800 s		0.997 m	
13	1.30 /s	0.768 s		0.918 m	
14	1.35 /s	0.741 s		0.857 m	

Table 4.7: JONSWAP wave spectrum for experimental testing.

JONSWAP spectrum	
Hs	0.08 m
Tp	1.0 s
Gamma	3.3
Duration	10 min
Number of waves	650

4.4 Sources of Error

The physical experiments are completed according to recommended practice on the wave flume lab of ESITC and University of Caen, while analysis are done using tools and numerical schemes considered to have high quality. Nevertheless, some errors are expected and these are described in the following section.

4.4.1 Wave flume

The wave flume used for the described work had never been used prior to the experiments. The flume had, at the time of the experiments, not received a certificate of completion declaring the quality, accuracy or general state. Inspections of the wave flume declared the following deviations, with descriptions of expected error. The following inaccuracies are not estimated to a specific value.

- The wave paddle was assembled with an uneven transversal displacement, resulting in a gap between the paddle and the right and left side of the flume of 4 mm and 1.4 mm, consequently. This produced waves with a skewed crest that traversed over the course of the wave propagation. The position of this skewness inflicted the gauge measurements as the transverse movement made the increased crest hit just some gauges.
- Side walls of the wave flume were bulging over the height of the flume, resulting in a variation of the wave flume width. This might have been contributing to the transversal skewness as described in the point above.
- The wave flume were installed without exact levelling, resulting in a deviance of water level from paddle to start of flume beach on 14 mm. This is resulting in an inaccuracy concerning the usage of depth dependent wave theories, wave generation and numerical models.
- Replacement of the water in the flume were a time demanding process, resulting in water laying in the flume for several weeks. This might, over time, change the water properties, due to e.g. bacteria and dirt, with changed electrical water resistance as a consequence. This could impact the resistive wave gauges, as they are highly dependent on the resistance. However, comparisons of tests done over a span of

time did not indicate clear signals of the problem occurring.

- Irregular and regular wave runs were calibrated before testing, but some deviations from the presented data are expected, and registered. However, deviances are small and not impacting the final result in a critical way.
- The wave flume is small, resulting in some deviations from recommended practice for lab work in wave flumes. The distance from the wave paddle to the first group of gauges should at least be one wave length, and the distance from the breakwater to the second gauge group should be long enough to prevent overtopping from hitting the gauges. Neither of these were satisfied. The short wave flume will also prevent proper development of the propagating waves.

4.4.2 Wave flume instruments

4.4.2.1 Wave gauges

The configuration described in Paragraph 4.1.1.1 must be done by hand, as the gauges are of an older model. This leads to a possible error if the fixation is not accurate at the marked configuration lines. The consequence of such an error is a proportional error in measured data. Clear indications of this error has not been detected in the analysed data, but unexplained deviances resulted in reconfiguration and retesting.

4.4.2.2 Load cell

Technical issues provoked a suspected electrical noise on the signal of 50Hz, which were cleaned using a low pass frequency filter (MathWorks, 2022), illustrated in Appendix A2. The disturbance on the raw signal has an amplitude of 0.6 Newton.

5 Results and Discussions

5.1 Preliminary testing

Preliminary testing were conducted in order to calibrate wave paddle and define the conditions in the flume without any interactions. The Results from the irregular wave run are presented in Table 5.1 and reflection from the beach for regular wave runs is displayed in Figure 5.1.

Table 5.1: Reflection coefficient, C_r, for irregular wave from wave absorbing beach in wave flume.

C_r	T_p [s]	H_s [m]
12.99 %	0.9426	0.07886

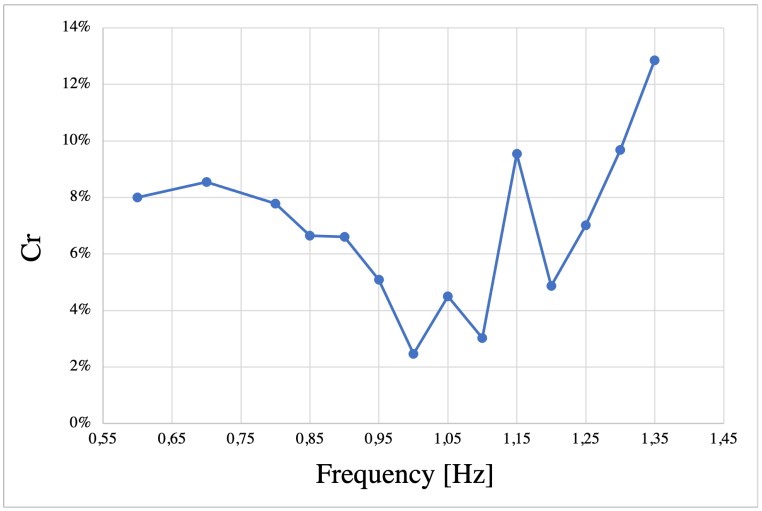

Figure 5.1: Reflection coefficient, C_r, for regular wave runs from wave absorbing beach in wave flume.

5.2 Rigid fixation

The rigid fixation prevented any movements of the floating body, and the focus of the tests were to investigate the effect of wave transmission and -reflection. The tests were conducted with an inclination of 15 degrees, for two configurations; the reference case and Configuration 5. A total of 30 tests were conducted, 28 regular wave runs and 2 irregular wave runs, as shown in Table 4.4. Tests with rigid fixation were the last to be tested, but

will be presented first for the benefit of a better foundation for comparison with other fixations.

5.2.1 Wave transmission

Wave transmission coefficients, C_t, for the reference case and Configuration 5 for regular wave runs are displayed in Figure 5.2, and two details must be highlighted. A clear separation between the transmission coefficients is revealed after $W/L = 0.42$ (run 3), where C_t for the porous Configuration 5 keeps decreasing rapidly, while it for the reference case decreases with a lower gradient. The decrease for Configuration 5 keeps a sharp gradient until $W/L = 0.60$ (run 7), where the gradient has a sharp decrease and flattens out for the remaining wave runs.

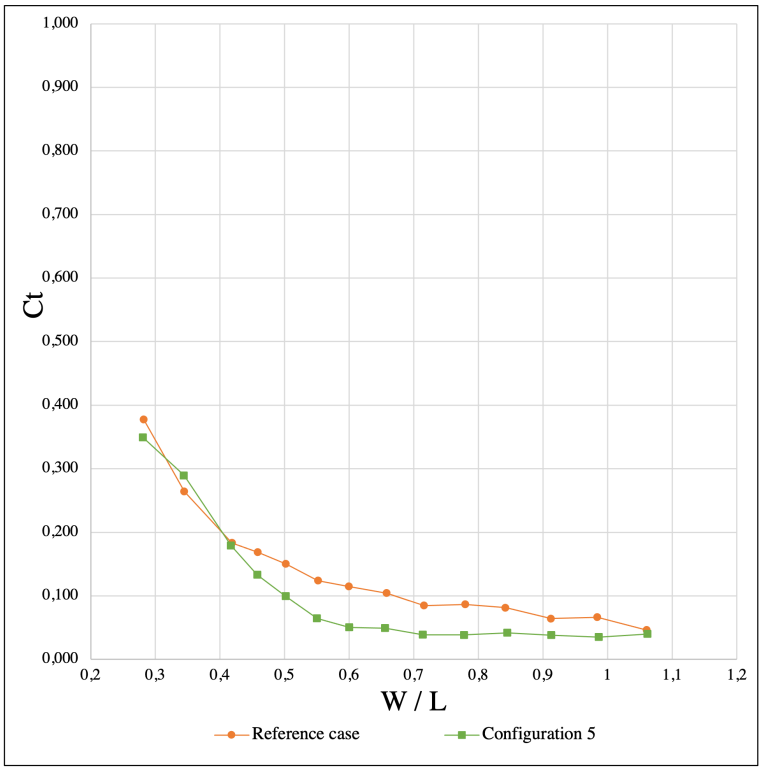

Figure 5.2: Transmission coefficient, C_t, for regular wave runs with rigid fixation.

Table 5.2: Irregular wave tests for rigid fixation, showing configuration, initial angle, ballast, reflection coefficient, C_r, wave properties for incident and transmitted waves, and transmission coefficient, C_t.

Model			**Incident waves**			**Transmitted waves**		
Configuration	**Angle**	**Ballast**	C_r	T_p [s]	H_s [m]	T_p [s]	H_s [m]	C_{t,H_s}
Ref	15*	N/A	22.01%	0.9410	0.08019	1.005	0.010230	13%
5	15*	N/A	18.81%	0.9426	0.07938	1.037	0.005873	7%

*Inclination also used in regular wave runs

Model configurations

Configuration		Chamber 1	Chamber 2	Chamber 3
Reference case	Top plate	No porosity		
	Bottom plate	No porosity		
Configuration 5	Top plate	5% (ø55)	17% (ø55)	23% (ø55)
	Bottom plate	5% (ø30)	10% (ø30)	6% (ø55)

5.2.2 Wave reflection

Wave reflection coefficients, C_r, for both configurations are displayed in Figure 5.3. C_r are slightly decreasing through the first half of the tests, before it stabilize slightly for the shorter wave lengths. The porous Configuration 5 has a lower C_r than the reference case.

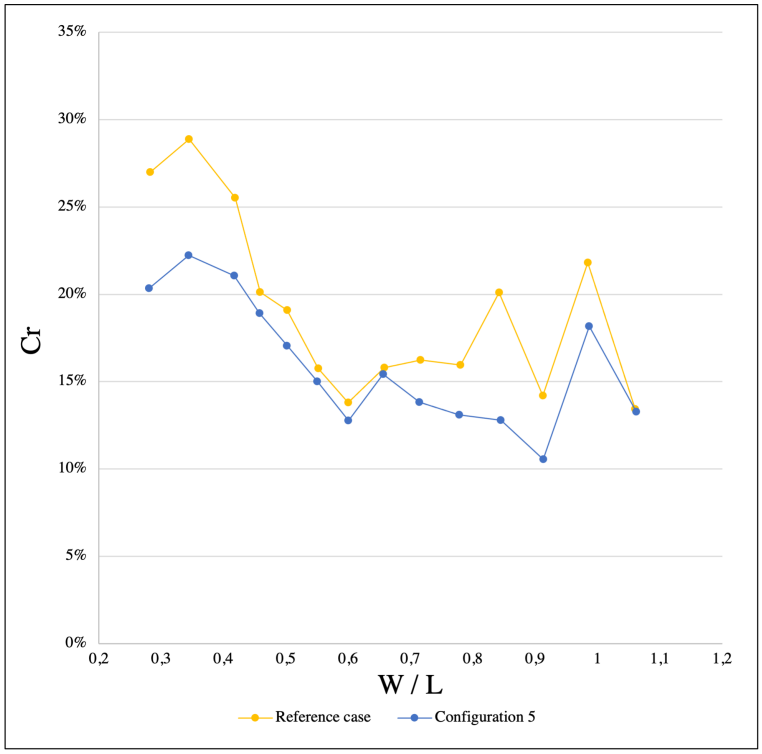

Figure 5.3: Reflection coefficient, C_r, for regular waves with rigid fixation.

5.2.3 Observations

Due to the rigid fixation, no movements of the model are observed through the runs. Hence, the observed hydraulic mechanisms are easier to isolate. The type of wave breaking had the same evolution for both configurations. The waves started with a collapsing breaking process from the first run, for both configurations. From $W/L = 0.42$ (run 3), a plunging breaking process was observed for the remaining runs. For the reference case, overtopping were observed from $W/L = 0.28$ to $W/L = 0.66$ (run 1-8). Some overtopping was observed for Configuration 5, primarily for the longer waves, but relatively insignificant compared to the reference case, as the incident wave collapsed in through the porous top plate, resulting in a non-laminar effect on the water flow and suspected higher dissipation of the waves.

The recorded reflection were higher for the longer waves than for other fixations, as described in Section 5.2.2. This increased reflection was visually observed, as the surface conditions were significantly more disturbed compared to tests with other fixations. The run-down process on the reference case was approximate laminar, hitting the lower part of the next incident wave, resulting in a significant rolling effect on the breaking wave,

see Figure A3.3 in Appendix. The difference between the wave attenuating process of porosity and the breaker process described, was not possible to interpret based on the observations.

5.3 Semi-rigid fixation

Semi-rigid fixation was the first test to be conducted. The main purpose was to retrieve information about the inclination effect on wave breaking mechanisms and wave transmission. Three configurations were tested to retrieve initial information about the effect of different inclinations and porosity. A total of 98 tests with regular waves were conducted, as shown in Table 4.4.

Inclination of 15-, 25-, and 35 degrees were tested for the reference case, Configuration 1 and Configuration 2, consequently. After inclination tests of the reference case, the inclination of 35 degrees was considered ineffective compared to the others, and not tested for the other configurations.

5.3.1 Wave Transmission

Transmission of waves is observed to have a steady decrease as the wavelength is decreasing. It is observed that for the longest wave lengths, the incident waves are barely affected by the breakwater, leading to high transmission, while for the shortest wave lengths, the transmission is significantly lower. Wave transmission coefficient, C_t, are displayed in the following graphs, Figure 5.4, 5.5 and 5.6, plotted according to the relation between the breakwater length and the wave length. There is no significant difference between C_t for the configurations at the same inclination. C_t is decreasing as the inclination is decreasing.

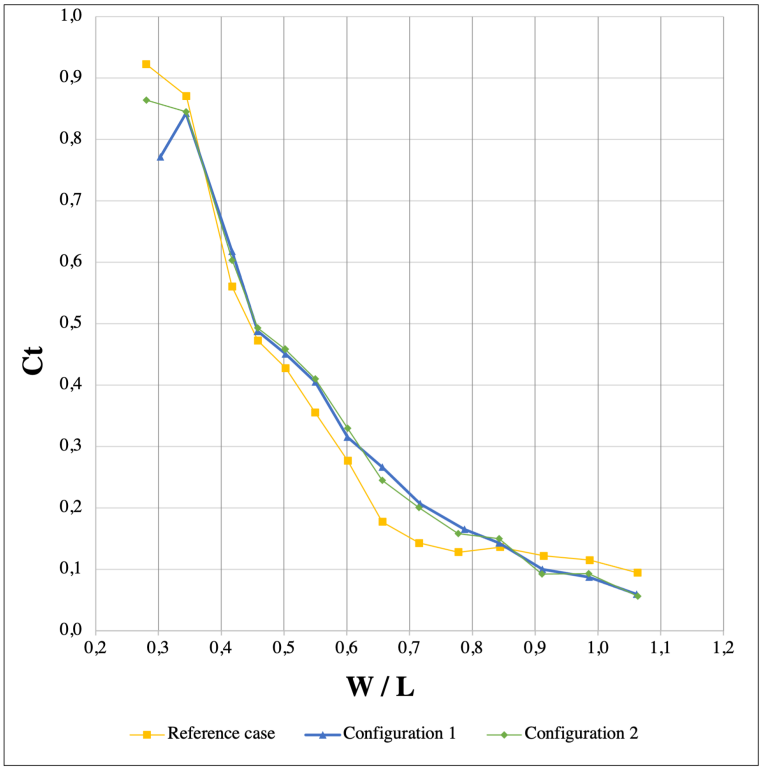

Figure 5.4: Transmission coefficient, C_t at 15 degrees inclination with semi-rigid fixation.

Model configurations

Configuration		Chamber 1	Chamber 2	Chamber 3
Reference case	Top plate	No porosity		
	Bottom plate	No porosity		
Configuration 1	Top plate	10% (ø30)	15% (ø30)	20% (ø30)
	Bottom plate	No porosity	5% (ø30)	10% (ø30)
Configuration 2	Top plate	10% (ø30)	20% (ø30)	5% (ø30)
	Bottom plate	No porosity	5% (ø30)	10% (ø30)

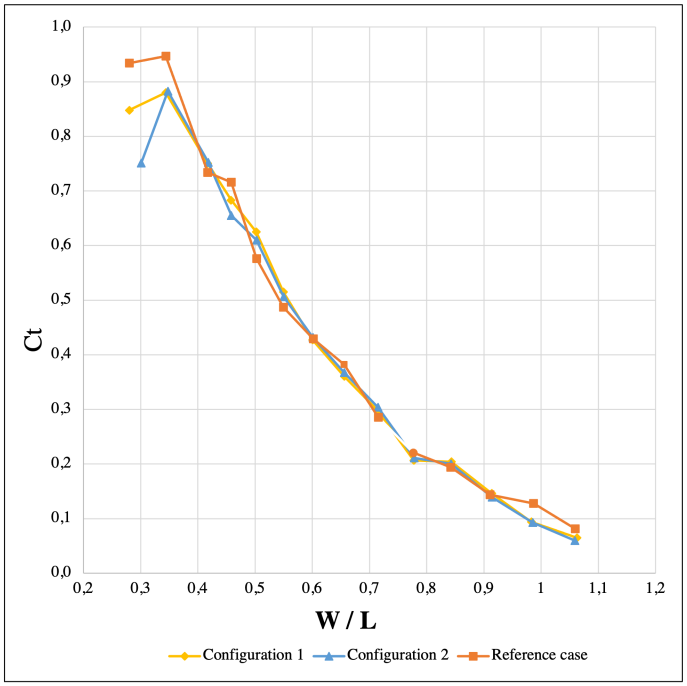

Figure 5.5: Transmission coefficient, C_t, at 25 degrees inclination with semi-rigid fixation.

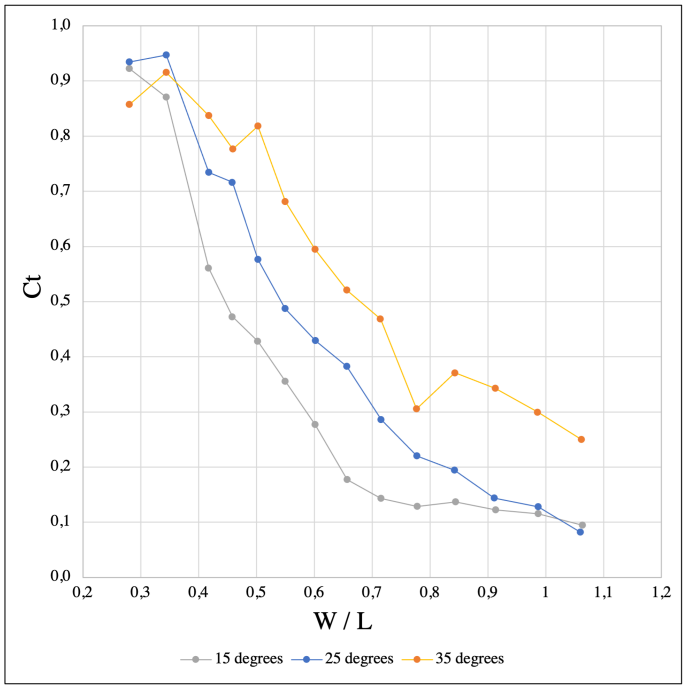

Figure 5.6: Transmission coefficient, C_t, for reference case with semi-rigid fixation.

5.3.2 Observations

The main purposes of the semi-rigid test were to investigate the wave breaking mechanisms and transmission due to the inclination. Observations of the design performance on aspects like body movement and water flow around the model were also noted.

For the inclination of 35 degrees, the dominant breaker type was surging, where most of the wave energy was transferred into the breakwater body and provoking big movements, making the breakwater producing new waves of a considerable size. Compared to the other inclinations, breaking was first observed on shorter wave lengths, after $W/L = 0.55$ (Run 6). For $W/L = 0.28$ to $W/L = 0.5$ (Run 1-5), primarily wave surge were observed, causing low wave dissipation and big body movements.

Inclination of 25 degrees and 15 degrees were having an increasing breaker effect on the waves. For 15 degrees inclination, breaking waves were observed for $W/L = 0.34$ (Run 2), and it was a visible decrease of energy transfer from the wave to the breakwater compared to higher inclinations, as wave energy dissipated more effectively in the breaking process.

The reference case had bigger occurrences of overtopping, causing a generally more disturbed sea state behind the breakwater. Configuration 1 and 2 had less overtopping, and the propagating waves were collapsing into the porous chambers, creating aerated water inside and under the breakwater.

5.3.3 Preliminary discussion

A good basis for further work was retrieved from the initial testing, as it isolated the effect of inclination and porosity. First indications in the results of the effect of the chosen porosities did not reveal big differences when it comes to wave transmission. Both visual observations and retrieved data are clearly showing advantageous effects due to a lower inclination.

It is drawn a preliminary conclusion based on the first round of tests that a lower inclination gives lower transmission, and this has been passed on to further testing.

5.4 Long-moored fixation

The main purpose of long-moored tests were to retrieve more in-depth information about the wave transmission and -reflection, effect of different configurations and model movements with a mooring configuration closer to what would be used for a full-scale model. A total of 94 tests were conducted, 10 with irregular waves and 84 with regular waves, as shown in Table 4.4.

5.4.1 Wave transmission

Transmission coefficients, C_t, for configurations tested with regular wave runs, are displaying the same trend as in the semi-rigid tests. As the wave length is decreasing, the transmission is decreasing. Neither of the configurations are showing significantly deviances compared to the others. Wave transmission coefficient, C_t, for regular wave rounds are displayed in Figure 5.7, plotted according to the relation between the breakwater length and the wave length. The average C_t for the regular wave runs is displayed in Figure 5.8. The reference case, Configuration 4 and Configuration 5 are, with small margins, displayed as the most effective.

Irregular wave tests were conducted on a total of 9 configurations, where some of them were tested with different inclinations. The results are displayed in Table 5.3. Inclination is dependent on the ballast amount and position, as well as configuration. The transmission coefficient for the significant wave height is in the span from $C_t = 0,47$ to $C_t = 0,59$. Configuration 8 and Configuration 4 are displayed as the most effective. Configurations with higher initial inclination resulted in a higher transmission coefficient. Spectrum plots for the irregular wave runs display better efficiency for high frequency wave dissipation, see Figure A3.4 in Appendix A3.

Model configurations

Configuration		Chamber 1	Chamber 2	Chamber 3
Reference case	Top plate	No porosity		
	Bottom plate	No porosity		
Configuration 1	Top plate	10% (ø30)	15% (ø30)	20% (ø30)
	Bottom plate	No porosity	5% (ø30)	10% (ø30)
Configuration 2	Top plate	10% (ø30)	20% (ø30)	5% (ø30)
	Bottom plate	No porosity	5% (ø30)	10% (ø30)
Configuration 3	Top plate	10% (ø30)	6% (ø55)	5% (ø30)
	Bottom plate	10% (ø30)	17% (ø55)	23% (ø55)
Configuration 4	Top plate	5% (ø55)	17% (ø55)	23% (ø55)
	Bottom plate	10%(ø30)	17% (ø55)	23% (ø55)
Configuration 5	Top plate	5% (ø55)	17% (ø55)	23% (ø55)
	Bottom plate	5% (ø30)	10% (ø30)	6% (ø55)

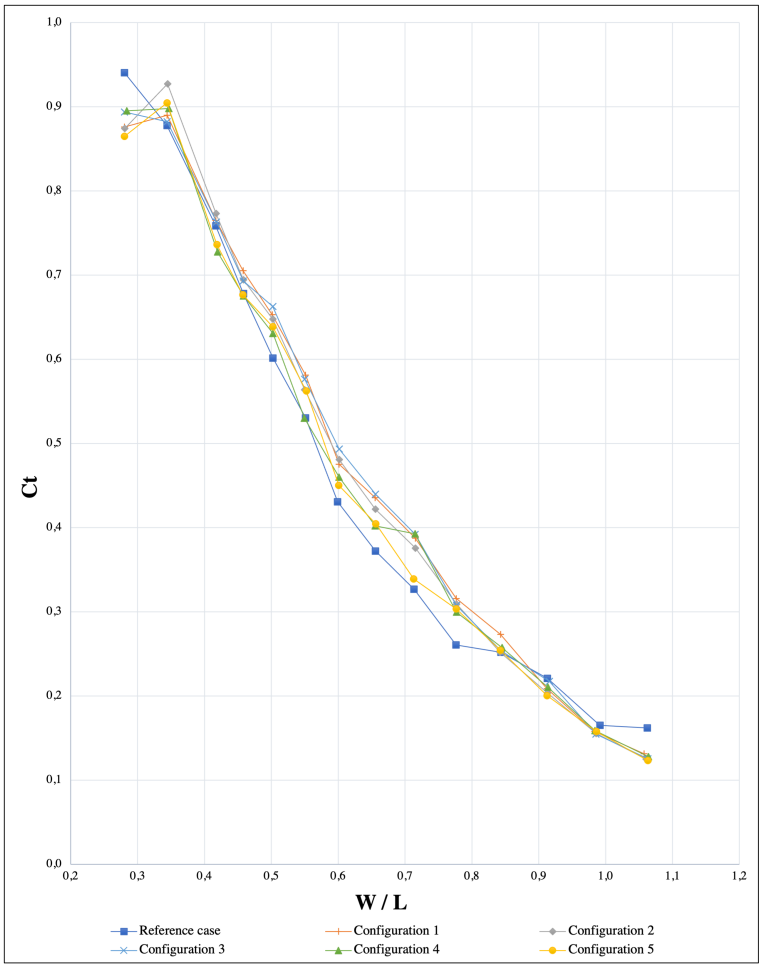

Figure 5.7: Transmission coefficient, C_t, for regular wave runs with long-moored fixation.

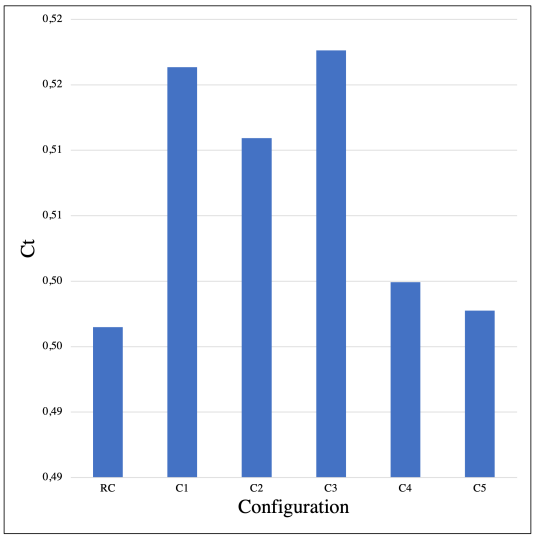

Figure 5.8: Average transmission coefficient, C_t, for Configuration 1-5 with long-moored fixation.

5.4.2 Wave reflection

Reflection coefficient, C_r, for regular runs are showing an increase in incident wave reflection for regular wave runs in the interval of $W/L = 0.42$ to $W/L = 0.46$ (run 3-4), before it is decreasing until $W/L = 0.78$ (run 10), and again increasing until the limit of the test scheme. The trend was representative for all configurations tested, where the reference case and Configuration 4 acted as the lower and highest extrema, consequently. Reflection coefficient, C_r, for regular wave runs are displayed in Figure 5.9. Results from irregular wave runs, as displayed in Table 5.3, revealed $C_r \approx 16 - 19\%$ for the configurations of the highest interest. The lowest reflection was from Configuration 7 ($C_r = 16,62\%$), whilst the highest was from Configuration 6 ($C_r = 29,73\%$). Higher inclination gave a higher reflection coefficient.

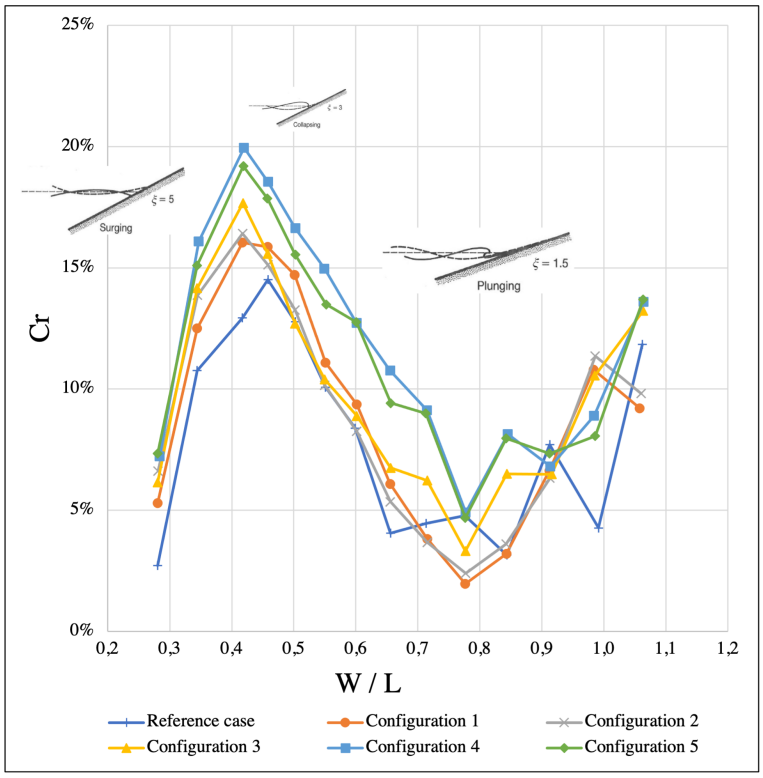

Figure 5.9: Reflection coefficient, C_r, for regular wave runs with long-moored fixation, with breaking mechanisms based on observations.

Table 5.3: Irregular wave tests for long-moored configurations, showing configuration, initial angle, ballast, reflection coefficient, C_r wave properties for incident and transmitted waves, and transmission coefficient, C_t.

Model			**Incident waves**			**Transmitted waves**		
Configuration	**Angle**	**Ballast**	C_r	T_p [s]	H_s [m]	T_p [s]	H_s [m]	C_{t,H_s}
Ref. case	23	2720g*	17.34 %	0.9424	0.07917	1.036	0.04272	54 %
1	29	2720g	19.91 %	0.9367	0.07874	1.040	0.04434	56 %
	19	2598g*	16.57 %	0.9397	0.07886	1.047	0.04036	51 %
2	31	2720g	21.16 %	0.9368	0.07883	1.035	0.04429	56 %
	19	2598g*	16.91 %	0.9353	0.07882	1.042	0.04050	51 %
3	20	2598g*	17.20 %	0.9378	0.07874	1.036	0.03943	50 %
4	21	2598g	19.66 %	0.9383	0.07890	1.045	0.03883	49 %
	20	2598g*	19.43 %	0.9427	0.07834	1.043	0.03639	46 %
5	21	2598g*	18.82 %	0.9362	0.07839	1.042	0.03968	51 %
6	22	2598g	29.73 %	0.9322	0.08079	1.024	0.04608	57 %
7	13	4150g**	17.90 %	0.9412	0.07989	1.043	0.04608	58 %
	19	4551g**	16.62 %	0.9390	0.07953	1.040	0.04290	54 %
8	16	2598g	18.94 %	0.9415	0.07836	1.054	0.03714	47 %

*Ballast and inclination also used in regular wave runs.
** Rocks in chamber 1 used as ballast.

Model configurations

Configuration		Chamber 1	Chamber 2	Chamber 3
Reference case	Top plate	No porosity		
	Bottom plate	No porosity		
Configuration 1	Top plate	10% (ø30)	15% (ø30)	20% (ø30)
	Bottom plate	No porosity	5% (ø30)	10% (ø30)
Configuration 2	Top plate	10% (ø30)	20% (ø30)	5% (ø30)
	Bottom plate	No porosity	5% (ø30)	10% (ø30)
Configuration 3	Top plate	10% (ø30)	6% (ø55)	5% (ø30)
	Bottom plate	10% (ø30)	17% (ø55)	23% (ø55)
Configuration 4	Top plate	5% (ø55)	17% (ø55)	23% (ø55)
	Bottom plate	10%(ø30)	17% (ø55)	23% (ø55)
Configuration 5	Top plate	5% (ø55)	17% (ø55)	23% (ø55)
	Bottom plate	5% (ø30)	10% (ø30)	6% (ø55)
Configuration 6	Top plate	23% (ø55)	Open chamber	17% (ø55)
	Bottom plate	5% (ø30)	No porosity	6% (ø55)
Configuration 7	Top plate	Rocks	23% (ø55)	17% (ø55)
	Bottom plate	5% (ø35)	No porosity	5% (ø55)
Configuration 8	Top plate	5% (ø55)	Foam	14% (ø30)
	Bottom plate	6% (ø55)	Foam	10% (ø30)

5.4.3 Observations

5.4.3.1 Wave breaking

Wave breaking mechanisms were again observed to be dependent on inclination. Breaking was observed more often for the lower inclination than for the two configurations with higher inclination, Configuration 1 at 29 degrees inclination and Configuration 2 at 31 degrees inclination. Wave breaking for the regular wave test runs were correlating between the different configurations, with small deviances. For $W/L = 0.28$ to $W/L = 0.42$ (run 1-3), surging were dominant, $W/L = 0.42$ to $W/L = 0.50$ (run 3-5) collapsing started to appear, and for $W/L = 0.50$ to $W/L = 1.06$ (run 5-14), plunging breaking were dominating for most configurations. Areas for breaking mechanism trends are illustrated in Figure 5.9. The surging in the first runs resulted in little energy dissipation, while it increased for shorter waves. For the porous configurations, there would be clear observations of the wave "falling" into the porous openings during its propagation, potentially reducing the vertical water pressure. Observations of models with low inclination revealed occasional immersion of the wave in front of the breakwater due to the end being too high in the water, making the propagating wave to transfer a bigger horizontal force to the model before the beaching process started.

5.4.3.2 Aeration and Overtopping

Aeration and overtopping were correlating, as the overtopping resulted in aerated water in the back of the model as it hit, and broke the water surface. Submerged bubbles in the water could be observed up to 15 cm behind the model, while bubbles on the surface were observed all the way to the flume beach. The reference case was dominating in terms of overtopping, as it was observed on every wave run from $W/L = 0.34$ to $W/L = 1.06$ (run 2-14). Overtopping on other configurations were less in terms of both magnitude and number of runs, as well as dependent on top plate porosity. For Configuration 1, 2, 4, 5, configurations with at least one top-plate with 20% porosity, overtopping was present from $W/L = 0.50$ or $W/L = 0.55$ (run 5 or -6), while overtopping was observed from $W/L = 0.46$ (run 4) for Configuration 3 which had a lower top plate porosity. Overtopping were present for all the configurations until $W/L = 0.84$ (run 11), with some occasional overtopping for $W/L = 0.91$ to $W/L = 1.06$ (run 12-14). For all porous configurations,

aeration was observed due to water circulating inside the chambers. As wave breaking developed into plunging waves, there would be observed blasts of air bubbles down from the bottom plate in the third chamber. These bubbles would, dependent on the force of the breaking wave, reach up to 15-20 cm under the model, from chamber 3. Another hydraulic phenomena was observed for Configuration 4 and -5, where the top plates had the highest porosities, as there was a flow of water running out from the top plates as the waves retracted, interrupting the next incoming wave and forcing it into a steeper breaking mechanism. Due to different submersion, the conditions in the different chambers were varying. Chamber 1, the deepest one, had a relative calm flow state without aeration, mainly caused by some hydrostatic pressure from passing wave as well as displaced water due to the rotation of the model. Chamber 2 had some aeration due to the plunging waves and a strong current passing through the chamber during wave breaking and model rotations. Chamber 3 had variations between a partially empty chamber during the high point of a rotation, and a fully filled chamber after a breaking wave, with a significant aeration level.

5.4.3.3 Breakwater motions

Movements could clearly be separated into two types, dependent on wave frequency, or W/L. At low frequency, low W/L, the model would be displaced horizontally while lifting the mooring line due to the incoming wave, followed by a retraction as the mooring line moved towards normal position and the water retracted from the model between the waves. This would result in bigger body movements, where the whole model moved horizontally while the end were moving vertically, making circular movements in the end of the model. As the frequency, or W/L, increases, the model would have less time retracting between the incident wave hits. This reduced the horizontal movement significantly, while the vertical movement decreased slower. From $W/L = 0.50$ (run 5), horizontal movements decreased from 7-10 cm to 0-1 cm, for all configurations. Vertical movement reduced from 7-10 cm to 4-6 cm. Observed model movements reduced to be slightly smaller for the porous models than for the reference model with no porosity. For the lowest frequencies, or W/L, the whole body followed the circular movement of the wave propagation, while as the waves became shorter, the ends of the model started moving unsynchronized in the vertical direction. There should also be noted how the movement caused by incident

waves changed the inclination of the model, thus influencing the inclination-dependent wave breaking.

5.4.4 Preliminary discussion

The transmission coefficients, C_t, for the different configurations are still following the same monotonic decrease as the wave lengths are decreasing. There is not revealed any clear indications in the results that certain configurations are performing better than others, as Figure 5.7 shows. It can be seen that the average values for Configurations 0, -4, and -5 in Figure 5.8 are slightly lower than the other tested configurations. The reference case and Configuration 5 are also among the best performing in terms of reflection, shown in Figure 5.9. For irregular wave runs, Configuration 8 performed well, making it a relevant configuration to be subject to further testing.

The reference case, Configuration 4, -5 and -8 will be subject to further testing based on the findings related to C_t for the long-moored fixation.

5.5 Short-moored fixation

The main purpose of the short-moored fixation tests were to examine the mooring load induced by the different configurations and the free body motions. Wave transmission and -reflection were also analysed. Regular wave run testing were conducted with fewer runs due to time limitations, where run 3, 6, 9 and 12 were skipped ($W/L = [0.42, 0.55, 0.71, 0.91]$). A total amount of 35 tests were conducted, 30 with regular waves and 5 with irregular waves, as shown in Table 4.4.

5.5.1 Wave transmission and -reflection

Wave transmission coefficients, C_t, for the three configurations tested are following the same uniform decline as presented in previous tests. As Figure 5.10 displays, C_t for short-moored tests are decreasing slightly faster than for the long-moored tests. The figure also display C_t for the reference case with the long-moored fixation, showing that the more rigid short-moored fixation has a lower wave transmission. Results show no clear deviance between the three configurations tested.

Reflection coefficients, C_r, are following the same trends as displayed in the previous fixation. Reflection coefficients, C_r, for short-moored fixation are displayed in Figure 5.11, with correlating trends as described for the long-moored fixation (see Figure 5.9). The reference case has a generally lower C_r than Configuration 5, both with and without 3D-pattern.

Table 5.4: Irregular wave tests for short-moored configurations, showing configuration, initial angle, ballast, reflection coefficient, C_r, wave properties for incident and transmitted waves, and transmission coefficient, C_t.

Model			**Incident waves**			**Transmitted waves**		
Configuration	**Angle**	**Ballast**	C_r	T_p [s]	H_s [m]	T_p [s]	H_s [m]	C_{t,H_s}
Ref	23	2720g*	16.20%	0.9412	0.07979	1.042	0.04300	54%
4	21	2598g	18.97%	0.9441	0.07880	1.040	0.03836	49%
5	21	2598g*	17.81%	0.9397	0.07926	1.039	0.04042	51%
5 (3d)	21	2598g*	18.50%	0.9382	0.07938	1.031	0.03754	47%
8	16	2598g	19.12%	0.9441	0.07873	1.047	0.03653	46%

*Ballast and inclination also used in regular wave runs

Model configurations

Configuration		Chamber 1	Chamber 2	Chamber 3
Reference case	Top plate	No porosity		
	Bottom plate	No porosity		
Configuration 5	Top plate	5% (ø55)	17% (ø55)	23% (ø55)
	Bottom plate	5% (ø30)	10% (ø30)	6% (ø55)

5.5.2 Mooring load

Mooring loads for the reference case, Configuration 4 and -5 for regular wave runs, are displayed in Figure 5.12. The figure displays the established average pull force, shaded by the average amplitude of the cyclic low-, and high force, explained in Figure A2.2 in the Appendix. As displayed, configurations with porosity have lower pull forces than the reference case, both in terms of average pull force and force amplitude. Longer waves are responded with higher force amplitudes. The distribution of the force amplitude for longer waves is uneven around the average, indicating that the high amplitude is sharp crested peak loads, while the relaxation state is a relative slower process. The distribution of force amplitude is equalizing as the wave length is decreasing.

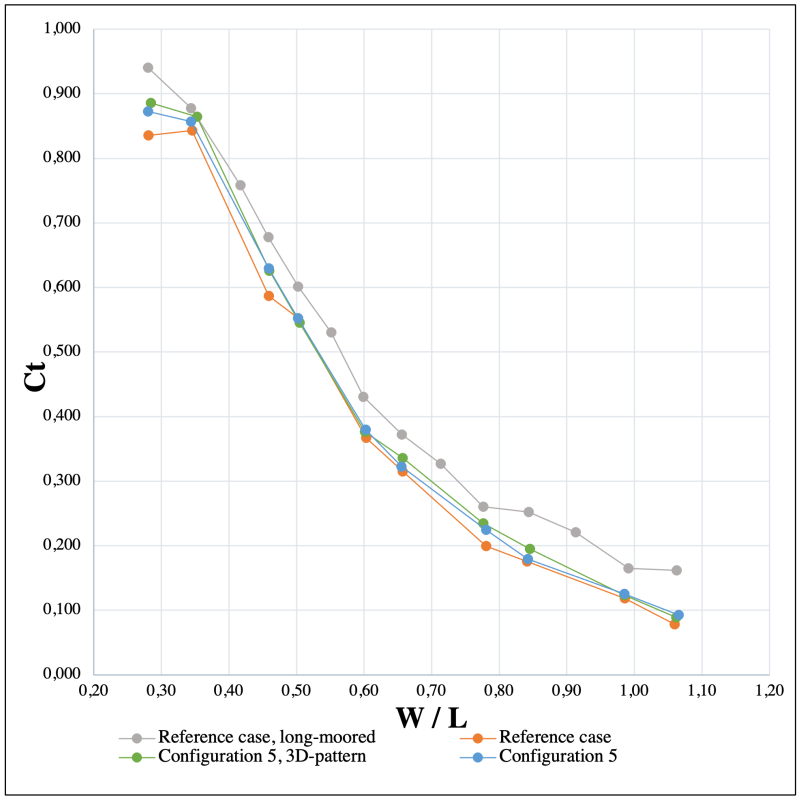

Figure 5.10: Transmission coefficient, C_t, for regular wave runs with short-moored fixation.

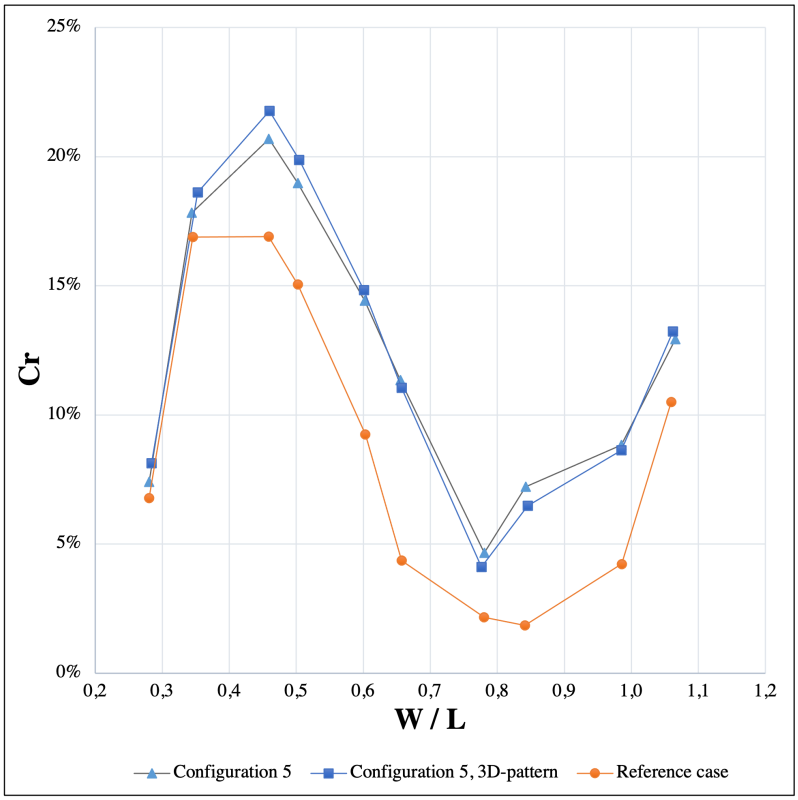

Figure 5.11: Reflection coefficient, C_r for regular wave runs with short-moored fixation.

Figure 5.13 displays the load spectrum for the reference case, Configuration 4, -5 and -8, for irregular wave runs. It can be seen that the reference case is having a higher mooring forces for the other tested configurations, and confirming that the trend from regular waves is valid for irregular waves as well. The mooring force spectrum has peaks around the peak frequency of the wave spectrum, 1 Hz, and for lower frequencies. The force peak around the peak frequency correlates to the incident wave force, while lower frequencies correlate to body movement resonance.

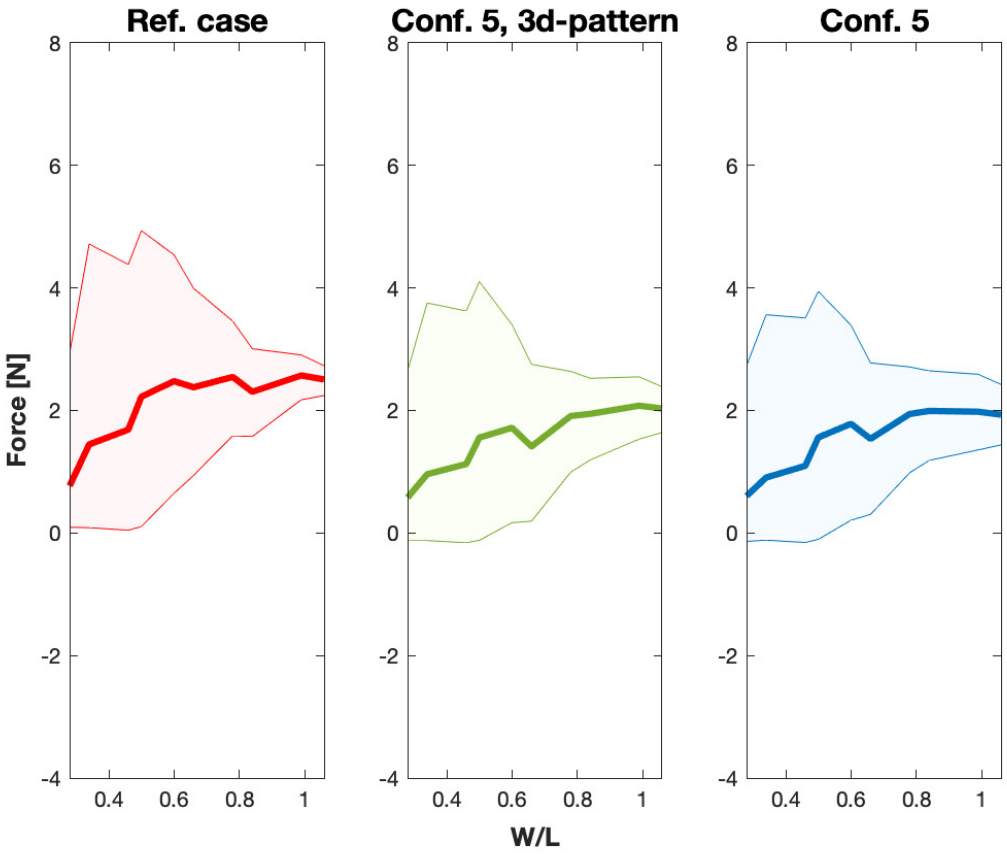

Figure 5.12: Mooring loads for the reference case and Configuration 5 (with/without 3d-pattern), subjected to regular wave runs.

Model configurations

Configuration		Chamber 1	Chamber 2	Chamber 3
Reference case	Top plate Bottom plate	No porosity No porosity		
Configuration 4	Top plate Bottom plate	5% (ø55) 10%(ø30)	17% (ø55) 17% (ø55)	23% (ø55) 23% (ø55)
Configuration 5	Top plate Bottom plate	5% (ø55) 5% (ø30)	17% (ø55) 10% (ø30)	23% (ø55) 6% (ø55)
Configuration 8	Top plate Bottom plate	5% (ø55) 6% (ø55)	Foam Foam	14% (ø30) 10% (ø30)

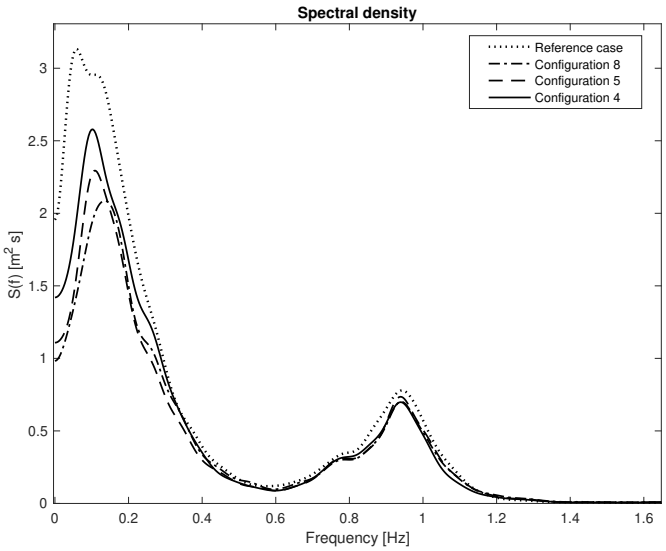

Figure 5.13: Load spectrum for irregular wave tests on reference case, Configuration 4, -5 and -8.

5.5.3 Breakwater Motion tracking

Breakwater motion tracking were conducted for four configuration; the reference case, Configuration 4, -5 and 9. The motion tracking is displayed in two ways. Figure 5.15 shows a scatter plot of the magnitude of motion density averaged around 0, for point A-C for each configuration. Figure 5.14 shows box plots of the movement in x- and y-direction for point A-C for every configuration. On each box, the central mark indicates the median, and the bottom and top edges of the box indicate the 25th and 75th percentiles, respectively. The whiskers extend to the most extreme data points not considered outliers, and the outliers are plotted individually using the '+' marker symbol. Point A-C are described in Figure 4.6.

Motions for the reference case are visibly higher for all points and direction, except for point A in y-direction. Configuration 8 has the best performance, as the peak values for the configurations are lower than the other configurations. The 25th and 75th percentiles are within the same range for Configurations 4, -5, and -9. The dominant direction for movements in point A and -C in all configurations is vertical. Point B has circular dominant movement for all configurations.

The density centre for the scatter plot for the motion tracking, in Figure 5.15, is varying dependent on both configuration and tracking point. The density centre for point B is

relatively homogenous for the four configurations. The density centre in point A and C are varying dependent on the configuration.

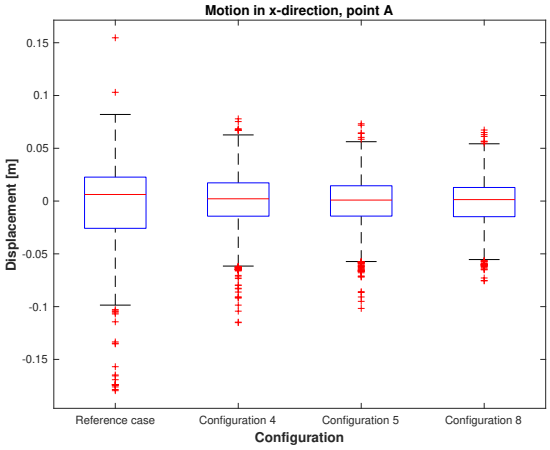

(a) Motion in point A, x-direction.

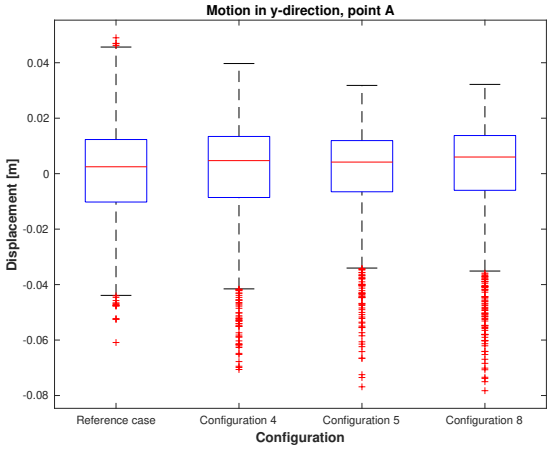

(b) Motion in point A, y-direction.

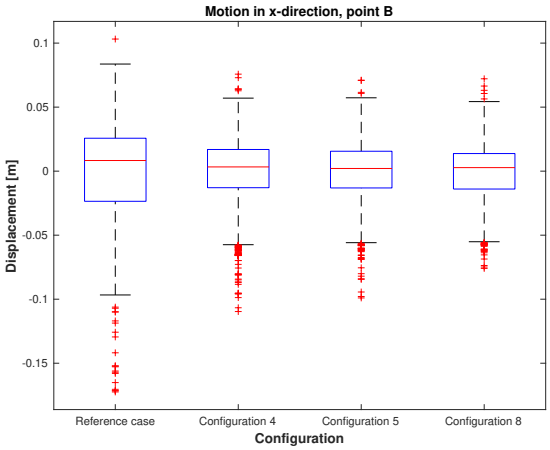

(c) Motion in point B, x-direction.

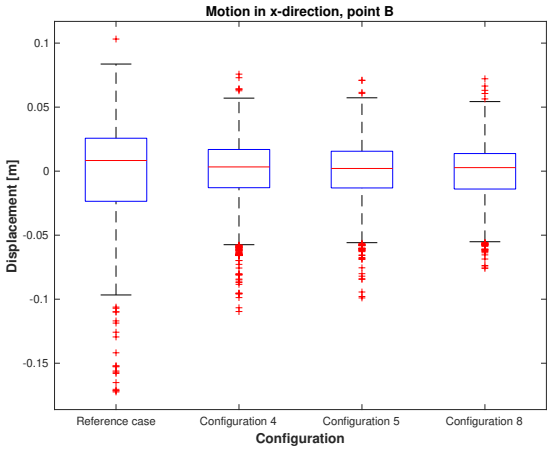

(d) Motion in point B, y-direction.

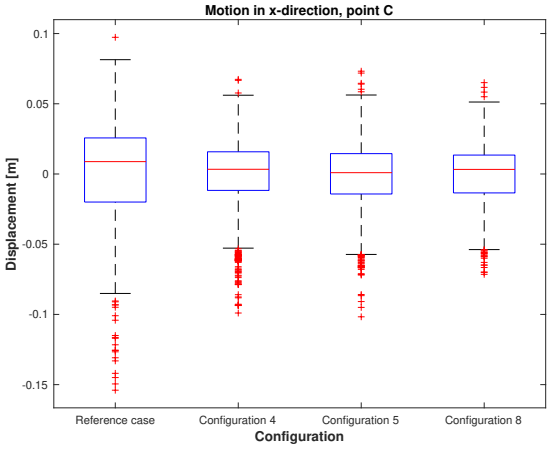

(e) Motion in point C, x-direction.

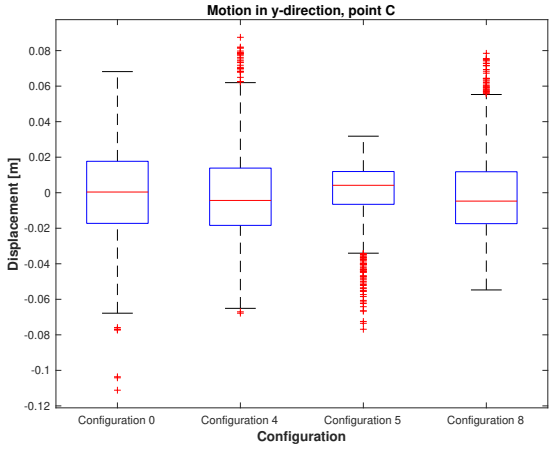

(f) Motion in point C, y-direction.

Figure 5.14: Box plot of motion in tracking points, in x- and y-direction.

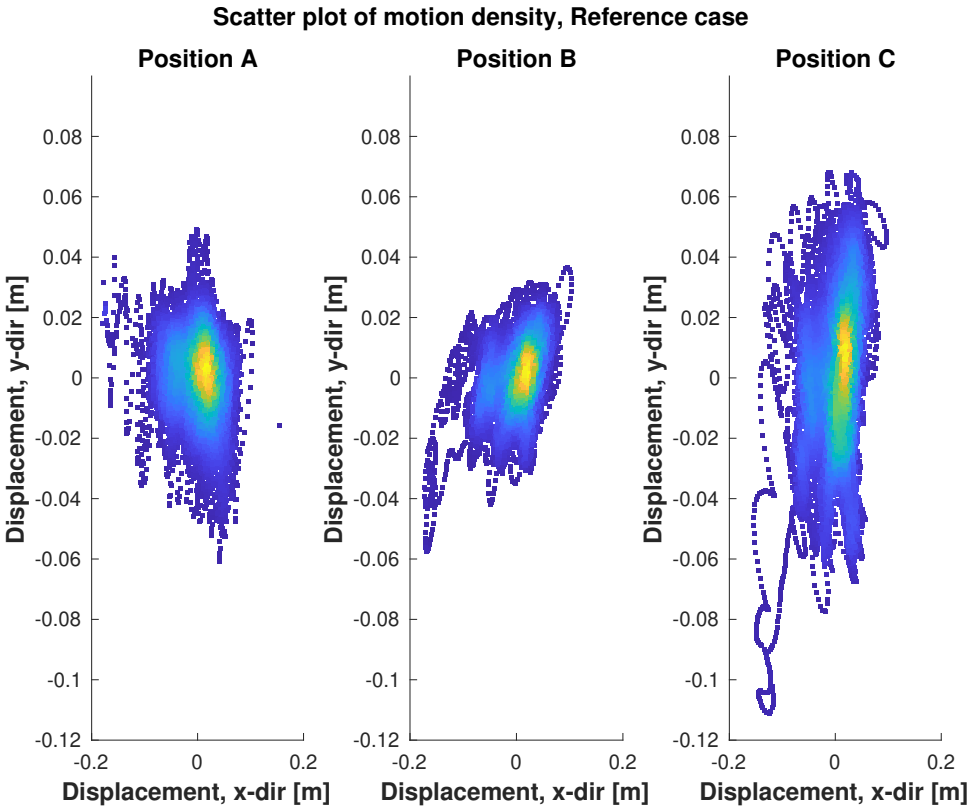

(a) Density scatter plot of movements zero-averaged motion for point A-C on the reference case.

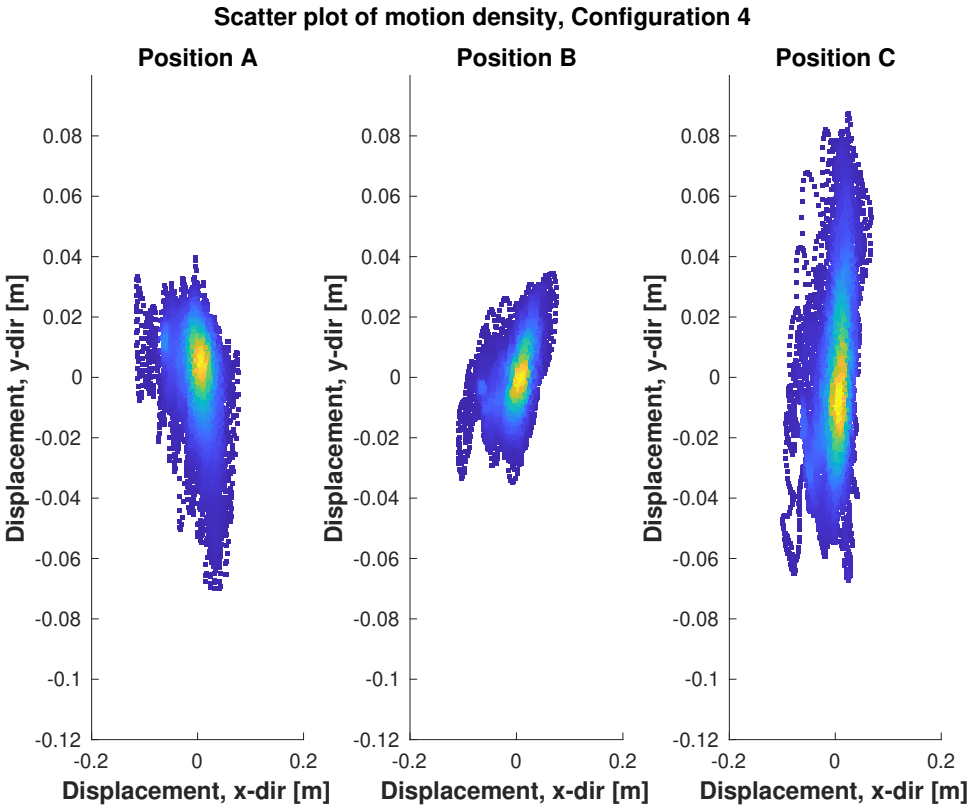

(b) Density scatter plot of movements zero-averaged motion for point A-C on Configuration 4.

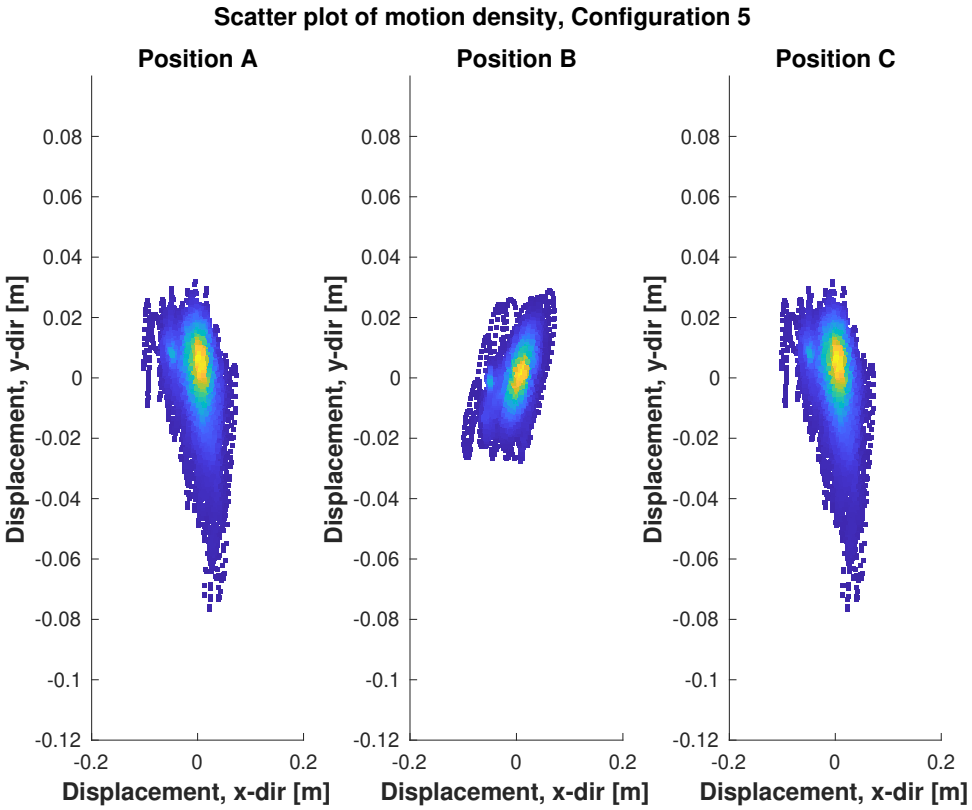

(c) Density scatter plot of movements zero-averaged motion for point A-C on Configuration 5.

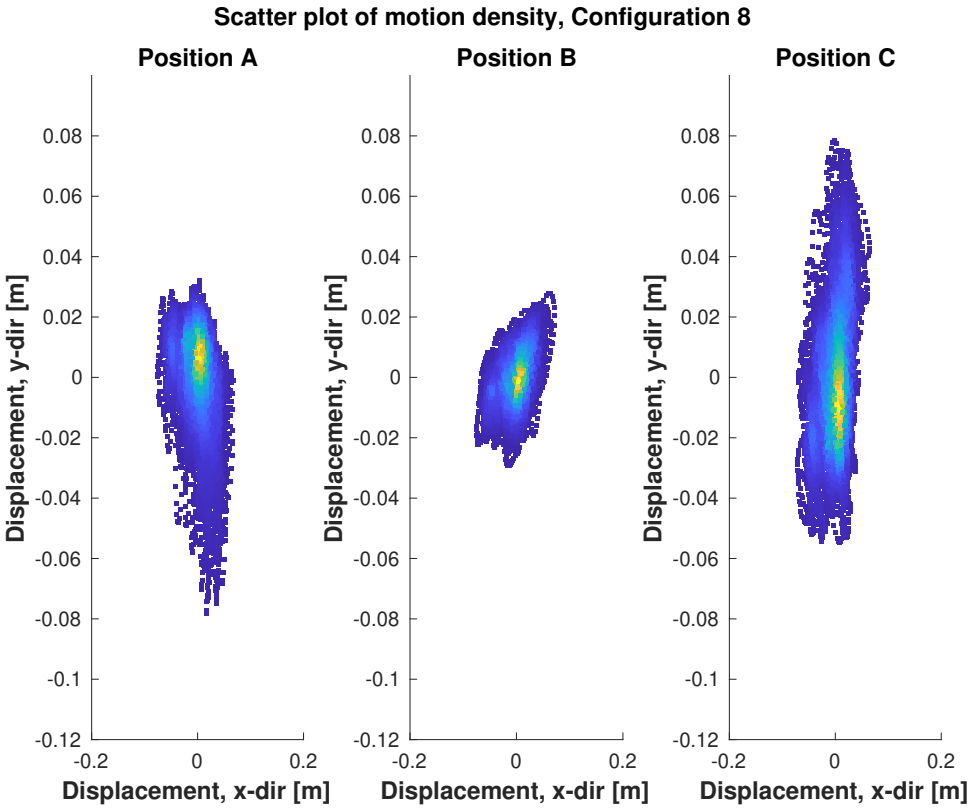

(d) Density scatter plot of movements zero-averaged motion for point A-C on Configuration 9.

Figure 5.15: Density scatter plot of movements from motion tracking of short-moored fixation.

5.5.4 Observations

The system has a higher stiffness due to the mooring system, reflected in the movements of the breakwater. Compared to the long-moored system, there is almost no added weight from the mooring line when the model is pushed by the incoming waves, resulting in quicker rotation and less suspension in the motion extrema, making deceleration visibly faster. However, the flexibility of the load-cell fixation is contributing to a dampening effect of the motion and force extrema. The increase in deceleration was not observed to make significant impact on the hydraulic performance of the model. The movements started circularly with resemblance to observations done with the long-moored tests, explained in Section 5.4.3, followed by a dominating vertical movement as the wavelength became shorter.

Wave breaking observations were, with minor deviances, equal to observations described in Section 5.4.3. Observations of aeration and overtopping were also correlating.

5.6 General discussions

5.6.1 Wave transmission

The ability to dissipate wave energy and stop its propagation is the main purpose of any breakwater. As a result, wave transmission performance is the most important factor to take into account when assessing the overall performance of the breakwater model tests in this study.

Measurements of wave transmission have resulted in data results of satisfying confidence due to few strong deviations. However, substantial errors were presented in section 4.4. Comparisons of different numerical schemes gives few deviations, exemplified by the biggest deviances for the reference case for long-moored fixation, shown in Table 5.5, and contributes to the confidence of the selected numerical schemes and its outputs. As both Njordr and Wavelab uses numerical schemes for reflection analysis, where the recommendation of four gauges makes basis for the validity, error-messages occurred in both programs, thus the preferred numerical method were the zero up-crossing method due to its simplicity (see section 4.1.1.1). The data validating is further discussed in

section 5.6.2, where the output for reflection analysis is displayed compared to each other.

Table 5.5: Incident waves from wave runs with the highest deviances between zero up-crossing analysis and Njordr wave synthesizer for the reference case for long-moored fixation

	Wave height [m]		
Wave run	Zero up-crossing	Njordr	Difference
1	0.0989	0.0918	0.0071
5	0.1029	0.0998	0.0031
10	0.1101	0.1010	0.0091
14	0.1102	0.0966	0.0136

Testing of the inclination of the breakwater shows an increased effect of the wave attenuation performance for the breakwater at lower inclinations. Results originate from semi-rigid tests with regular runs (see Figure 5.6) and irregular runs of long-moored fixations (see Table 5.3). Observations from lower inclinations present more breaking waves, which have a higher dissipation effect due to hydraulic mechanisms than surging waves (Iafrati (2011)). The test scheme did not include horizontal inclination, as the expected effect will change the preliminary terms for the tests. Too low inclination did also result in unwanted horizontal energy transfer to the end of the breakwater during the preliminary testing during the design process, also observed and presented in Section 5.4.3.

Results from related studies presented in Section 2.1 display an advantageous effect from porosity of floating breakwaters. However, these results were not confirmed as only small deviances were discovered in the set-ups with half-rigid fixations (see Figure 5.6), set-up for long-moored fixation (see Figure 5.7) and short-moored fixation (see Figure 5.10). Results from rigid fixation presented a clear result showing a better wave attenuating performance by the porous configuration. These results correlate with the results presented in section 2.1 concerning porous plate breakwaters. These results give two possibilities:

1. Floating, inclined breakwaters *are not* having advantageous effects due to the type of porous surfaces tested in these experiments, but rigid, porous, inclined plate breakwaters have advantageous effects compared to solid slopes.

2. Floating, inclined breakwaters *are* having advantageous effects due to the type of porous surfaces tested in these experiments, similar to the effect displayed in

the testing of a rigid porous breakwater. However, another effect overruns this performance, contributing to wave transmission from the floating breakwater.

Possibility number 1 is not fully rational, as the effect of porosity should not be diminished simply as a consequence of an increase in allowed free body movements of the breakwater model. Due to the observations of similar hydraulic mechanisms for the breaking wave, indicating similar dissipating mechanisms, possibility number one is regarded as a plausible, but unlikely reason for the results displaying less correlating magnitude of transmission coefficient for the two free- and one semi-free floating fixations.

Possibility number 2 can be explained by looking at the free body movement, as this is the most plausible reason for the increased transmission, an assumption also based on the fact that movements are the general weakness of floating breakwaters. Waves are assumed to transmit due to three reasons:

- Wave energy going under the model, due to limitations of model depth.
- Energy going through, in terms of overtopping and water transmission through the model.
- Wave energy transferred to the model, initiating movement, makes the model itself propagate waves, acting as a wave paddle.

Figure 5.16 shows transmission coefficients, C_t, for all fixation set-ups, for the reference case. As the tests allow more movements, transmission increases. In the transition from rigid to semi-rigid fixation, it allows rotation around the ballast and some horizontal movement, while it limits vertical movement of the ballast. The transition leads to a significant increase in long wave transmission. From semi-rigid to short-moored, rotations changes from the ballast to the rotational centre of the free body, while the possibility for horizontal and vertical movements increases. One observes increasing change in transmission for mediocre wave lengths. Transition from short-moored to long-moored leads to increased horizontal and vertical, thus rotational, movement, and an overall increased transmission. Test runs with long waves have the biggest differences in terms of transmission, compared to the rigid fixation, and increased motion leads to increased transmission. Concluding on one specific movement being the main contributor to the increased transmission is not possible based on the data, as neither of the tests isolate

one specific movement. However, due to the inclined bottom of the breakwater, every movement will result in a load transfer to the volume of water underneath the model which has its resultant in the propagation direction of the transmitted wave.

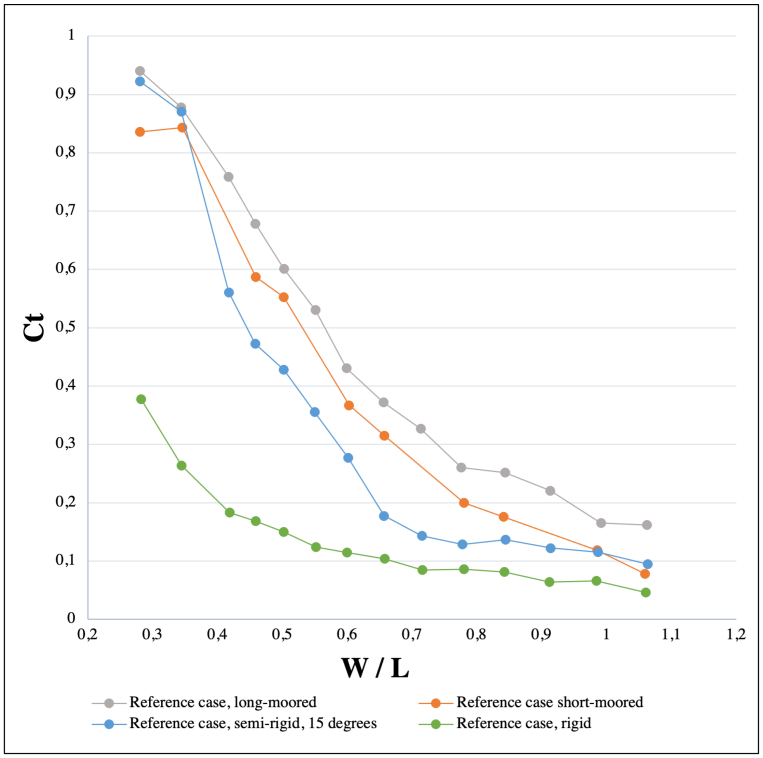

Figure 5.16: All fixation set-ups for the reference case.

The performance of the reference case has a tendency to be among the best in all the tests with fixations allowing motion. This is believed to come from three different reasons. It could be a result due to less surface friction, making the waves break solely because of the slope, and not the surface friction. This can result in less force transmission between the waves and the model, thus resulting in less model movements that propagate waves. As motion tracking reveals generally bigger movements for the reference case, this theory depends on whether certain movements propagate more waves than others, as discussed in the previous paragraph. The ballast- and body weight of the reference case is higher than the other configurations, leading to a lower submersion, lower gravitational centre and increase in the added water mass, thus the required motion-propagating force. The effects combined can reduce the wave propagating movements and lead to a general increase in energy dissipation. The third possibility is that wave breaking mechanisms for the non-porous configuration are dissipating more energy than the combination of wave breaking and porosity related mechanisms for the porous configurations. This is explained

closer in Section 5.6.2.

Alterations to the model that contribute to a decrease in movements will, based on the above discussions, contribute to a decrease of C_t. As the movements are decreasing, tests indicate that porous models will have an increasing positive effect on the wave attenuating performance of the model, compared to solid surfaces. Lower inclination gives higher wave dissipation due to wave breaking, but too low inclination can change the terms of the intended effect from the breakwater.

Comparison to the reference location (see section 3.4.1) are displayed in Table 5.6, where transmission coefficients, C_t, for regular wave runs, long-moored fixation, with corresponding parameters to the reference location are listed. Except for C_t corresponding to the mean period, T_m, the performance of the tested design is poor compared to the breakwater located at the reference location, where the following values for transmission coefficient, C_t, were stated in Section 3.4.1,

$$C_{r,H_s} = \frac{H_{s,inner}}{H_{s,outer}} = 0.17 \tag{5.1}$$

and

$$C_{r,H_{max}} = \frac{H_{max,inner}}{H_{max,outer}} = 0.16. \tag{5.2}$$

Table 5.6: Wave transmission from experimental tests with scaled values corresponding to reference location parameters.

			Transmission coefficient, C_t	
Parameter	Reference location	Scaled values	Reference case	Configuration 5
T_p	5.0 s	1.0 s	0.431	0.450
T_m	3.8 s	0.76 s	0.163	0.158
s_{0,H_s}	0.038	0.038	0.759	0.736
$s_{0,H_{max}}$	0.064	0.064	0.431	0.450

5.6.2 Wave reflection

Measured reflection coefficients, C_r, displayed an unintuitive result, as there were two peaks for C_r (see Figure 5.9 and 5.11). The first peak were located at $W/L = 0.42$, or at

a frequency of 0.800 Hz (run 3). The trend were for all configurations, with the reference case as the averaged less reflective. Low C_r for the reference case were also results from the irregular wave tests, see Table 5.3 and 5.4. The increase resulting in the first peak has 6 possible explanations that can contribute to the trend, where a combination is likely to occur:

1. The output from Njordr, the analytical program used, is affected by the combination of a lower amount of gauges than recommended and the wave conditions in front of the breakwater.
2. A standing wave phenomena occurs at the position of the measuring nodes, contributing to insufficient base of data for the analysis program to interpret.
3. Due to a high wave transmission, the artificial beach in the flume transmits a reflected wave back to the gauges in front of the breakwater.
4. The natural frequency of the breakwater is located within the frequency spectrum where the phenomena occur, leading to an increase in movements for the breakwater.
5. Movement of the breakwater caused by the waves makes the breakwater act as a wave generator, sending waves back towards the incident waves.
6. Incident wave energy is not fully dissipated in the porous chambers, resulting in reflection.

Assessment of the first alternative required testing of different numerical schemes. Long-moored reflection tests were conducted using 3 gauges in the Njordr software, and by using four gauges in the Njord and WaveLab software. Figure 5.17 displays the correlation between the three tests, excluding the alternative. The tests exclude alternative two as well, due to the model being moved towards the artificial beach in order to make room for the fourth gauge. This action will shift the location and occurrence of any standing wave, thus the result rules out the alternative.

Reflection analyses of the artificial wave flume beach (see Figure 5.17) displays a homogenous result significantly lower than the reflection peak assessed from the breakwater tests, hence the results exclude possibility three.

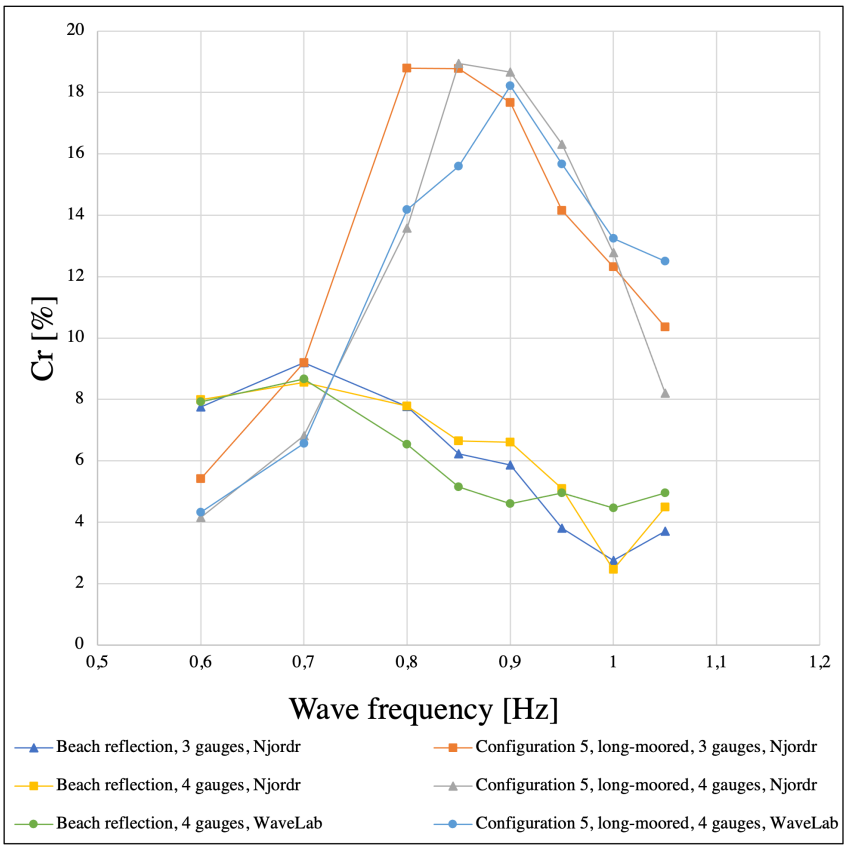

Figure 5.17: Reflection coefficients, C_r, for short-moored tests and wave flume beach using different analysing schemes.

Natural frequency can be estimated, amongst others, conducting physical experiments or using an analytical calculation. Due to slow flow mechanisms around and through the model, physical testing proved to be insufficient as the model simply floated with a stable speed towards its equilibrium state without any resonance indicating a natural frequency, neither in heave nor rotation, when attempted tested within the wave flume. Analytical calculations, based on Fossen (2011), gave a natural frequency of 0.74 Hz for heave and 14.12 Hz for roll. However, simplified calculations results in an insufficient basis for conclusion. Natural frequency in heave direction as an explanation for increased reflection is plausible. Calculations are displayed in Appendix A4.

Model movements are following the circular movement of the wave for lower frequencies, or a low W/L with a uniform vertical movement for the end parts of the model (described in section 5.4.3). As the waves are getting shorter, and the wave breaking are developing from surging to collapsing, the end parts start to displace vertically unsynchronized to each other, an effect strongest for the wave lengths corresponding to the first peak in the

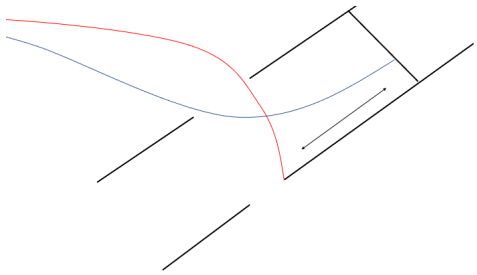

Figure 5.18: Reflection from laminar processes inside chambers.

displayed reflections. The effect is due to shorter wave lengths, and a more concentrated hydraulic pressure from the wave. This indicates that an increase in unsynchronized movements makes a wave propagating effect. Consequently, it is not necessarily reflected waves making the reflection trend registered through tests, but rather a wave directed towards the incident waves, produced by the movements of the breakwater. As the wave breaking develops from collapsing to plunging breaking, more energy is dissipated in the process, and movement and reflection decreases.

Reflection curves from perforated or slotted Jarlan-type breakwaters have tendencies of the same reflection curves as seen in the reflection results for this thesis (Huang et al. (2011), see Figure 2.2. However, neither of the designs of the Jarlan-type breakwaters are representative of the one in this experiment, although the concept of the reflection curves can be applied. The reflection is dependent on the incident and reflected wave phase, and the distance from the perforated plate to the reflecting medium. This can either be the transverse plates between the breakwater chambers or the bottom porous plates reflecting laminar waves or currents coming into the chambers. There can be observed a varying reflection coefficient, C_r, for the rigid fixation, but not as significant as the C_r peak seen for long-moored and short-moored fixation. This effect can be increased by the breakwater body motion, as the transverse wall inside the chambers will be more vertical at the motion extrema. Although this can be a contributing part for the porous model, it is not applicable for the non-porous model. Figure 5.18 illustrates the process.

Tests with rigid fixation displays expected results in terms of reflection coefficient, C_r, based on existing studies (see section 2.1), where the porous breakwater has a lower coefficient than the non-porous model. This correlates to the decreased transmission coefficient, C_t, hypothetically due to the hydraulic dissipating mechanisms observed for the porous configurations. However, the reference case has lower C_r than the other

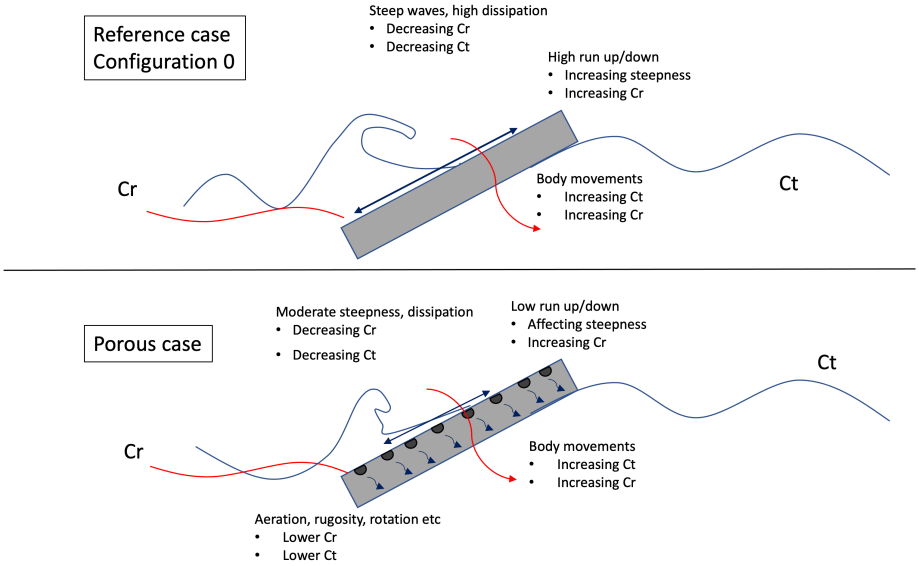

Figure 5.19: Dominate processes during wave breaking.

Table 5.7: Contribution to wave transmission and -reflection.

Process	C_t		C_r	
	Reference	Porous	Reference	Porous
Body movements	+	+	+	+
Run-up/down			(+)	
Wave breaking dissipation	− − −	−−	− − −	−
Porous chambers		−		(−/+)
	−	−	−−	(−/+)

configurations for the tests with fixations that allow motions, at the same time as C_t is equal. Figure 5.19 is an illustration of the domination processes during wave breaking, and Table 5.7 is grading the different contributions. The energy equilibrium requires higher dissipation effect for the non-porous reference configuration in order to present an explanation of the phenomena.

In order to explain the different reflection contributions for the porous and non-porous configurations, the processes will be elaborated separately.

- Body movement is approximate uniform for the two configurations, with correlating decrease as the reflection peak decreases. This explains the overall decrease, but not why the contribution from the non-porous configuration is lower. The motion for this configuration is observed to be slightly higher than for the porous configuration.

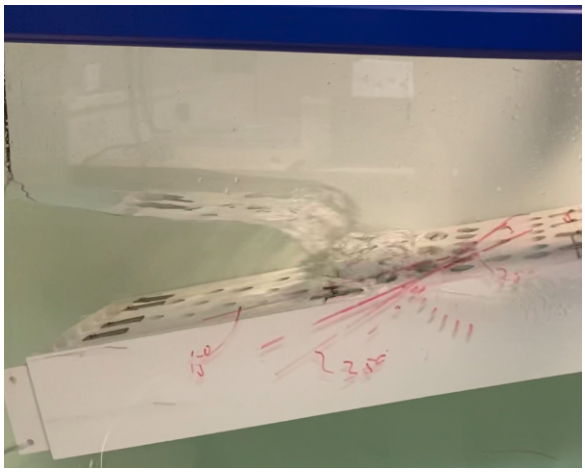

(a) Top position for wave breaking on non-porous plate.

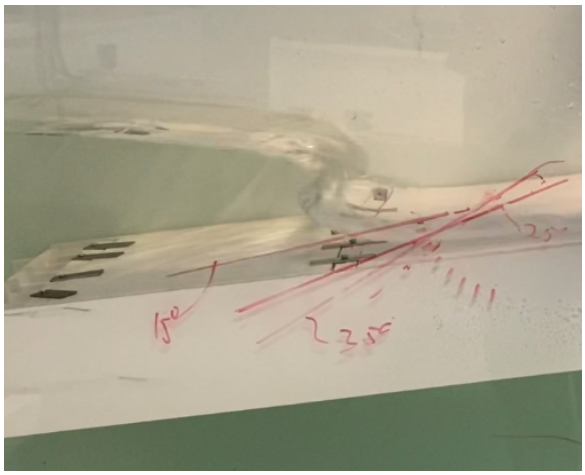

(b) Top position for wave breaking on non-porous plate.

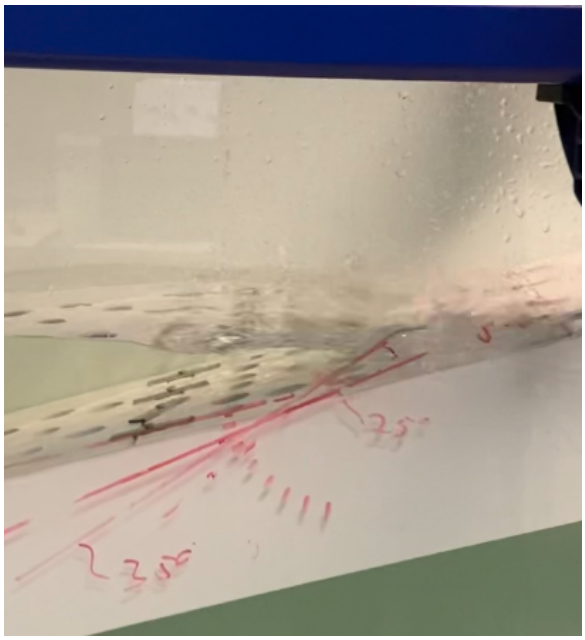

(c) Broken wave on porous plate.

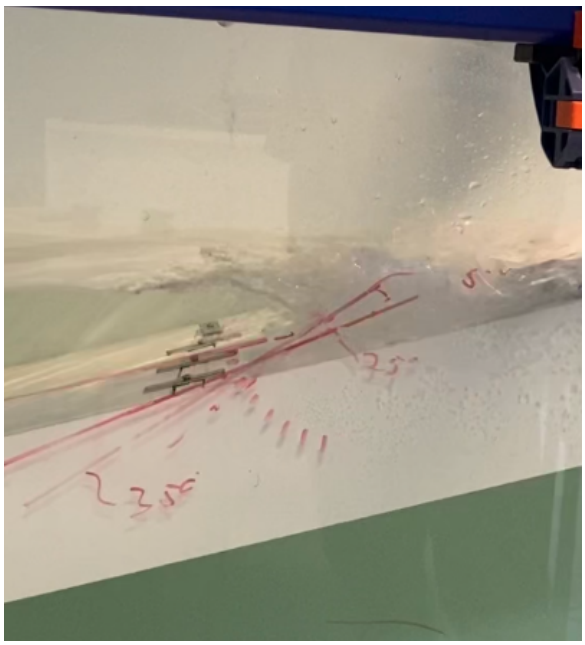

(d) Broken wave on non-porous plate

Figure 5.20: Still-frames from wave breaking on porous and non-porous configurations.

However, the motion response is estimated to be similar, and will not explain the difference.

- Aeration, rugosity, rotation etc., in the porous chambers is expected to decrease the reflection for the porous configurations and give an advantage compared to the non-porous reference configuration based on existing studies (see section 2.1). However, the effect of the process is unclear. Transmission coefficients, C_t, for rigid tests decrease for shorter wave lengths, indicating an increased effect. Reflection coefficient, C_r, for rigid tests are varying compared to each other throughout the whole spectrum of tested waves, making the effect vague. Referring to alternative 6 presented above, about reflection trends similar to Jarlan-type breakwaters, the reflection can also increase due to the chambers. As the foundation in terms of experimental results is weak, no definitive conclusion can be drawn of the porous chambers' contribution of the energy dissipation for the non-rigid configurations. Hence, the contribution is believed to be lower, but the magnitude is very uncertain. The porous chambers are also expected to be the reason for the lower mooring force recorded. A lower mooring force indicates that less energy is transferred to the model, thus more energy is transmitted, reflected or dissipated in the chambers.

- The run-up/down, R_u/R_d for the porous configurations are not extensive, and gives a low contribution to both incident wave steepness increase and wave reflection. This process is stronger for the non-porous configuration. R_d is visibly increasing the steepness of the incident wave. It is also believed to contribute to some wave reflection. Rockmanual (2007) presents methods for run-up calculations, presented in section 3.2.

- The wave breaking is visibly stronger for the non-porous configuration due to the higher wave steepness. The breaking process is dominated by the processes linked to surrounding air, surface tension and viscous dissipation, not the friction towards the slope, due to the low rugosity of the non-perforated PVC-plates. Wave breaking mechanisms are described in Section 3.1. Figure 5.20 shows still-frames from the wave breaking for the non-porous and the porous configuration. As displayed, the non-porous configuration contributes to a higher wave height during breaking and more aerated and turbulent water after the wave is broken. The wave breaking

dissipation for the non-porous configuration is believed to be of a higher benefit for the magnitude of reflected wave than for the non-porous configuration.

The second peak is based on other parameters than the first. Wavelength are significantly shorter and steepness increased. Observations of the conducted tests describes how a uniform plunging breaking process is dominant for all cases, a plunging distributed over a relative short time due to the input wave parameters of high frequency, or high W/L. The movement in the breakwater is observed to be relative small and measured C_t is small. Force measurements reflect how the mooring line is in constant stress, preventing the model from retracting, but the stress is not increasing as C_r increases. These factors make the model resemble a traditional fixed beach, where we can simplify the wave breaking dissipation to be uniform for the highest frequencies, or highest W/L. As the wave energy is dissipating during the breaking process, a decreasing amount of energy is transmitted to movement and transmission. As the wave height is uniform, it is evident that the energy equilibrium must be stabilized by an increase in reflected wave energy as the other processes decreases.

The reflection trends are the output results from this study that have the highest degree of uncertainty. However, the reflection performance of the breakwater does not degrade the overall performance of the model. The reflection coefficient is relatively low compared to conventional breakwaters (Jarlan, 1961) and other floating breakwaters presented in the literature search (Wang and Sun, 2010; Shih, 2012; Ji et al., 2019). Even though, the processes leading to the reflection trends must be analysed in order to understand the behaviour of the different model parameters. Future experiments should investigate the effects more closely. As a remedy to the uncertainties, the following experiments are recommended.

- Rigid testing using other porosities in order to isolate the effect of a porous model.
- Rigid testing using other inclinations to investigate the effect of the porosity compared to angle.
- Testing using a fixation-rig that allows only one of the following motions: rotation around the rotational centre, horizontal displacement and vertical displacement, in order to isolate the contributing effect of each movement.

- Rough surface of the non-porous model to investigate solely the effect of reduced R_u and R_d.

5.6.3 Wave breaking mechanisms

Wave breaking has been varying dependent on fixation and configurations, described in the observations for the tests conducted. Table 5.8 displays wave steepness and Irribarren number, explained in Section 3.1, for the regular wave runs. Referring to Figure 3.1, there should have been observed plunging and breaking earlier in the wave runs used in the conducted tests. As the inclination decreases during wave impact, further breaking should have been observed. However, this has not been the case in the tests where the model has had a horizontal degree of freedom. Breaking mechanisms were weakened due to horizontal movement, which suspended the impact force towards the wave. As a result, breaking criteria according to Battjes (1974) are considered inapplicable for wave breaking mechanisms towards a free floating beach with allowed horizontal movements. Observations also indicate that the porosity has an impact on the validity of the theory. Wave breaking criteria were applicable for the rigid fixation tests.

Table 5.8: Steepness and Irribarren number for regular wave runs and different inclinations.

			Irribarren number			
Wave run	Period [s]	Frequency [Hz]	Steepness	15 degrees	25 degrees	35 degrees
1	1.67	0.60	0.023	1.76	3.07	4.61
2	1.43	0.70	0.031	1.51	2.63	3.95
3	1.25	0.80	0.041	1.32	2.30	3.46
4	1.18	0.85	0.046	1.25	2.17	3.26
5	1.11	0.90	0.052	1.18	2.05	3.07
6	1.05	0.95	0.058	1.11	1.94	2.91
7	1.00	1.00	0.064	1.06	1.84	2.77
8	0.95	1.05	0.071	1.01	1.75	2.64
9	0.91	1.10	0.077	0.96	1.68	2.52
10	0.87	1.15	0.085	0.92	1.60	2.41
11	0.83	1.20	0.092	0.88	1.54	2.31
12	0.80	1.25	0.100	0.85	1.47	2.21
13	0.77	1.30	0.108	0.81	1.42	2.13
14	0.74	1.35	0.117	0.78	1.36	2.05

5.6.4 Mooring forces

Porosity leads to a decrease in average mooring forces, as well as lower force amplitude for longer wave lengths. Average wave force increased as the wave length decreased, but force amplitude decreased. Lower mooring force correlates with the movement of different breakwater configurations, where porous configurations have lower motions than the non-porous configuration (previously discussed in section 5.6.1 and 5.6.2). Mooring forces and mooring systems are not one of the main scopes of this thesis, hence more in-depth tests were not conducted. However, mooring system is of significance, and existing studies have published results where reduced mooring forces for porous structures are documented (e.g. Wang and Sun (2010) and Ji et al. (2016), presented in 2.1). Tests of mooring forces correlated with expectations based on these results. Alternative mooring systems are briefly discussed in Section 5.8.5. As the mooring forces reduces, less anchorage systems are required, as well as lower requirements for mooring line dimensions and connections. This will lead to increased durability and survivability when facing extreme weather conditions. However, due to relatively large movements by the breakwater, the system is prone to high frequency stress cycles, as shown in Figure 5.13. This increases the risk for fatigue in the mooring system, especially in connections. Preventive measures and design alterations should be done according to the risk.

5.7 Aqua cultural performance

The aqua cultural performance of the breakwater cannot be concluded without conducting biological testing in a marine environment similar to the projected localization for the prototype. However, as presented in Section 2.2, several physical details and responses can be observed and designed in order to adapt to previous studies.

5.7.1 Sheltering for fish and other marine species

As the model were of a basic design in this experiment, while focussing on wave attenuating features, no detailed sheltering designs were done. However, by observing the behaviour of the body movements and the hydraulic flow, we can see potential for locations for shelter structures.

- 3D-structures can be built on the bottom of the breakwater. There is limited current action from the middle of the body and downwards, allowing structures to be built without being too impacted by external forces. However, there is a limitation in terms of sunlight (Hadary et al., 2022).
- Oyster cages on the surface of the breakwater will have access to sunlight, facilitate oyster growth and could have wave attenuating qualities, but could also improve the flow conditions (Hadary et al., 2022).
- The inside of the breakwater chambers will act as shelters for marine species. With the three-chambers design as used in the presented design, there are three different hydraulic conditions in the chambers. Different species will be able to find habitat in the different flow regimes, suitable for its preferences. 3D-patterns and constructed shelters inside the chambers are a solution that will impact both the conditions for marine species and hydrodynamic flow. Depending on the surface design, there will be realistic solutions for sustainable sunlight conditions.

5.7.2 Aeration

As observations describe, aeration around the breakwater is present due to porosity and overtopping. As a remedy for decrease in dissolved oxygen (Grundvig et al., 2014), breakwater movement due to waves will act as a mechanical paddle. This can facilitate better conditions for adjacent infrastructure, like fish farms, as well as facilitate marine growth on the structure itself.

5.7.3 Low-depth habitat in deep water

The breakwater can be used for protection of fish farms, an infrastructure often placed in deep waters. As presented in Section 2.2.2, low-depth species, like the fish species lumpsuckers, can be used in the installations to prevent salmon lice. As a remedy for a huge yearly loss of the deployed fish (Stranden, 2021), the presented model can be used as a habitat for the escaped fish. Due to the placement of the breakwater, a low-depth marine ecosystem is likely to form, especially if facilitated with deployed species from such an existing ecosystem.

5.8 Alternative design solutions

As this thesis is presenting an experimental work with a specific time limit, design testing and its development had to be terminated in order to assure the tests conducted had a satisfying quality. The following paragraphs are design considerations that did not become a part of this thesis.

5.8.1 Aquaculture ropes

Trailing ropes is a design proposal with both bio enhancing, and wave dissipative, advantages. As the effect of mussel ropes (Rinde et al., 2019), general surface growth (Hadary et al., 2022) and free floating habitats (Perkol-Finkel et al., 2006) were presented, this is a design that has the potential to facilitate growth, water cleansing and weight, as well as manipulate drag forces. The added weight and drag forces are very likely to have an effect on the behaviour of the model. Added chain on a sloping breakwater has been shown to improve performance (Sohrabi et al., 2021). The proposed design might contribute to decreased upwards movements due to increased drag force, decreased influence from low energy waves due to added weight and decrease of current transfer underneath the breakwater. Different applications for aquaculture ropes and nets are shown in Figure 5.21.

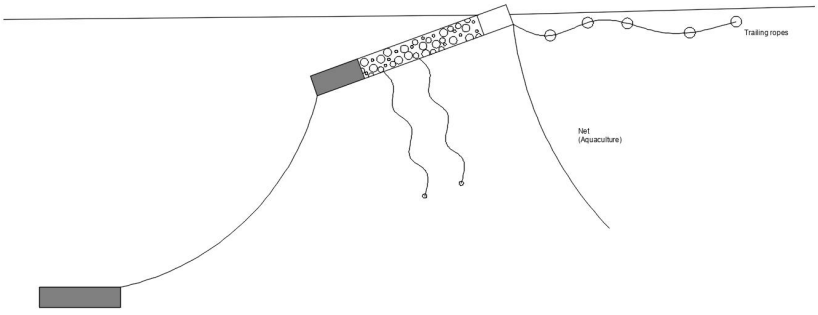

Figure 5.21: Design proposal with aquaculture ropes

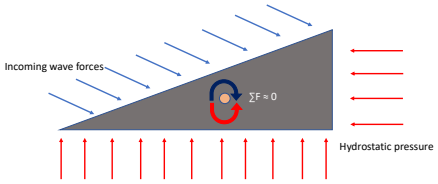

Figure 5.22: Simplified free-body force diagram for triangular design

5.8.2 Triangular design

The initial design discussions altered between a rectangular and triangular design. A triangular design will have advantages and disadvantages compared to the rectangular design, and should be tested in order to compare the results.

As discussed in Section 5.6.1 and 5.6.2, the rectangular design has a rotating movement that displaces water and causes wave propagation. As the backside and bottom of a triangular design are perpendicular and aligned with the water surface, the displacement of water during rotation of the model will be significantly smaller. Additionally, the rotational movement is likely to be reduced as the rotational centre during wave action will be impacted by a higher amount of opposing forces, illustrated in Figure 5.22, reducing the expected dominating degrees of freedom in the 2D-plane to two; heave and sway.

The inclination of a triangular design will not be possible to alter with a basic design. The inclination will as well, opposite to the rectangular design, have a more rigid position as incoming waves are hitting the model, due to the reduced rotation compared to the rectangular model. Hence, it will require less testing to find the ideal inclination, and design can more easily be based on previously studies with inclined plates, described in Section 2.1.

5.8.3 Direction chambers

As discussed in Section 5.6.1 and 5.6.2, wave propagation in both directions from the model is strongly connected to the model movements. To reduce the model-movement propagated wave in the transmitted direction, direction chambers are a proposed design. These will prevent the displaced water from propagating, and rather push it backwards,

through the model and towards the next round of incident waves. See illustration in Figure 5.23.

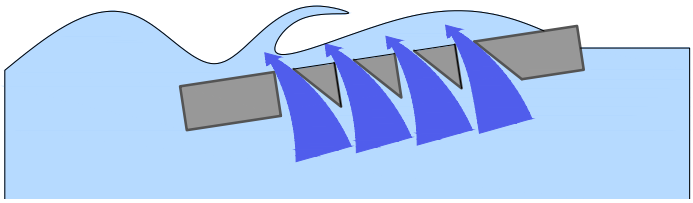

Figure 5.23: Direction chambers.

5.8.4 3D-pattern

3D-pattern were briefly tested in the experiments. but are likely to have multiple other layouts. As shown in Figure 5.24, hydraulic responses as eddies and aeration were observed. This response should be further manipulated by changing the layout in order to find advantageous configurations. Suggestions for designs are shown in Figure 5.25.

5.8.5 Mooring system

Two mooring systems are prospected for the model in the 2D-plane. For a full-scale prototype, systems to prevent rotation might also be necessary. One mooring system works in the windward direction, holding the breakwater in its place. The other mooring system is in the leeward direction, with the purpose of holding the breakwater in its place in the case of waves or currents from the opposite direction. It might also be a desired effect that the leeward directed mooring system is pulling the breakwater under the water in the case of heavy load from currents and waves incident from the unfavourable direction. This type of mooring system can also contribute to a reduction in horizontal movements, thus potentially enhancing the performance of the breakwater. A proposition for mooring system is displayed in Figure 5.26. Furthermore, several published articles are studying mooring systems, and further investigation is recommended for future work.

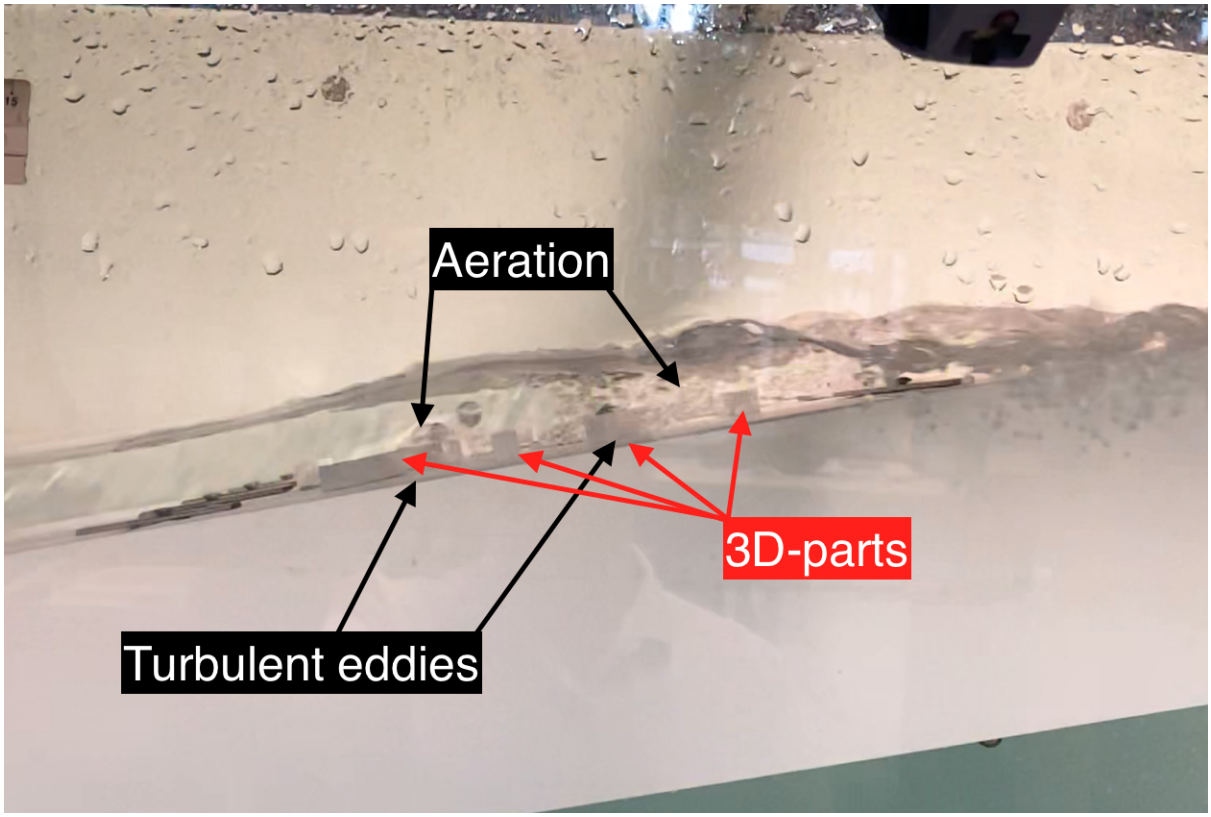

Figure 5.24: Hydraulic responses due to 3D-structure.

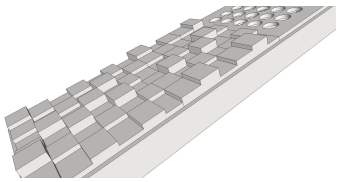

(a) Irregular 3D-pattern

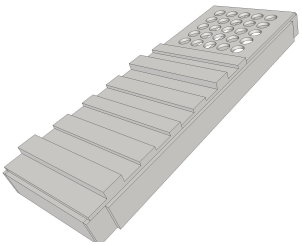

(b) Transverse 3D-structure

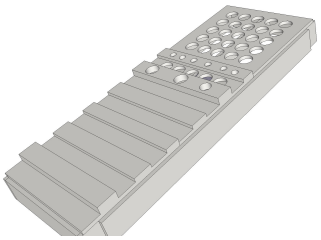

(c) Transverse 3D-structure, with extra porosity

(d) Irregular 3D-pattern, with extra porosity

Figure 5.25: Design alternatives for surface 3D-structure

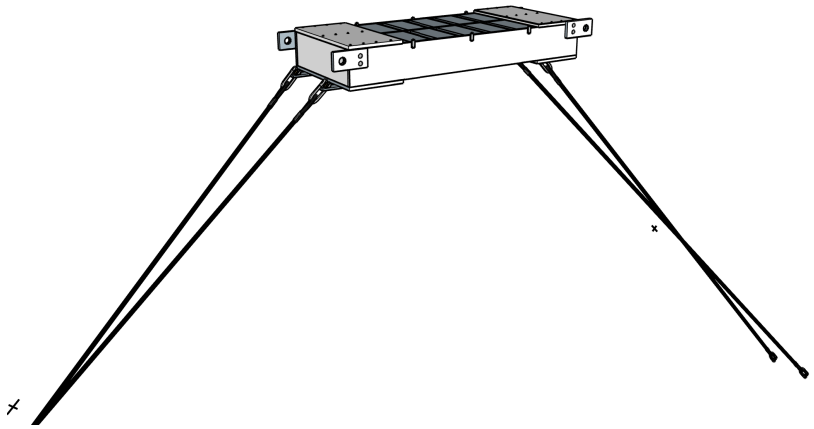

Figure 5.26: Proposed mooring system.

6 Conclusions and Recommendations for future work

6.1 Conclusions

In this Master thesis, the aim was to develop a new design of a floating breakwater, while enhancing biodiversity and aquaculture by conducting a literature search and experimental studies of the proposed design.

A literature search of state-of-the-art examples for combined perforated, floating and inclined breakwaters did not give any results, but performance and details for the following types of breakwaters were presented: one type of perforated solid breakwaters, several inclined, porous plate breakwaters, several porous floating breakwater and one inclined floating breakwater, as well as other design with interest for the study. Main findings were a reduced transmission- and reflection coefficient, mooring load and body movement for the porous floating breakwaters. Special considerations for floating coastal structures and enhancement of marine biodiversity were presented.

Experimental studies of one inclined, non-porous reference case and 8 inclined, porous configurations were conducted, with four different fixation types exposed to regular and irregular waves. Different parameters were analysed, where the main findings are described below:

- **Wave transmission** is, for a fixation that allows model movements, found to be decreased due to inclination, shorter wavelengths, more rigid fixations and for certain porous configurations exposed to an irregular wave state. The trend for transmission coefficient for configurations exposed to regular waves showed an inconsiderate difference when comparing the non-porous reference case to porous configurations.

  Results from the rigid fixation revealed an increased effect in terms of reduced wave transmission for the porous configuration, both for regular and irregular waves.

  Comparisons to an existing breakwater on a reference location revealed a poorer performance for the inclined breakwater based on transmission coefficient.

- **Wave reflection coefficient** for the moored fixations in regular waves, had one peak for $W/L = 0.42$, before decreasing to $W/L = 0.78$ and increasing again for the rest of the test scheme. The non-porous reference case had the best performance.

  For the fixed fixation, for both regular and irregular waves, the porous fixation had a lower refection coefficient.

  Results from tests with irregular runs on moored fixations displayed homogenous results for the non-porous and porous configurations, and an increased reflection due to increased inclination.

- **Body motions** were found to decrease for porous configurations, correlating with a decreased **mooring force**, for both regular and irregular wave runs. Long wave lengths gave a lower average mooring force, but higher force amplitudes, while average mooring force increased and amplitude decreased as wave lengths shortened. The decreased motions and mooring forces will contribute to an increased durability and better survivability when facing extreme weather conditions.

- **Wave breaking** were an important parameter explaining trends in transmission, reflection, body motions and mooring forces, and inclination were a leading parameter when manipulating the breaking mechanisms.

- Observations of the processes inside, and around, the breakwater indicated potential for **eco-engineering** that contribute to **biodiversity enhancement**. **Aeration** of the surrounding water were enhanced by porosity and overtopping, giving a clear oxygenation of the water. **Current actions** in the internal chambers of the breakwater can be adapted to different species, and colonization of marine species on the breakwater can improve its performance by contributing to increased surface rugosity.

6.2 Recommendations for Future Work

- Breakwater body motions has been regarded as a main contributor to wave transmission and -reflection. Isolating motions to vertical, horizontal and rotational around the rotational centre will reveal whether certain motions contribute more than others. Testing of rigid fixation with different inclinations should be conducted

in order to assess the breaking, transmission and reflection performance.

- Further developments on the design are recommended in terms of surface rugosity, trailing ropes, directional chambers, triangular design and alternative mooring systems. Isolation of each effect should be conducted. Motion manipulating designs are recommended to be prioritized.
- A thorough in-situ biological study should be conducted on a reference location based on the current, aeration and physical conditions displayed from experimental results in order to investigate the potential for the breakwater to act as a floating artificial reef.
- Testing of the design in a bigger wave flume is recommended in order to investigate the wave propagation in front and in the back of the model, with higher accuracy.

References

Andersen, T. L., Eldrup, M. R., and Frigaard, P. (2017). Estimation of incident and reflected components in highly nonlinear regular waves. *Coastal Engineering*, 119:51–64.

Battjes, J. A. (1974). Computation of set-up, longshore currents, run-up and overtopping due to wind-generated waves.

Bayram, A. (2000). Experimental study of a sloping float breakwater. *Ocean Engineering*, 27:445–453.

Behera, H. and Ng, C.-O. (2017). Oblique wave scattering by a system of floating and submerged porous elastic plates.

Brown, D., Christian, W., and Hanson, R. (2022). Tracker. https://www.hydrosoft.civil.aau.dk/wavelab/ [Accessed: 2022-05-07].

Cho, I. and Kim, M. (2013). Transmission of oblique incident waves by a submerged horizontal porous plate. *Ocean Engineering*, 61:56–65.

Christakos, K., Björkqvist, J.-V., Tuomi, L., Furevik, B. R., and Breivik, Ø. (2021). Modelling wave growth in narrow fetch geometries: The white-capping and wind input formulations. *Ocean Modelling*, 157. Article 101730.

Christakos, K., Varlas, G., Cheliotis, I., Spyrou, C., Aarnes, O. J., and Furevik, B. R. (2020). Characterization of wind-sea-and swell-induced wave energy along the norwegian coast. *Atmosphere*, 11(2):166.

Christensen, E. D., Bingham, H. B., Friis, A. P. S., Larsen, A. K., and Jensen, K. L. (2018). An experimental and numerical study of floating breakwaters. *Coastal Engineering*, 137:43–58.

CIRIA/CUR/CETMEF (2007). *The rock manual: the use of rock in hydraulic engineering*, volume 683. Ciria.

EdinburghDesigns (2016). Edinburgh designs. http://www4.edesign.co.uk [Accessed: 2022-02-10].

Firth, L., Thompson, R., Bohn, K., Abbiati, M., Airoldi, L., Bouma, T., Bozzeda, F., Ceccherelli, V., Colangelo, M., Evans, A., et al. (2014). Between a rock and a hard place: environmental and engineering considerations when designing coastal defence structures. *Coastal Engineering*, 87:122–135.

Fossen, T. I. (2011). *Handbook of marine craft hydrodynamics and motion control*. John Wiley & Sons.

Google (2021). Google scholar. https://scholar.google.com [Accessed: 2021-12-15].

Google Maps (2022). Google maps. https://maps.google.com [Accessed: 2022-05-17].

Grundvig, H., Bergheim, A., Makridis, P., and Gausen, M. (2014). Diffused-air system improves oxygen levels in sea cage culture. *Global Aquaculture Advocate*.

Hadary, T., Martínez, J. G., Sella, I., and Perkol-Finkel, S. (2022). Eco-engineering for climate change—floating to the future. In *WCFS2020*, pages 409–421. Springer.

Hanssen-Bauer, I., Drange, H., Førland, E., Roald, L., Børsheim, K., Hisdal, H., Lawrence, D., Nesje, A., Sandven, S., Sorteberg, A., et al. (2015). Klima i norge 2100. *Bakgrunnsmateriale til NOU Klimatilpassing., Norsk klimasenter, Oslo, Norway*.

Huang, Z., Li, Y., and Liu, Y. (2011). Hydraulic performance and wave loadings of perforated/slotted coastal structures: A review. *Ocean Engineering*, 38(10):1031–1053.

Hughes, S. A. (1993). *Physical models and laboratory techniques in coastal engineering*, volume 7. World Scientific.

HydraWiki (2019). Wave gauge calibration. http://wiki.hydralab.eu/index.php?title=Wave_Gauge_Calibration [Accessed: 2022-02-10].

Iafrati, A. (2011). Energy dissipation mechanisms in wave breaking processes: spilling and highly aerated plunging breaking events. *Journal of Geophysical Research: Oceans*, 116(C7).

IPCC (2022). Climate change 2022: Impacts, adaptation, and vulnerability. contribution of working group ii to the sixth assessment report of the intergovernmental panel on climate change. http://pure.iiasa.ac.at/id/eprint/17819/ [Accessed: 2022-05-04].

Jarlan, G. (1961). A perforated vertical wall breakwater. *The Dock and Harbour Authority*, (486):394–398.

Jensen, J., Svendsbøe, R., Thom, P., Fransson, M., and Edvardsen, E. (2018). *Molohandboka*, volume 1. Kystverket.

Ji, C.-Y., Bian, X.-Q., Cheng, Y., and Yang, K. (2019). Experimental study of hydrodynamic performance for double-row rectangular floating breakwaters with porous plates. *Ships and Offshore Structures*, 14(7):737–746.

Ji, C.-Y., Chen, X., Cui, J., Gaidai, O., and Incecik, A. (2016). Experimental study on configuration optimization of floating breakwaters. *Ocean Engineering*, 117:302–310.

Koftis, T. and Prinos, P. (2005). On the hydrodynamic efficiency of floating breakwaters. In *Arabian Coast Conference*.

Kundu, S., Gayen, R., and Datta, R. (2018). Scattering of water waves by an inclined elastic plate in deep water. *Ocean Engineering*, 167:221–228.

Lin, C.-Y. and Huang, C.-J. (2004). Decomposition of incident and reflected higher harmonic waves using four wave gauges. *Coastal engineering*, 51(5-6):395–406.

Mansard, E. P. and Funke, E. (1980). The measurement of incident and reflected spectra using a least squares method. In *Coastal Engineering 1980*, pages 154–172.

MathWorks (2022). Lowpass filter design in matlab. https://www.mathworks.com/help/dsp/ug/lowpass-filter-design.html [Accessed: 2022-02-05].

Meylan, M. H., Bennetts, L. G., and Peter, M. A. (2017). Water-wave scattering and energy dissipation by a floating porous elastic plate in three dimensions. *Wave Motion*, 70:240–250.

Misund, B. (2021). Fiskeoppdrett. Store norske leksikon, https://snl.no/fiskeoppdrett [Accessed: 2022-05-06].

Norconsult (2017). Resultater fra bølgemåling.

Oliver, J., Aristhages, P., Cederwall, K., Davidson, D., and Graaf, F. (1994). *Floating Breakwaters: A Practical Guide for Design and Construction*, volume 85. Pianc.

Perkol-Finkel, S., Zilman, G., Sella, I., Miloh, T., and Benayahu, Y. (2006). Floating and fixed artificial habitats: effects of substratum motion on benthic communities in a coral reef environment. *Marine Ecology Progress Series*, 317:9–20.

Rao, S., Shirlal, K. G., Varghese, R. V., and Govindaraja, K. (2009). Physical model studies on wave transmission of a submerged inclined plate breakwater. *Ocean Engineering*, 36(15-16):1199–1207.

Rinde, E., Sørensen, E. T., Walday, M. G., Christie, H., Staalstrøm, A., Barkved, L. J., Simmons, H., Borchgrevink, H. B., et al. (2019). Reetablering av biologisk mangfold i oslos urbane sjøområder. Norsk institutt for vannforskning.

Røge Eldrup, M. and Lykke Andersen, T. (2019). Estimation of incident and reflected wave trains in highly nonlinear two-dimensional irregular waves. *Journal of Waterway, Port, Coastal, and Ocean Engineering*, 145(1). 04018038.

Shih, R.-S. (2012). Experimental study on the performance characteristics of porous perpendicular pipe breakwaters. *Ocean engineering*, 50:53–62.

Sohrabi, S., Lotfollahi Yaghin, M. A., Aminfar, M. H., and Mojtahedi, A. (2021). Experimental and numerical investigation of hydrodynamic performance of a sloping floating breakwater with and without chain-net. *Iranian Journal of Science and Technology, Transactions of Civil Engineering*, pages 1–13.

Stranden, A. (2021). Hvert år dør 50 millioner rensefisk i norske oppdrettsanlegg. Forskning.no, https://forskning.no/fisk-fiskehelse-fiskesykdommer/hvert-ar-dor-50-millioner-rensefisk-i-norske-oppdrettsanlegg/1627630 [Accessed: 2022-05-06].

Teh, H. and Ismail, H. (2013). Hydraulic characteristics of a stepped-slope floating breakwater. In *Proceedings of the 4th International Conference on Energy and Environment ICEE*, pages 1–4. IOP publishing.

WaFo (2017). Wafo. https://www.maths.lth.se/matstat/wafo/ [Accessed: 2022-02-05].

Wang, H. and Sun, Z. (2010). Experimental study of a porous floating breakwater. *Ocean Engineering*, 37(5-6):520–527.

Wavelab (2019). Wavelab. https://www.hydrosoft.civil.aau.dk/wavelab/ [Accessed: 2022-05-02].

Zelt, J. and Skjelbreia, J. E. (1993). Estimating incident and reflected wave fields using an arbitrary number of wave gauges. In *Coastal Engineering 1992*, pages 777–789.

Appendix

A1 Wave flume

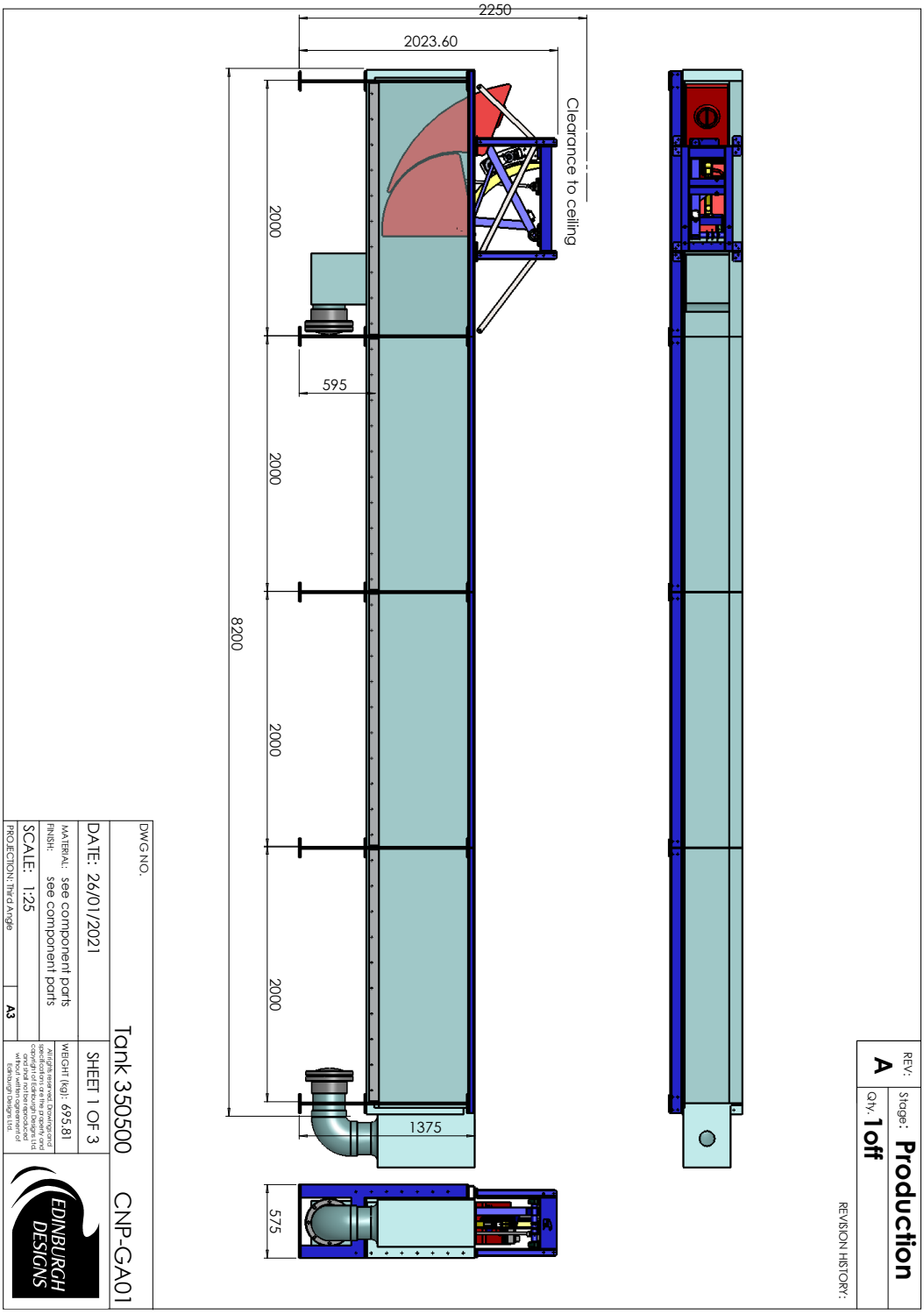

Figure A1.1: Wave Tank at ESITC.

REV:	Stage: **Production**
A	Qty.

REVISION HISTORY:

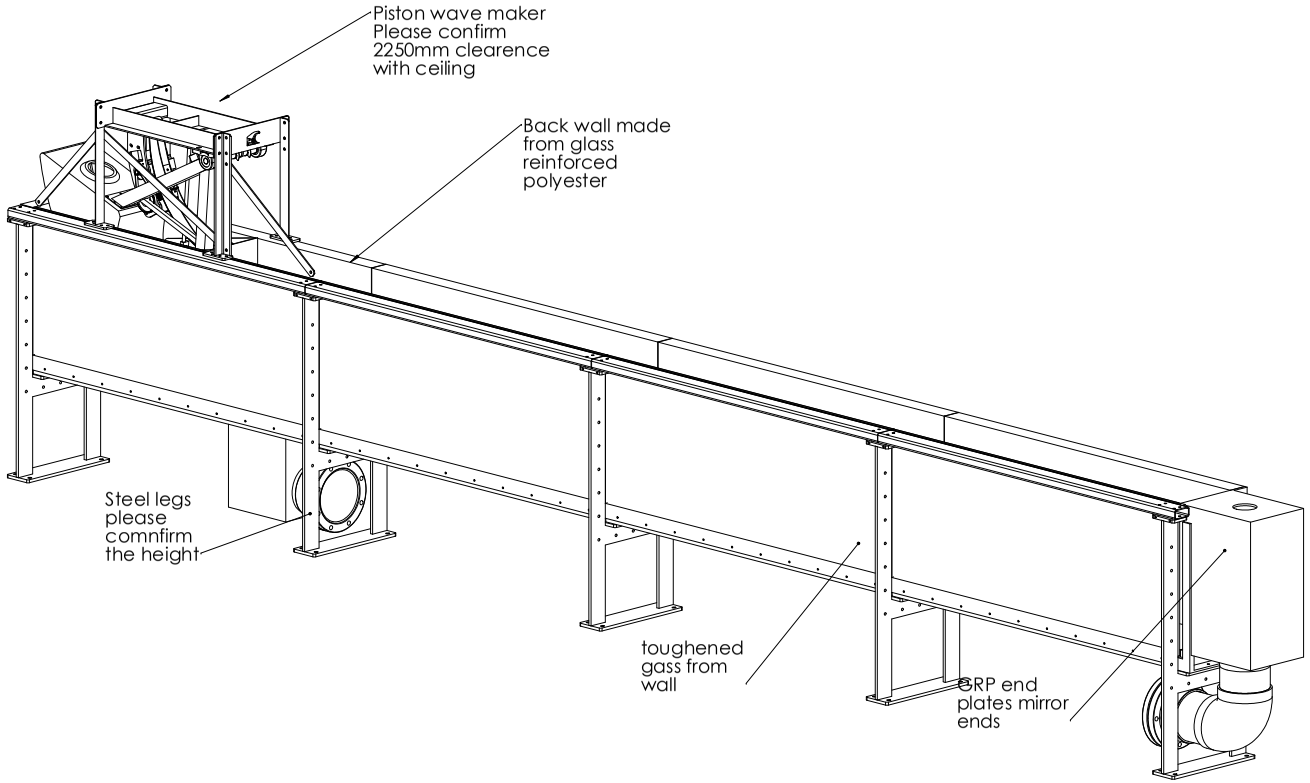

DWG NO.	Tank 350500	CNP-GA01
DATE: 26/01/2021	SHEET 2 OF 3	
MATERIAL: see component parts FINISH: see component parts	WEIGHT (kg): 695.81	
SCALE: 1:50		EDINBURGH DESIGNS
PROJECTION: Third Angle **A3**		

REV:	Stage: **Production**
B	Qty.

REVISION HISTORY:

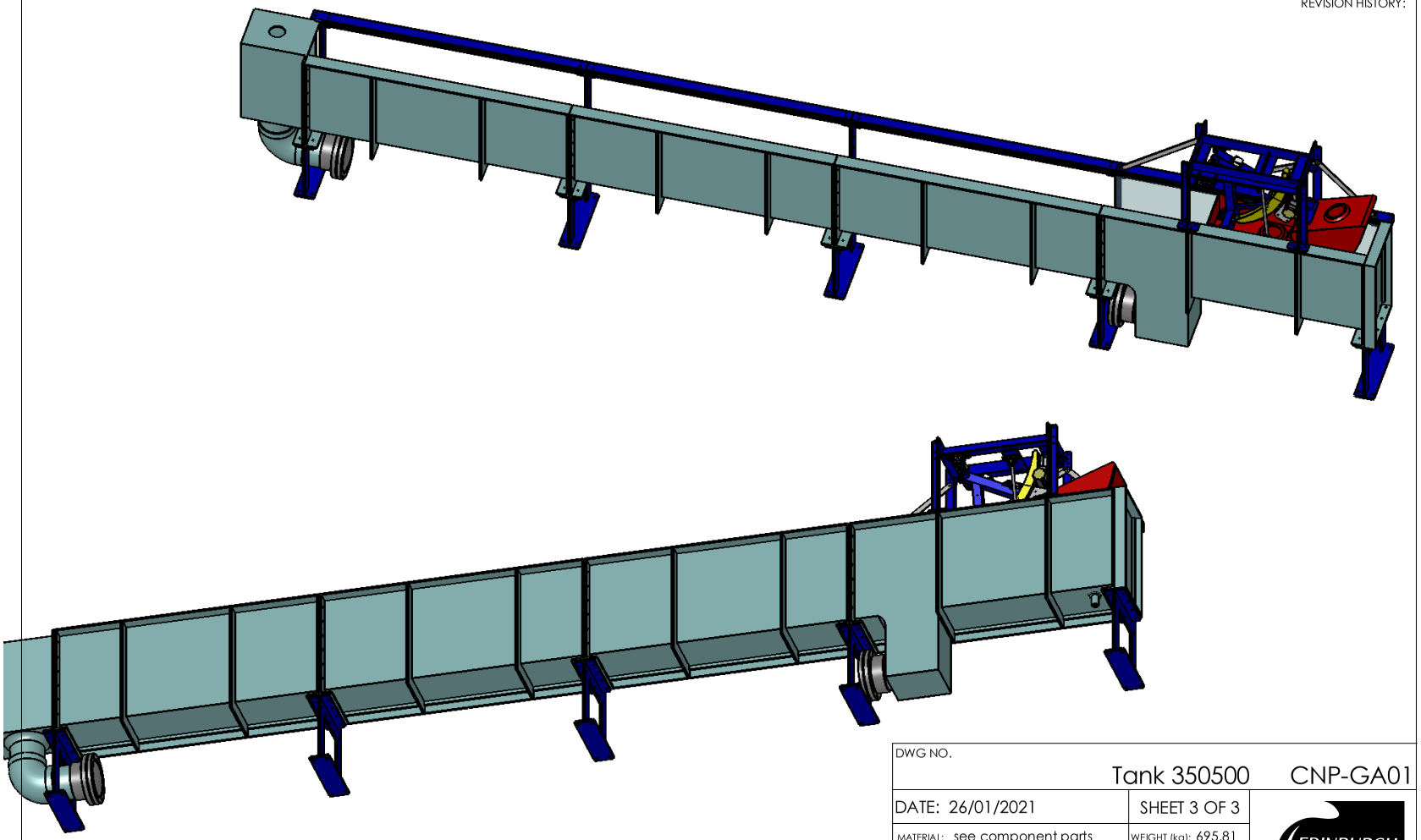

DWG NO.	Tank 350500	CNP-GA01
DATE: 26/01/2021	SHEET 3 OF 3	
MATERIAL: see component parts FINISH: see component parts	WEIGHT (kg): 695.81	
SCALE: 1:50		
PROJECTION: Third Angle	**A3**	

EDINBURGH DESIGNS

A2 Load cell signal

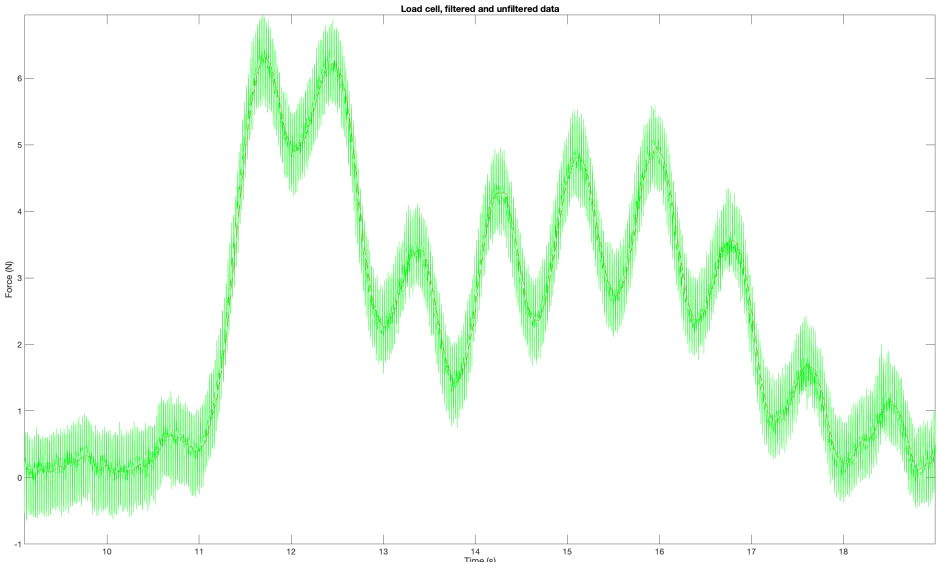

Figure A2.1: Load cell, filtered and unfiltered data.

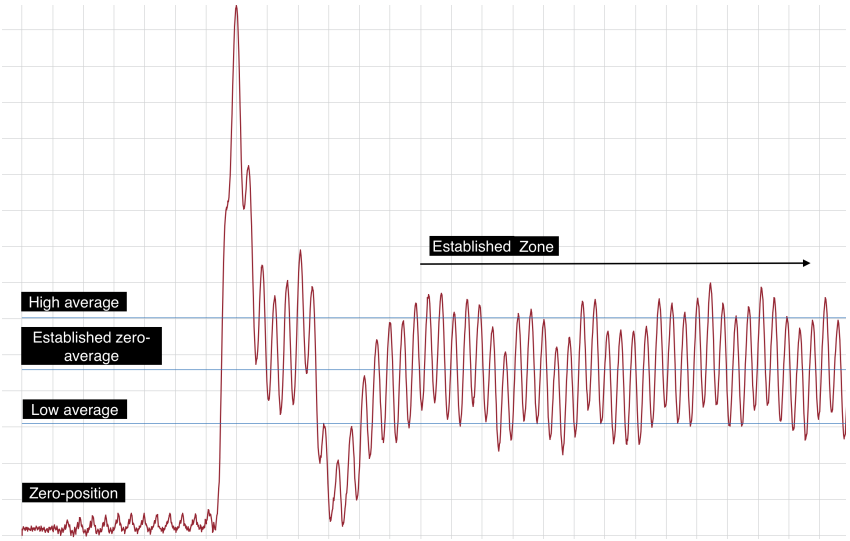

Figure A2.2: Explanation of established zero, high-, and low force amplitude.

A3 Images of the model, laboratory, results and test facilities

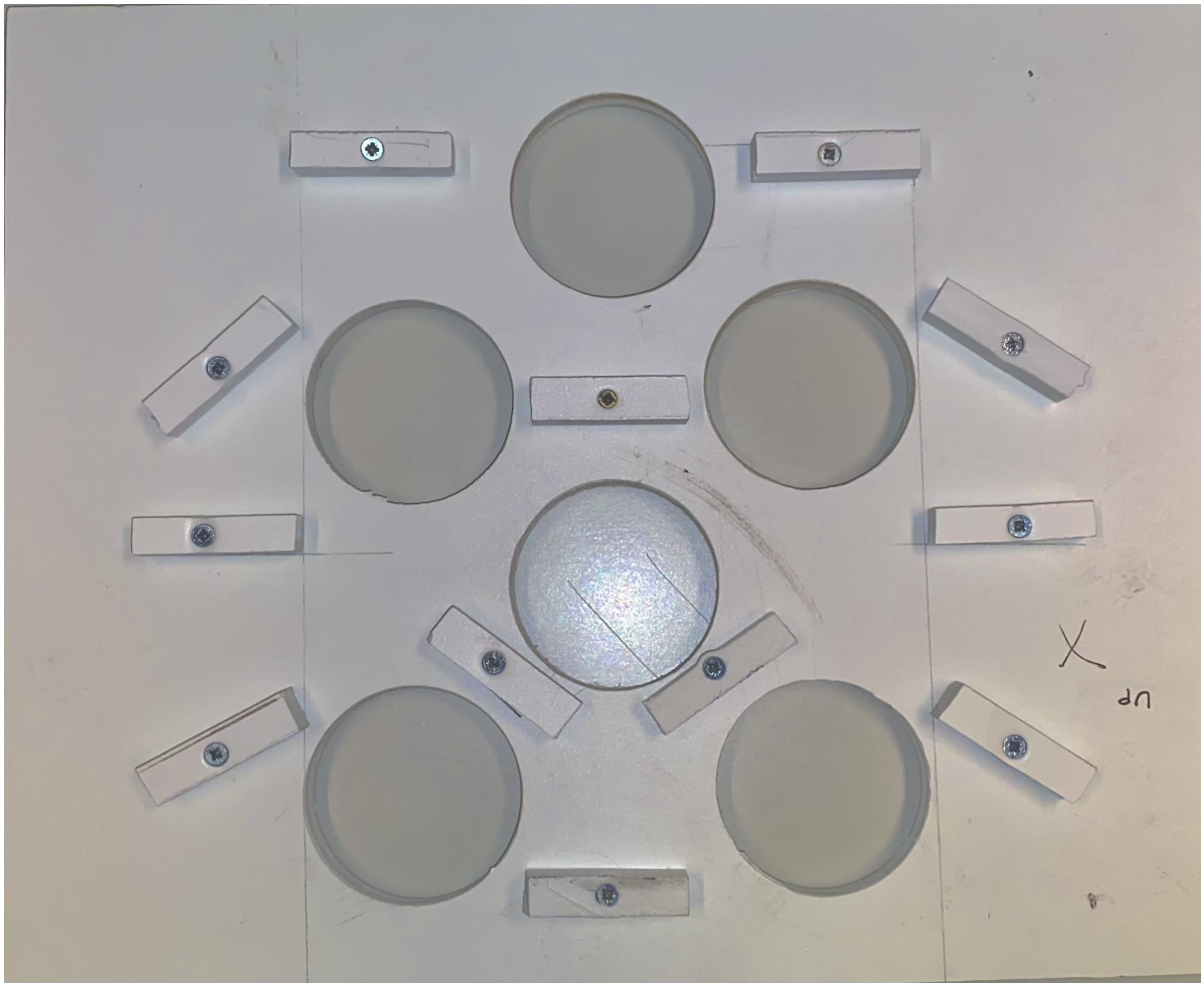

Figure A3.1: 3D-pattern on porosity plate.

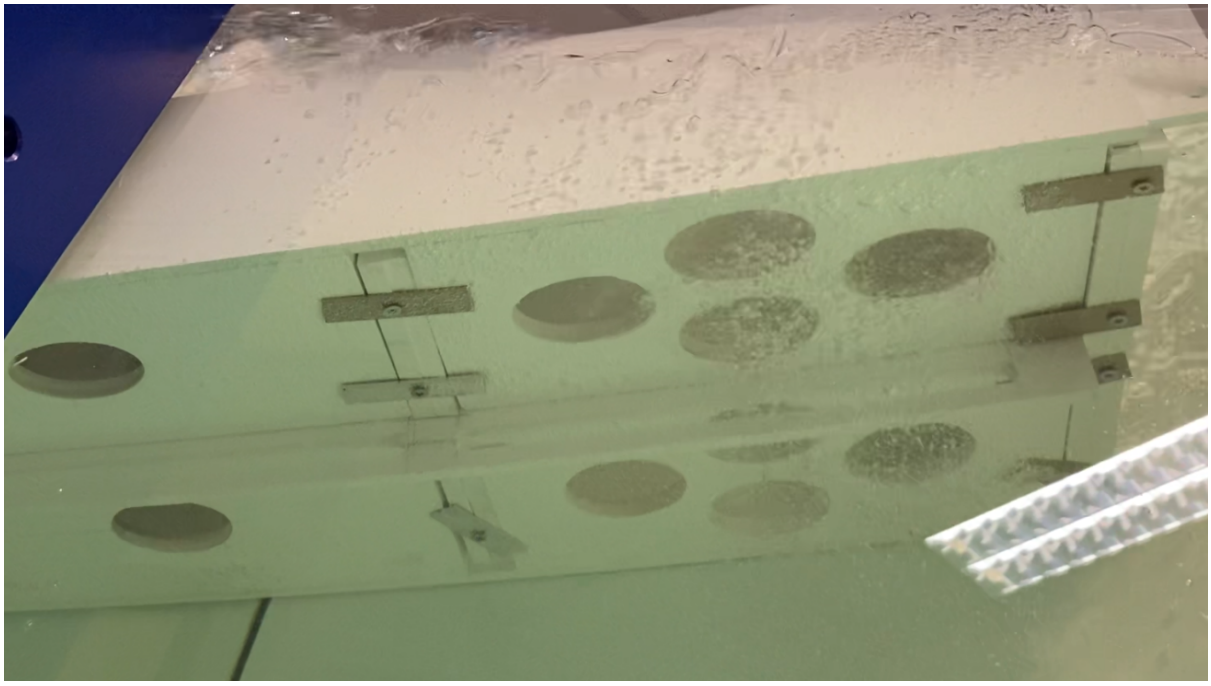

Figure A3.2: Aeration under chamber three during laboratory tests.

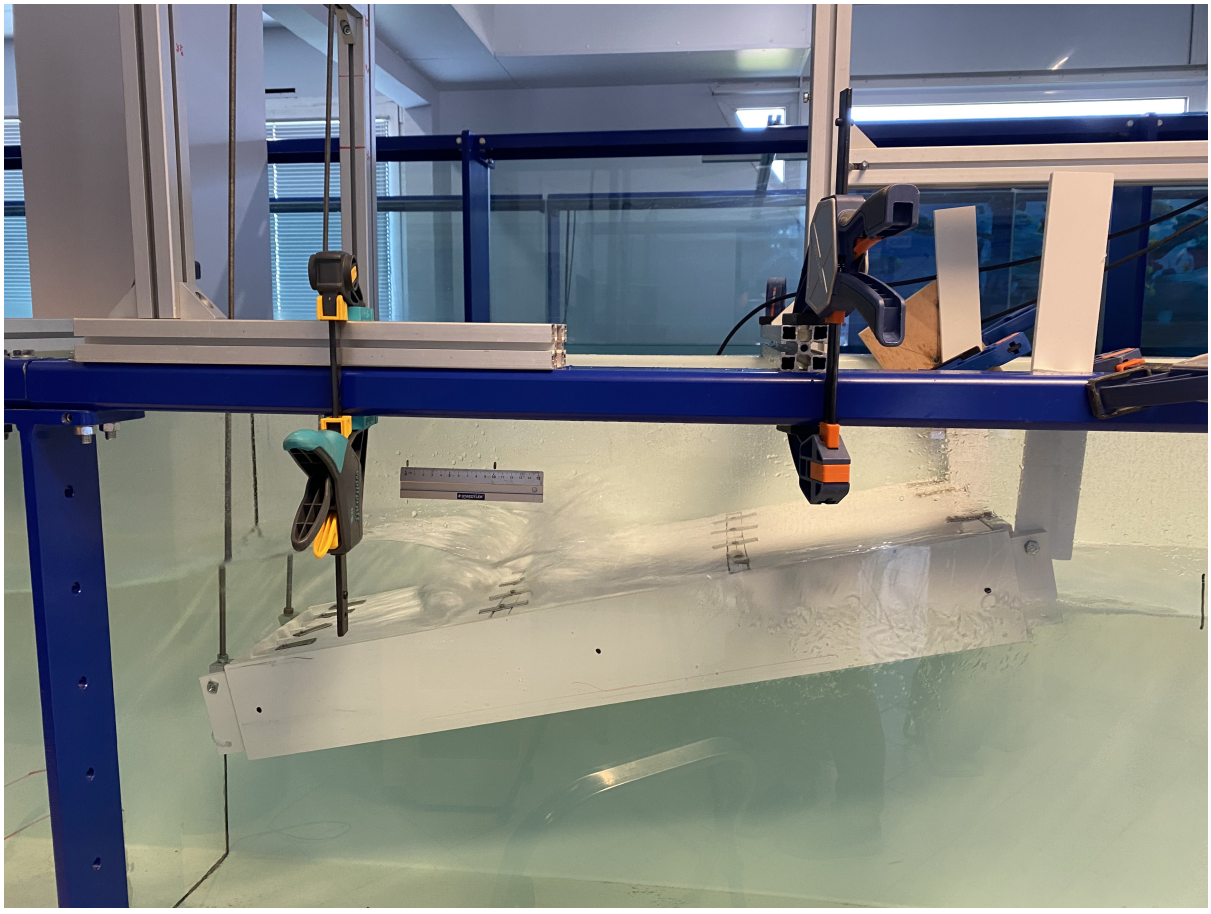

Figure A3.3: Rolling wave breaking during fixed set-up testing of configuration 0.

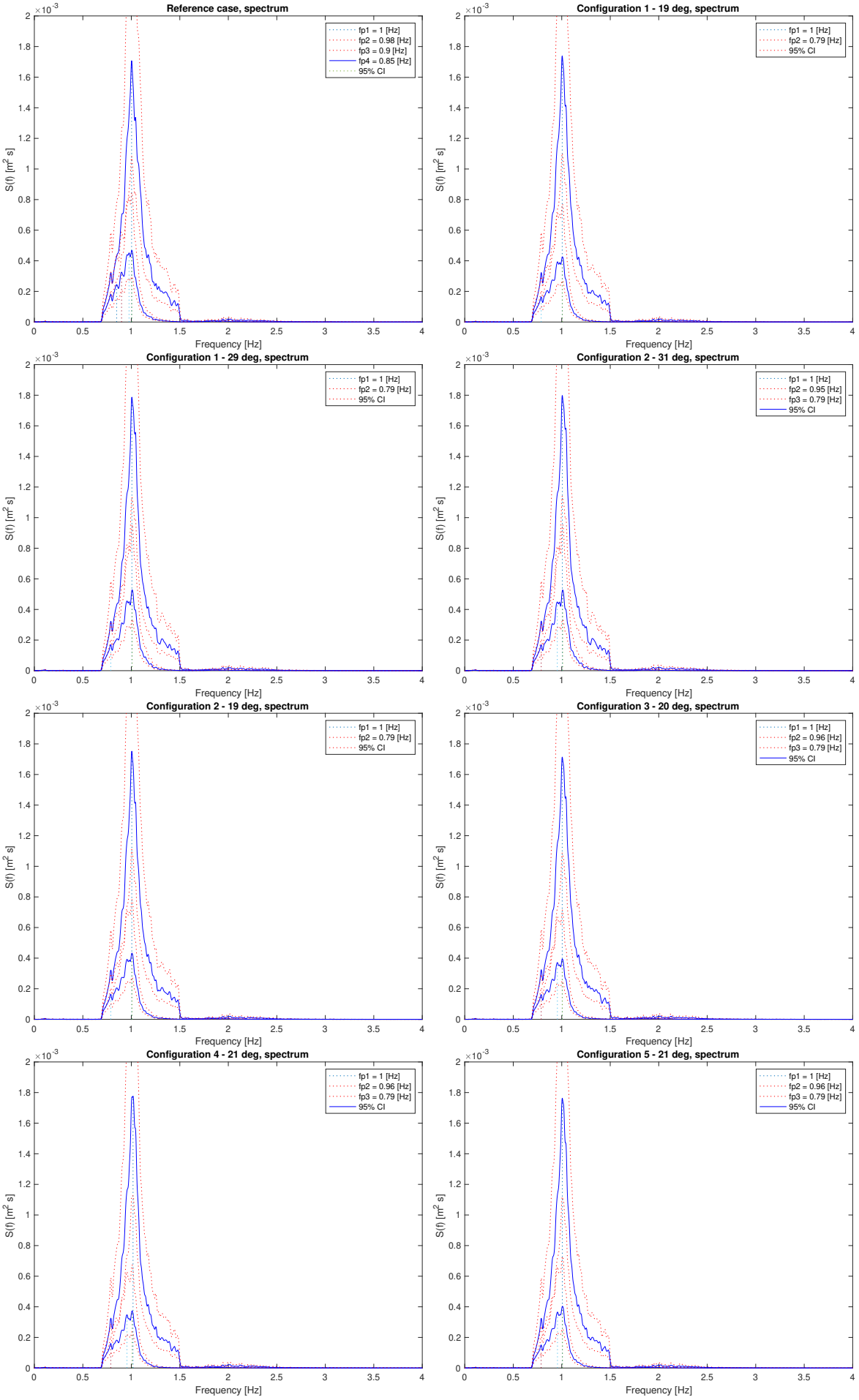
Reference case, spectrum
fp1 = 1 [Hz]
fp2 = 0.98 [Hz]
fp3 = 0.9 [Hz]
fp4 = 0.85 [Hz]
95% CI
Configuration 1 - 19 deg, spectrum
fp1 = 1 [Hz]
fp2 = 0.79 [Hz]
95% CI
Configuration 1 - 29 deg, spectrum
fp1 = 1 [Hz]
fp2 = 0.79 [Hz]
95% CI
Configuration 2 - 31 deg, spectrum
fp1 = 1 [Hz]
fp2 = 0.95 [Hz]
fp3 = 0.79 [Hz]
95% CI
Configuration 2 - 19 deg, spectrum
fp1 = 1 [Hz]
fp2 = 0.79 [Hz]
95% CI
Configuration 3 - 20 deg, spectrum
fp1 = 1 [Hz]
fp2 = 0.96 [Hz]
fp3 = 0.79 [Hz]
95% CI
Configuration 4 - 21 deg, spectrum
fp1 = 1 [Hz]
fp2 = 0.96 [Hz]
fp3 = 0.79 [Hz]
95% CI
Configuration 5 - 21 deg, spectrum
fp1 = 1 [Hz]
fp2 = 0.96 [Hz]
fp3 = 0.79 [Hz]
95% CI
S(f) [m² s]
Frequency [Hz]

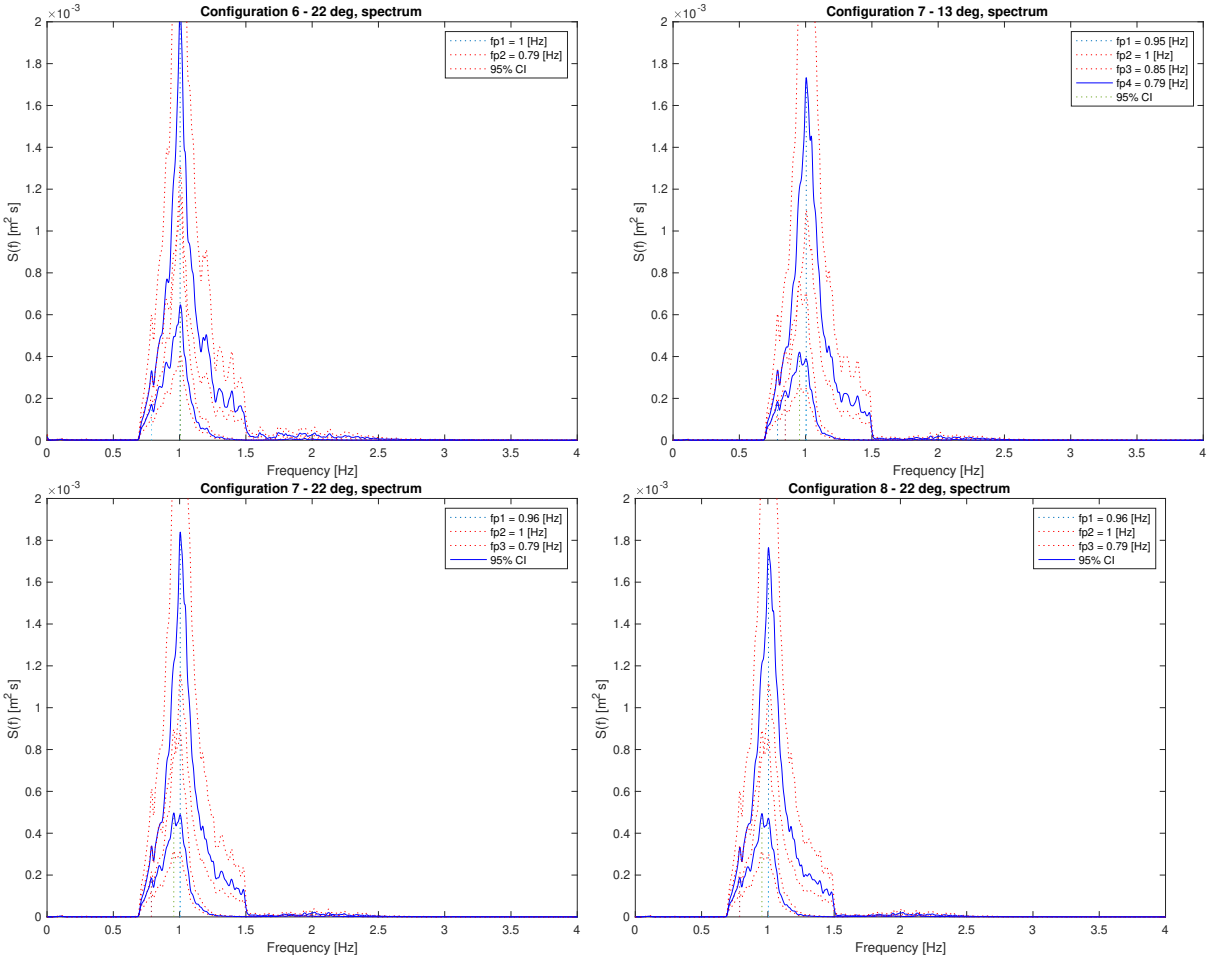

Figure A3.4: Wave spectrums for irregular wave runs.

A4 Natural frequency calculations

Moment of inertia:	Plane								
Frame:									
		z	x	y	Amount		c,y	Iy', part	Ix', part
Sidewalls	Outer	100	10	900	2		490	8,33E+05	7,50E+07
	Inner	80	10	980	2		490	4,27E+05	4,18E+07
Middle wall		130	10	880	1		490	1,83E+06	1,61E+08
transverse wall	Nr1	100	140	20	2		380	1,17E+07	1,67E+06
	Nr2	100	140	20	2		660	1,17E+07	1,67E+06
	End	100	300	20	1		940	2,50E+07	1,67E+06
	Start	100	140	20	2		50	1,17E+07	1,67E+06
	Ballast, end	100	300	10	1		95	2,50E+07	8,33E+05
	Ballast, wall	80	10	40	4		70	4,27E+05	1,71E+06
Top plate		10	320	260	3		810	2,67E+04	2,17E+04
Bottom plate		10	155	260	6		810	1,29E+04	2,17E+04

Angle: 20 degrees

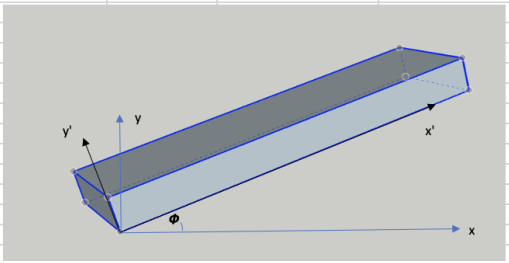

yc'	xc'	yc	xc	Ay	Ax	m (kg)	Iy, part	Ix, part	Iy', contributi	Iy, contribution
450	5	153,9090645		1000	90000	1,08	1,00E+06	7,77E+08	6,71E+07	5,49E+06
490	5	167,5898702		800	78400	0,9408	5,14E+05	7,71E+08	5,34E+07	2,75E+06
440	5	150,4888631		1300	114400	0,6864	2,21E+06	1,01E+09	8,82E+07	8,67E+06
10	70	3,420201433				0,336	1,41E+07	1,48E+06	3,17E+08	7,05E+08
10	70	3,420201433		14000	2000	0,336	1,41E+07	1,48E+06	2,57E+09	7,05E+08
10	150	3,420201433		30000	2000	0,36	3,01E+07	1,48E+06	1,50E+10	1,51E+09
10	70	3,420201433		14000	2000	0,336	1,41E+07	1,48E+06	4,82E+08	7,05E+08
5	150	1,710100717		30000	1000	0,18	3,01E+07	7,37E+05	6,00E+08	1,53E+09
20	5	6,840402867		800	3200	0,0768	5,14E+05	1,56E+06	2,17E+07	3,88E+07
130	160					1,4976				
130	77,5					1,4508				
			Total	91900	293000	7,2804				

Figure A4.1: Material and structural properties.

Constants						
g	9,81	m/s^2				
rho	1000	kg/m^3				
angle	0,349	rad	20	degrees		
Variables						
z	+/ - 0.010	m	Observed heave			
Ballast	2,2	kg				
Zc,ballast	70	mm				
Total weight	9,4804	kg				
Projected submerged length	553	mm				
CG, y local axis	232,9	mm				
CG, y main axis	218,8	mm				
Draft, local axis	588,0	mm				
Draft, main axis	201,1	mm				
CG,x						
KG	369,2					
KB	625,7					
BG	256,6					
Iy, local	1,92E+10					
Iy, main	5,22E+09					
Displaced volume						
	Submerged	60 %				
Fully submerged						
	Ballast	428000	mm^3			
	Transverse wall 1	560000	mm^3			
Partially submerged	Outer sidewalls	1080000	mm^3			
	Inner sidewalls	940800	mm^3			
	Middle wall	686400	mm^3			
	Transverse wall 2	336000	mm^3			
Total		4031200	mm^3	Delta, **Δ**		
		A'	Awp (m^2)			
Waterplane area (Awp)	Ballast	*Fully submerged*				
	Transverse wall 1	Fully submerged				Changes in displaced volume is dependent on movement. Highly relevant due to big relative movements.
	Outer sidewalls	2000	2,13E-03	m^2		
	Inner sidewalls	1600	1,70E-03	m^2		
	Middle wall	1300	1,38E-03	m^2		
	Transverse wall 2	5600	5,96E-03	m^2		
	Top plate	3200	3,41E-03	m^2		
	Bottom plates	9300	9,90E-03	m^2		
Total			2,45E-02	m^2		
BMy	1294	mm	Iy / Delta			
GMy	1037,8	mm	Bmy - BG			
KMy	1407,0	mm	KG + Gmy			

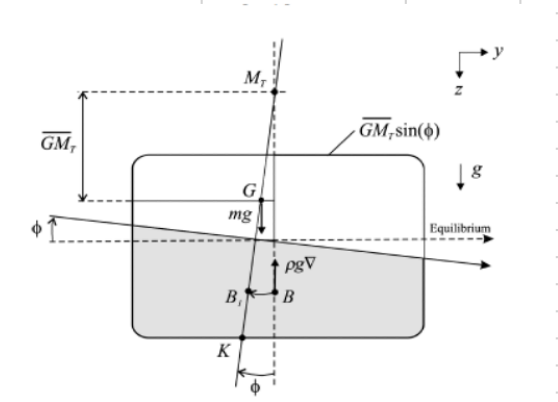

Figure A4.2: Calculations of displaced volume, water plane area and factors based on the method of Fossen (2011).

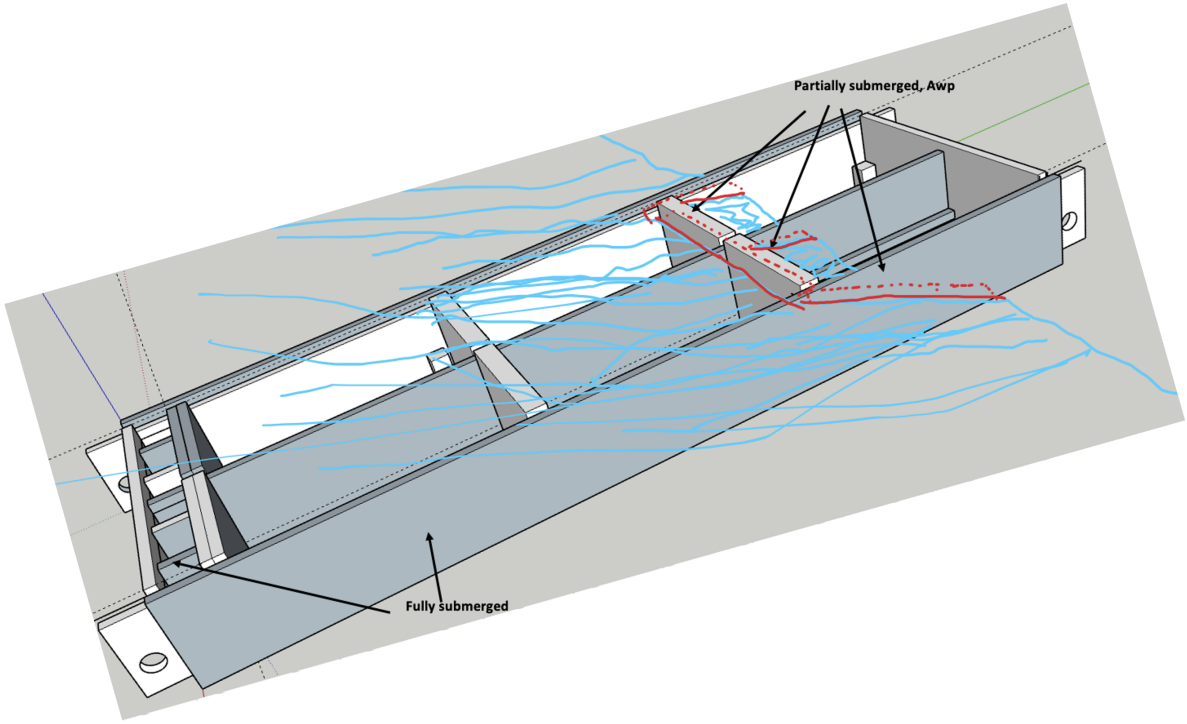

Figure A4.3: Illustration of partially submerged model frame.

C33	2,40E+02	T_heave	1,34E+00	Frequency	0,74
C44	4,10425E+13	T_roll	7,08E-02	Frequency	14,12
C55					

$$C_{33} = \rho g A_{wp}(0)$$

$$C_{44} = \rho g \nabla \overline{GM}_T$$

$$C_{55} = \rho g \nabla \overline{GM}_L$$

$$\omega_{n3} = \sqrt{\frac{C_{33}}{m + A_{33}(\omega_{heave})}}$$

$$\omega_{n4} = \sqrt{\frac{C_{44}}{I_x + A_{44}(\omega_{roll})}}$$

$$\omega_{n5} = \sqrt{\frac{C_{55}}{I_y + A_{55}(\omega_{pitch})}}$$

Figure A4.4: Natural frequency in heave and rotation, related to C_{33} and C_{44}, consequently.